CONTRACT NUMBER: NAS 9-14722

DRL NUMBER: T-707

DRD NUMBER: MA-559T

REPORT: MDC E1478

NASA CR-147716

Development of S-BAND ANTENNA INTERFACE DESIGN

VOLUME I

FINAL REPORT

MCDONNELL DOUGLAS ASTRONAUTICS COMPANY - EAST

MCDONNELL DOUGLAS CORPORATION

CONTRACT NUMBER: NAS 9-14722
DRL NUMBER: T-707
DRD NUMBER: MA-559T
REPORT: MDC E1478

COPY NO. 2

Development of S-BAND ANTENNA INTERFACE DESIGN

30 APRIL 1976

REPORT MDC E1478

VOLUME I
FINAL REPORT

Prepared by E. A. Kuhlman
E. A. Kuhlman
Program Manager

Approved by Dave Freeman
D. J. Freeman
Chief Advanced Space Avionics Engineer

Approved by G G McKee
G. G. McKee
Director, Avionics Engineering

MCDONNELL DOUGLAS ASTRONAUTICS COMPANY - EAST
Saint Louis, Missouri 63166 (314) 232-0232

MCDONNELL DOUGLAS CORPORATION

DISTRIBUTION LIST

NASA Lyndon B. Johnson Space Center
R&T Procurement Branch
Attn: George Gaffney, Mail Code BC73(27)
Houston, Texas 77058
One Copy

NASA Lyndon B. Johnson Space Center
Technical Library Branch
Attn: Retha Shirkey, Mail Code JM6
Houston, Texas 77058
Four Copies

NASA Lyndon B. Johnson Space Center
Technical Utilization Office
Attn: John T. Wheeler, Mail Code AT3
Houston, Texas 77058
One Copy

NASA Lyndon B. Johnson Space Center
Electromagnetic Systems Branch
Attn: H. Dean Cubley, Mail Code EE3
Houston, Texas 77058
Eleven Copies

THIS PAGE INTENTIONALLY LEFT BLANK

ABSTRACT

The construction of an analytical thermal model of an S-band antenna in a typical Space Shuttle Orbiter installation is discussed. The selection and modeling of orbital and entry thermal environment inputs for the thermal analyses are discussed. The results of analyses for a variety of orbital thermal environments and entry initial conditions are given. Design and fabrication details of a thermal test fixture which physically approximates the Orbiter installation are discussed. The design and fabrication of two electrical test fixtures which electrically simulate the Orbiter surface shape and thermal protection system are discussed.

THIS PAGE INTENTIONALLY LEFT BLANK

CONTENTS

PRECEDING PAGE BLANK NOT FILMED

THIS PAGE INTENTIONALLY LEFT BLANK

CONTENTS

PRECEDING PAGE BLANK NOT FILMED

LIST OF PAGES

Title

iii thru xii
1-1 thru 1-2
2-1 thru 2-2
3-1 thru 3-2
4-1 thru 4-2
5-1 thru 5-34
6-1 thru 6-12
7-1 thru 7-26
8-1 thru 8-2
A-1 thru A-4
B-1 thru B-4
C-1 thru C-2

LIST OF TABLES

LIST OF TABLES

THIS PAGE INTENTIONALLY LEFT BLANK

CONCLUSIONS

The conclusions reached from an evaluation of the results obtained during this program are:

(a) The antenna temperature extremes are within specification requirements for military aircraft antennas (-66 to 177°C (-85 to 350°F)).

(b) Large temperature gradients do not exist in the antenna during any environmental condition because of the insulation afforded by the TPS.

(c) An active thermal control plan is not required.

(d) The rate of temperature change of the antenna due to orbital heat flux variations is slow.

(e) The temperature of the interior interface (i.e., crew cabin wall) moderately affects the antenna temperatures.

(f) Continuous antenna operation over extended periods raises the antenna temperatures approximately 11°C (20°F).

(g) A thermal test fixture has been designed and fabricated which is independent of TPS thickness and can be used for both orbital and entry heating environments.

(h) Electric test fixtures have been designed and fabricated which simulate the TPS and local shape for upper and lower Shuttle Orbiter body locations.

THIS PAGE INTENTIONALLY LEFT BLANK

CONCLUSIONS

The conclusions reached from an evaluation of the results obtained during this program are:

(a) The antenna temperature extremes are within specification requirements for military aircraft antennas (-66 to 177°C (-85 to 350°F)).

(b) Large temperature gradients do not exist in the antenna during any environmental condition because of the insulation afforded by the TPS.

(c) An active thermal control plan is not required.

(d) The rate of temperature change of the antenna due to orbital heat flux variations is slow.

(e) The temperature of the interior interface (i.e., crew cabin wall) moderately affects the antenna temperatures.

(f) Continuous antenna operation over extended periods raises the antenna temperatures approximately 11°C (20°F).

(g) A thermal test fixture has been designed and fabricated which is independent of TPS thickness and can be used for both orbital and entry heating environments.

(h) Electric test fixtures have been designed and fabricated which simulate the TPS and local shape for upper and lower Shuttle Orbiter body locations.

THIS PAGE INTENTIONALLY LEFT BLANK

INTRODUCTION

The purpose of this program was: (1) to construct a thermal model of an S-band antenna installed in a typical spacecraft structure, which is thermally protected by an external thermal protection system (TPS) and to analyze both orbital and entry thermal environments; (2) to design, fabricate and deliver a thermal test fixture which can be used to verify the thermal analyses by thermal vacuum tests; and (3) to design, fabricate and deliver two electrical test fixtures which simulate large and small radius spacecraft structures that are covered with external insulation for thermal protection during entry.

The Space Shuttle Orbiter is representative of current and future generation spacecraft designs and was, therefore, used as the baseline for the thermal analyses, the thermal test fixture and the electrical test fixtures required by this program. The Orbiter, unlike previous manned spacecraft which depended on ablating heat shields to dissipate entry heating, is covered with a thermal protection system (TPS) consisting principally of a low density, reusable, silica insulation bonded to the Orbiter structural skin. The insulation is locally sized to limit the maximum skin temperature. However, since the antenna aperture provides a surface discontinuity and a local heat sink, the antenna temperatures can differ from those on the surrounding skin surface. In terms of antenna performance, the thermal insulation is equivalent to covering the antenna and the surrounding ground plane with a dielectric sheet which affects the radiation patterns and impedance and the coupling to other antennas on the spacecraft.

An analytical thermal model of an S-band antenna mounted in the Space Shuttle Orbiter was constructed. The model includes a detailed representation of the antenna components, the Orbiter structure, the TPS internal insulation and heat sources.

The thermal model was used to determine the response of the antenna to a variety of orbital environments and to aerodynamic heating during entry from either hot or cold orbital conditions. The space irradiation was determined for spacecraft orbits in the Space Shuttle Reference Mission II timelines. Worst case hot and cold antenna temperatures were obtained for both operating and nonoperating modes of the antenna. The results of these analyses show that the temperatures, at any point on the antenna, remain between -63 and 128°C (-82 and 262°F) for all conditions considered.

A thermal test fixture was designed, fabricated and delivered. The test fixture design was based on the analytical thermal model to permit direct comparison of data from thermal vacuum tests with results obtained from that analytical model. Thermocouple locations on the tests fixture were selected to coincide with nodes in the analytical model.

Two electrical test fixtures were designed, fabricated and delivered. The test fixture shapes and simulated TPS configurations were based upon antenna locations on the upper and lower forward Orbiter body. The upper and lower Orbiter body locations represent large and small radius of curvature antenna ground planes, respectively.

THIS PAGE INTENTIONALLY LEFT BLANK

INTRODUCTION

The purpose of this program was: (1) to construct a thermal model of an S-band antenna installed in a typical spacecraft structure, which is thermally protected by an external thermal protection system (TPS) and to analyze both orbital and entry thermal environments; (2) to design, fabricate and deliver a thermal test fixture which can be used to verify the thermal analyses by thermal vacuum tests; and (3) to design, fabricate and deliver two electrical test fixtures which simulate large and small radius spacecraft structures that are covered with external insulation for thermal protection during entry.

The Space Shuttle Orbiter is representative of current and future generation spacecraft designs and was, therefore, used as the baseline for the thermal analyses, the thermal test fixture and the electrical test fixtures required by this program. The Orbiter, unlike previous manned spacecraft which depended on ablating heat shields to dissipate entry heating, is covered with a thermal protection system (TPS) consisting principally of a low density, reusable, silica insulation bonded to the Orbiter structural skin. The insulation is locally sized to limit the maximum skin temperature. However, since the antenna aperture provides a surface discontinuity and a local heat sink, the antenna temperatures can differ from those on the surrounding skin surface. In terms of antenna performance, the thermal insulation is equivalent to covering the antenna and the surrounding ground plane with a dielectric sheet which affects the radiation patterns and impedance and the coupling to other antennas on the spacecraft.

An analytical thermal model of an S-band antenna mounted in the Space Shuttle Orbiter was constructed. The model includes a detailed representation of the antenna components, the Orbiter structure, the TPS internal insulation and heat sources.

The thermal model was used to determine the response of the antenna to a variety of orbital environments and to aerodynamic heating during entry from either hot or cold orbital conditions. The space irradiation was determined for spacecraft orbits in the Space Shuttle Reference Mission II timelines. Worst case hot and cold antenna temperatures were obtained for both operating and nonoperating modes of the antenna. The results of these analyses show that the temperatures, at any point on the antenna, remain between -63 and 128°C (-82 and 262°F) for all conditions considered.

A thermal test fixture was designed, fabricated and delivered. The test fixture design was based on the analytical thermal model to permit direct comparison of data from thermal vacuum tests with results obtained from that analytical model. Thermocouple locations on the tests fixture were selected to coincide with nodes in the analytical model.

Two electrical test fixtures were designed, fabricated and delivered. The test fixture shapes and simulated TPS configurations were based upon antenna locations on the upper and lower forward Orbiter body. The upper and lower Orbiter body locations represent large and small radius of curvature antenna ground planes, respectively.

Mr. E. A. Kuhlman, Program Manager, was responsible for the overall technical direction of this program. Other members of the McDonnell Douglas Astronautics Company-East (MDAC-E) engineering staff who contributed to this program were L. H. Ebbesmeyer, E. A. Eiswirth, H. W. Kipp, G. D. Mitchell and C. D. Poore. Mr. Eiswirth provided the major effort for the design of the thermal model and performed the thermal analyses. Mr. R. B. Lewis, MCAIR Numerical Drafting Group, developed the frame contours of the simply curved surfaces for the electrical test fixtures. Test fixture fabrication was supervised by E. F. Disser and B. J. Myers of the McDonnell Aircraft Co. (MCAIR), Advanced Material Fabrication Facility. Messers. Disser and Myers also offered numerous suggestions which simplified the electrical and thermal test fixture designs.

Mr. H. D. Cubley of the Antenna System Section of the Electromagnetic Systems Branch, NASA Lyndon B. Johnson Space Center, Houston, Texas was the technical monitor for this program.

The units used for the physical quantities defined in this report are given in both the International System of Units (SI) and the U.S. customary units in the text. U.S. customary units are used in the drawings and in some of the graphs and tables.

This report is designated as Volume I in anticipation of additional work related to this contract which will be reported in a subsequent volume.

The task numbers used in the text correspond to the tasks given in the Statement of Work, Exhibit "A," of Contract NAS 9-14722, dated 1 July 1975.

THERMAL ANALYSES

The Thermal Analyses Task (Task 2.3.1) consisted of developing an analytical thermal model of an S-band antenna (design specified by NASA-JSC) and selecting orbital and entry thermal environments based on the Space Shuttle Baseline Reference Mission II. The objectives were: (1) to determine the dynamic temperature response of the major structural features of the array antenna; (2) to determine the necessity for supplying power to maintain the antenna temperature; and (3) to prepare a thermal control plan for maintaining the antenna within acceptable thermal limits. This section discusses the analytical thermal model, the thermal environment and the thermal response of the antenna. The results of these analyses indicate that active thermal control is not required.

Thermal Model

An antenna thermal model was constructed to evaluate the effects of orbital and entry thermal environments on an S-band antenna, mounted in a typical Space Shuttle Orbiter installation at both upper and lower body locations (figure 1). The external Orbiter wall consists of an aluminum skin-stringer structure covered with a reusable surface insulation (RSI), which combined with a strain isolation pad (SIP), serves as the thermal protection system (TPS). The RSI is bonded to the SIP and the SIP to the skin with RTV-560. Thermal properties of the antenna and TPS materials included in the thermal model are tabulated in Appendix A. A typical cross-section of TPS and structure is shown in figure 2. The thickness of the RSI is dependent upon the local heat input. The antenna is mounted in this structure with a supporting frame which holds the antenna aperture surface (typically a dielectric cover) flush with the skin surface. The TPS covers, and is bonded to, the antenna surface in the same way as it is to the surrounding skin. The RSI is not continuous but is cut into 15.2 x 15.2 cm (6.0 x 6.0 in.) tiles. The tile rows are offset 7.6 cm (3.0 in.) to minimize the gap heating. The gap width between tiles is nominally 1.27 $\pm$ .51 mm (0.050 $\pm$ 0.020 in.). Heating at the bottom of the gaps is insignificant and is not considered in the thermal model. The antenna configuration and its relationship to the surrounding structure, internal insulation and heat sources greatly influence the antenna temperature.

Baseline antenna design. - The analytical model was based on the design shown in figure 3. The antenna consists of five circularly polarized radiating elements arranged in a symmetrical array. The elements are essentially open-ended ridged waveguides with orthogonal ridge pairs excited from a 90° hybrid at the base of each element. The elements are fed from a power division and phasing circuit board, which also serves as a mechanical base for holding the elements in place. The circuit board assembly is attached at three points to the sleeves surrounding each radiating element. The sleeves hold the elements in place, flush with the ground plane.

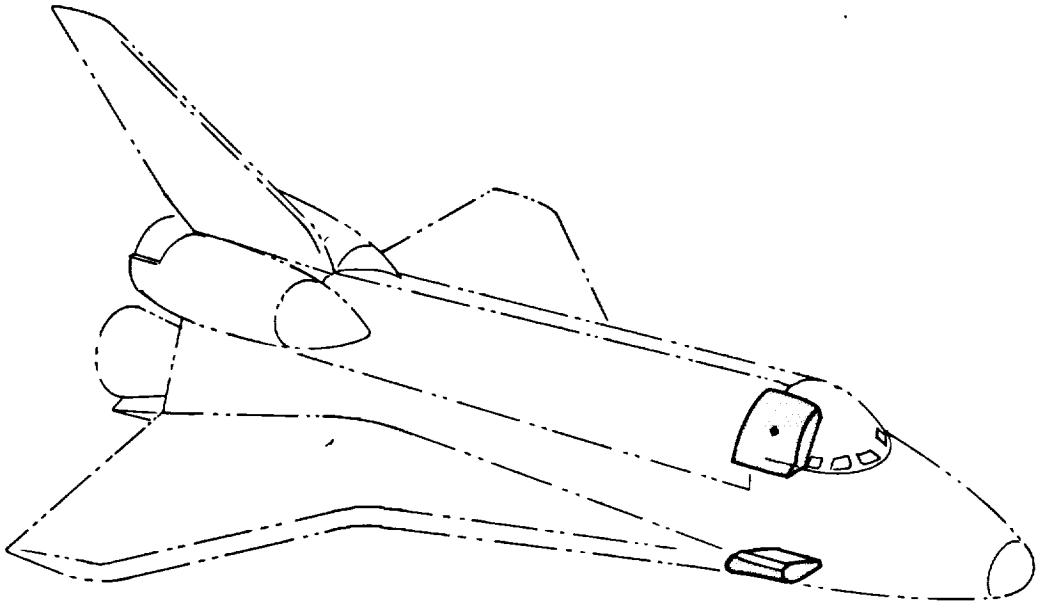

FIGURE 1 S-BAND ANTENNA LOCATIONS ON SPACE SHUTTLE ORBITER

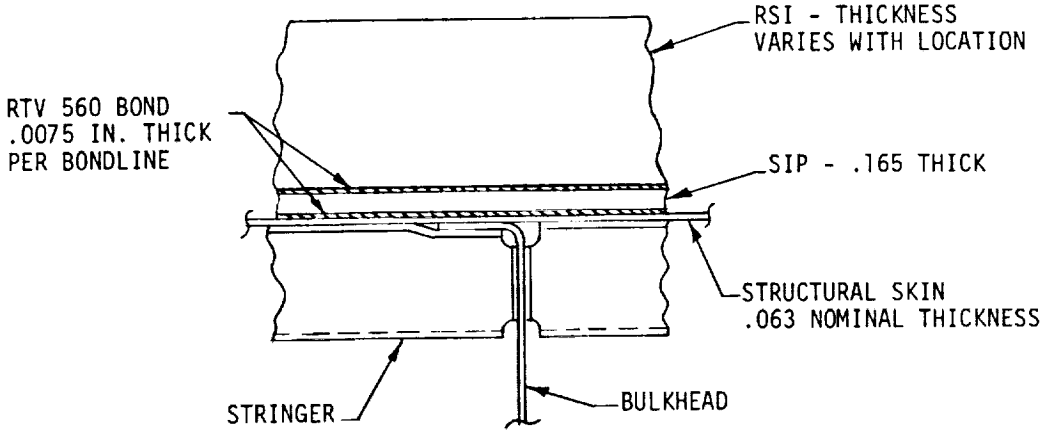

DIMENSIONS IN INCHES

FIGURE 2 TYPICAL TPS/STRUCTURE CONFIGURATION

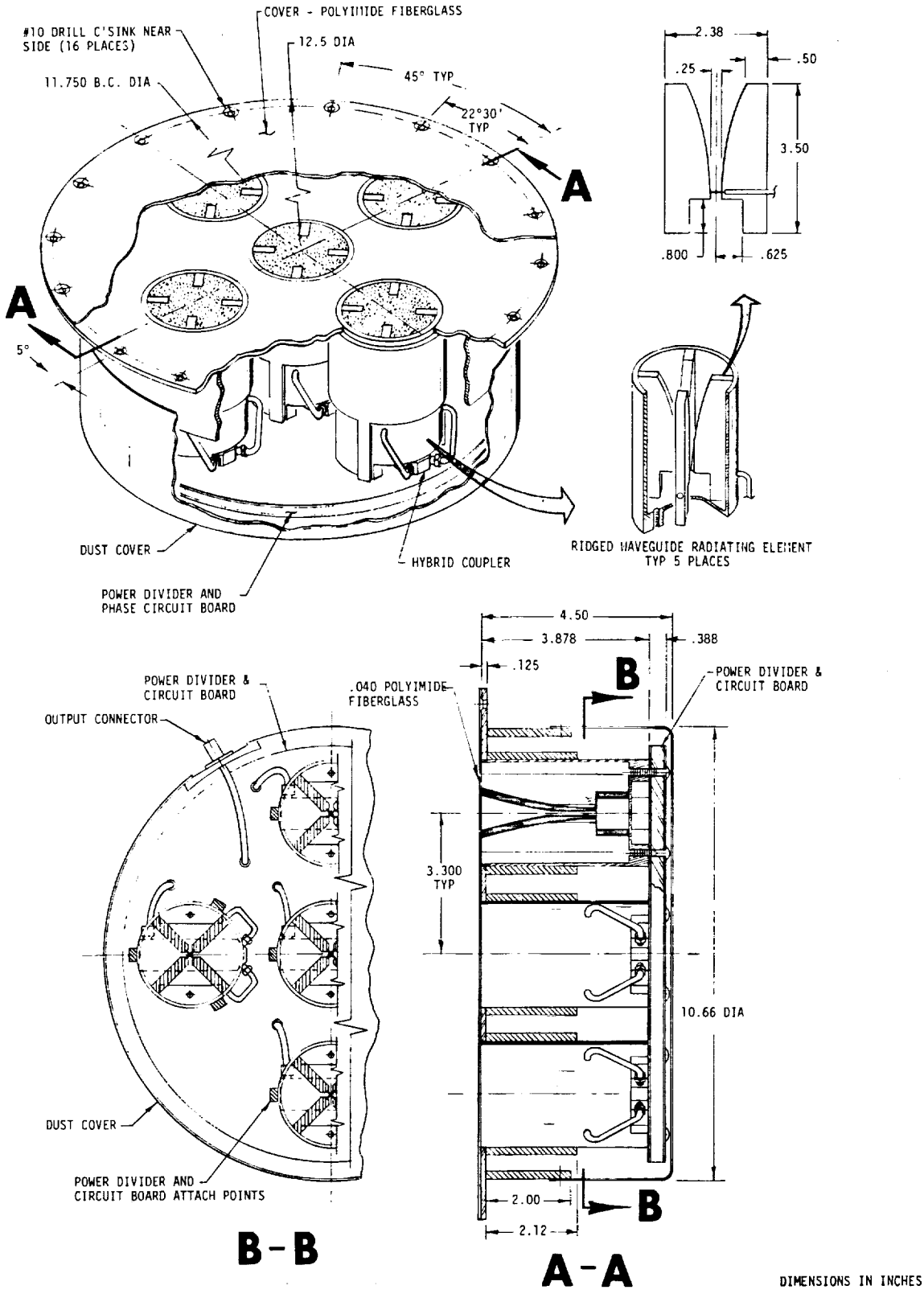

FIGURE 3 BASELINE S-BAND ANTENNA

Analytical thermal model. - A 324 node thermal model (ANTENA) of the S-band antenna and its surrounding structure and insulation was constructed using the MDAC-E thermal analysis program, HEATRAN. The model configuration, illustrated in figure 4, includes a 1/4 (90 degree) section of the antenna and a 61 cm (24 in.) square section of the surrounding skin-stringer structure and TPS. This size was required so that the edges of the model would be approximately adiabatic in the transverse direction. The distribution of the nodes of the model is as follows:

Skin and TPS	111 nodes
Antenna radiating elements	100 nodes
Circuit board, dust cover, antenna flange and plate	49 nodes
Internal insulation	12 nodes
Radiosity	52 nodes

The location of each of the thermal model nodes is tabulated in Appendix B. Figure 5 shows the arrangement of the model thermal nodes in the TPS, structure and internal insulation surrounding the antenna. Since only the antenna and the TPS bondline temperatures are of interest and since the transverse temperature gradients in the TPS are small with respect to the normal gradients, the curvature of the surface was neglected. The impressed heating rates were assumed to be constant over the model surface and the TPS thickness was assumed to be equal to that directly above the antenna, i.e., 1.04 cm (0.415 in.) and 4.44 cm (1.748 in.) for the upper and lower antenna locations, respectively. This is a reasonable approximation since the local TPS thickness is sized to limit the maximum skin temperature regardless of the local heating. It was necessary to model the skin and TPS in rectangular coordinates even though the antenna is rotationally symmetric because of the stringers attached to the vehicle skin. The conductance in the direction parallel to the stringers is almost double that along the perpendicular path. To accommodate this condition, the skin and the stringers were lumped together as nodes with different conductances in the parallel and perpendicular directions. The 111 nodes in the TPS and skin are arranged in seven layers of sixteen nodes each as shown in figure 5. The RSI includes five of the seven, equidistant nodes in the normal direction. The RTV bondlines and SIP were combined into one lumped node in the normal direction.

Figures 6 thru 9 illustrate the node locations within the antenna. Figure 6 is the top view; the cross-sectional views designated in figure 6 are shown in figures 7 and 8. Figure 9 is a detailed schematic of the nodes within one of the radiating elements. The nodal distribution is sufficiently detailed in the antenna section of the model to evaluate component interface temperatures and gradients. The forward radiating element contains thirty nodes and the associated hybrid coupler nine. The center radiating element is divided into eighteen nodes and its coupler contains six. The outboard radiating element has thirty nodes and its coupler has seven. The thermal model program is written so as to allow power to be dissipated in the element ridges to simulate heating due to the losses in the antenna during operation. All of the radiating element external nodes, the dust cover, mounting flange and circuit board are connected in the thermal model via a radiosity network which accounts for

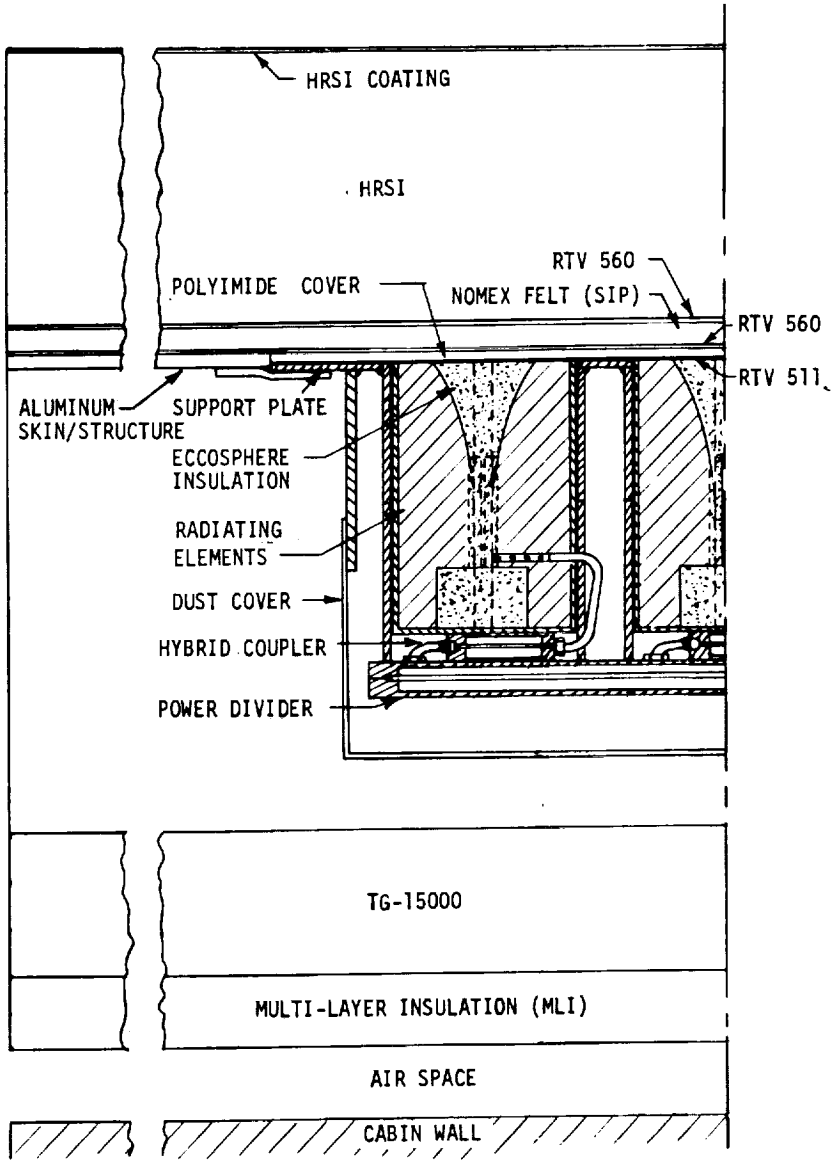

FIGURE 4 CROSS-SECTION OF S-BAND ANTENNA ANALYTICAL THERMAL MODEL

heating due to gray body radiation among components. Geometric view factors within the antenna were calculated using the MDAC-E thermal radiation analyzer program (RADQ).

The internal insulation (figure 4) of the thermal model, a 61 cm (24 in.) square section, contains only one node in the transverse direction. However, the insulation layers are divided into eleven nodes in the normal direction. This simplification causes no significant error since the cabin wall temperature is constant and the transverse temperature gradients are small. Radiosity connectors are used to link the antenna dust cover to the inside of the skin and to the TG-15000 insulation.

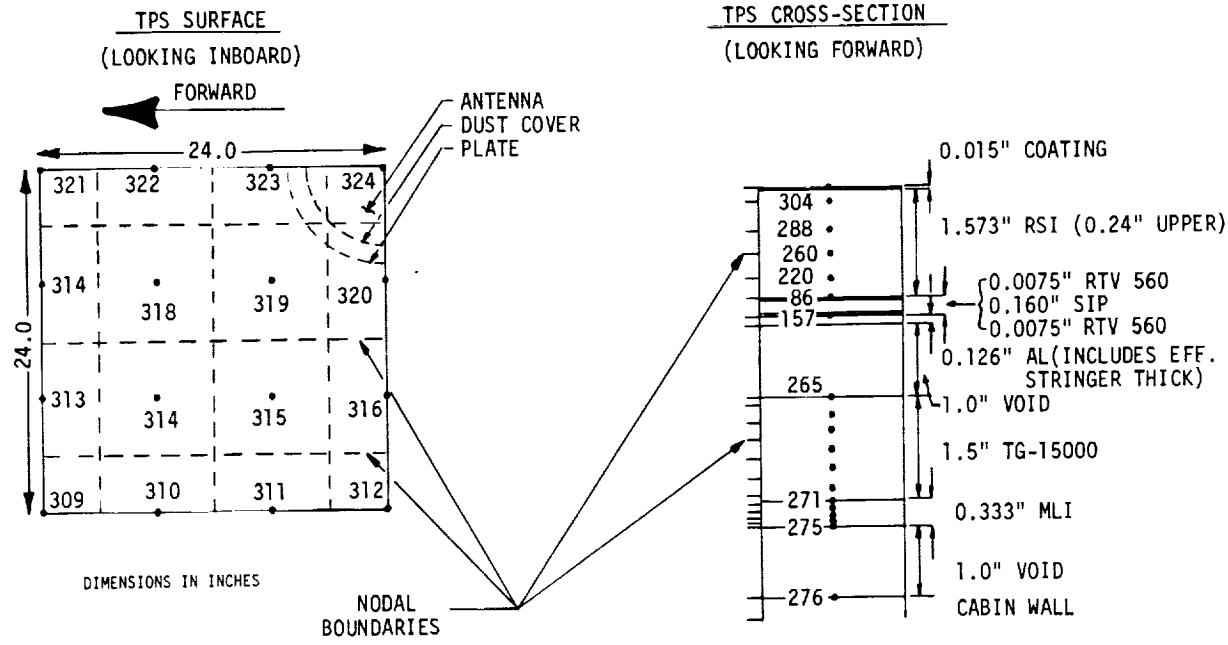

FIGURE 5 ANTENNA THERMAL MODEL NODAL DISTRIBUTION - TPS/STRUCTURE/ INTERNAL INSULATION

The HEATRAN program uses the initial temperature level of each of the 324 nodes in the thermal model along with the boundary conditions, cabin wall temperature and TPS surface heat transfer rate history to determine the transient temperature response at each of the nodes. Orbital equilibrium temperatures are determined by computing the temperature changes over several orbits and extrapolating each node temperature history in an exponential manner to the equilibrium level. The matrix solution techniques used in these analyses were either Gaussian elimination or Gauss-Seidel iteration depending on the rate of change in the applied heat flux. A sample output listing is shown in Appendix C.

Thermal Environment

The S-band antenna thermal environment consists of two parts, that associated with the external TPS surface and that at the interface within the vehicle. The external environment is composed of either irradiation from the Sun and Earth during orbital flight or aerodynamic heating during entry. The orbital environment was derived from an analysis of the Space Shuttle Baseline Reference Mission II timelines for Options 1, 2 and 3. The entry environment was based on entry surface temperatures provided by NASA. The internal environment is controlled by the capability of the antenna to accept or reject heat from the spacecraft interior.

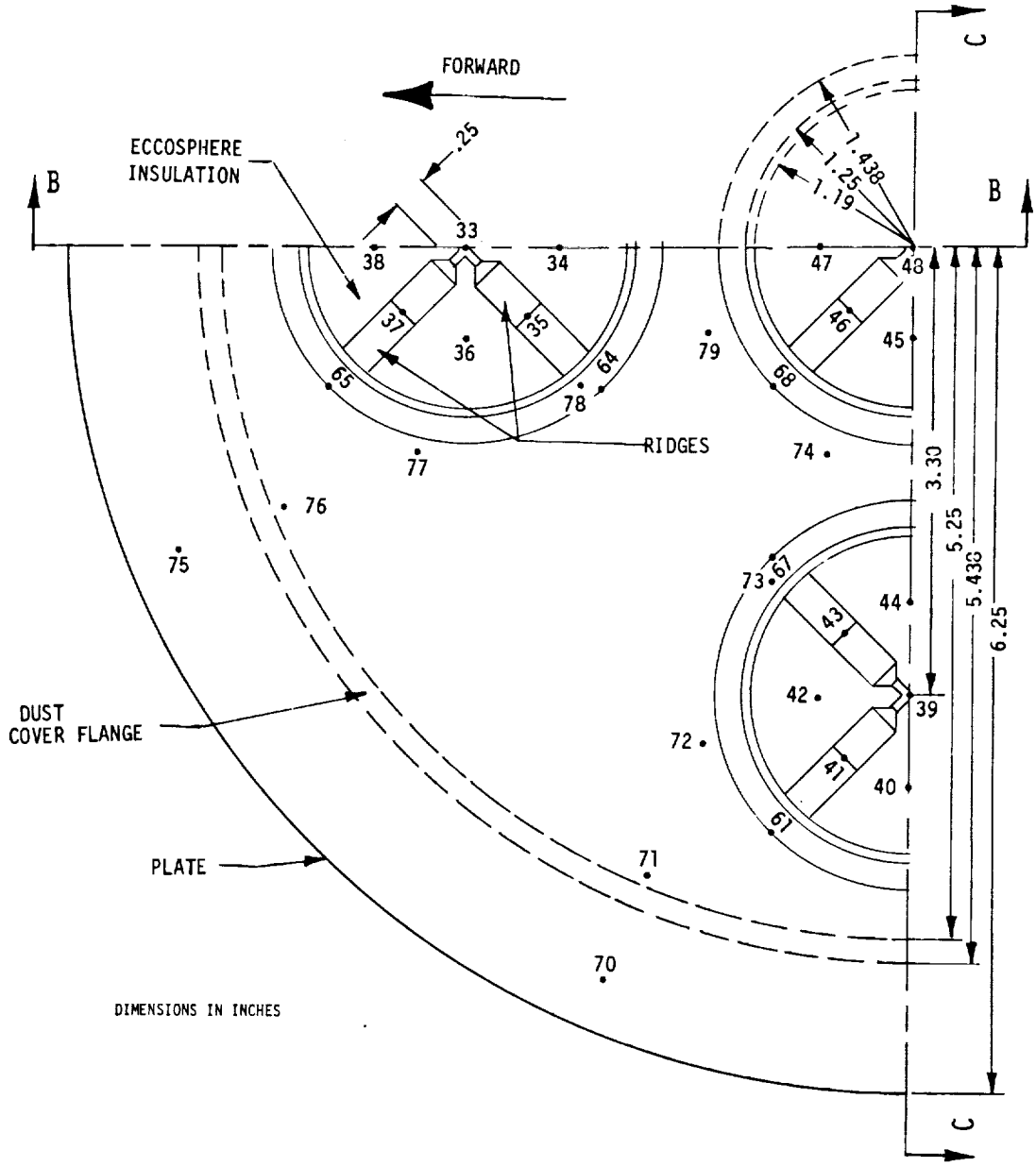

FIGURE 6 ANTENNA THERMAL MODEL NODAL DISTRIBUTION - ANTENNA TOP VIEW

Interior boundary condition. - For all of the baseline entry and orbital thermal environments, the spacecraft/S-band antenna interface, located at the cabin wall (figure 4), is isothermal at 33°C (92°F). To determine the effect of this condition on the array, the wall temperature was changed ±17°C (30°F) for two specific analyses.

Exterior boundary condition in orbit. - The external surface of the spacecraft is subject to three orbital irradiations; direct solar, Earth reflected solar (albedo) and Earth emitted infrared. The level of each of these fluxes

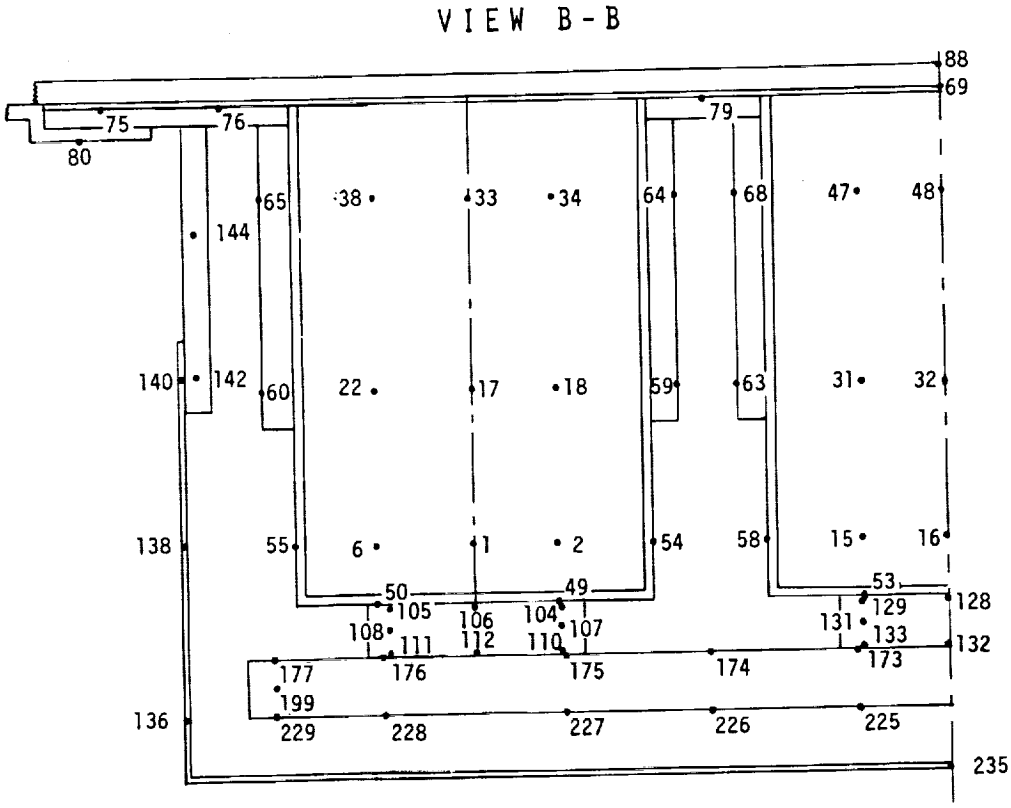

FIGURE 7 ANTENNA THERMAL MODEL NODAL DISTRIBUTION - ANTENNA CROSS-SECTION LOOKING OUTBOARD

at a specified surface is dependent on the spacecraft orbit and attitude because: (1) the irradiation is a function of the angle between the receiver and the radiation source and (2) part or all of a surface may be shaded by other surfaces or by the Earth.

The thermal analyses of the antennas at the respective locations were conducted for the extreme heat flux conditions, i.e., the maximum and minimum total absorbed heat flux. This approach yielded the upper and lower antenna temperature extremes. All other orbits would provide antenna temperatures within this range. In addition to the extreme cases, a spacecraft thermal conditioning case typical of all Mission II options was analyzed to provide typical initial antenna temperatures for entry. The incident and absorbed values of each of the thermal radiation fluxes were determined using the RADQ program. This program accounts for the orientation and optical properties of the receiving surface and also the extent and duration of shading during the orbit.

Since the principal portion of the total irradiation is direct solar, maximum and minimum heating conditions were approximated by rotating the spacecraft such that each antenna surface received sunlight over its entire area for all or none of the orbit. The percentage of a mean solar day that a

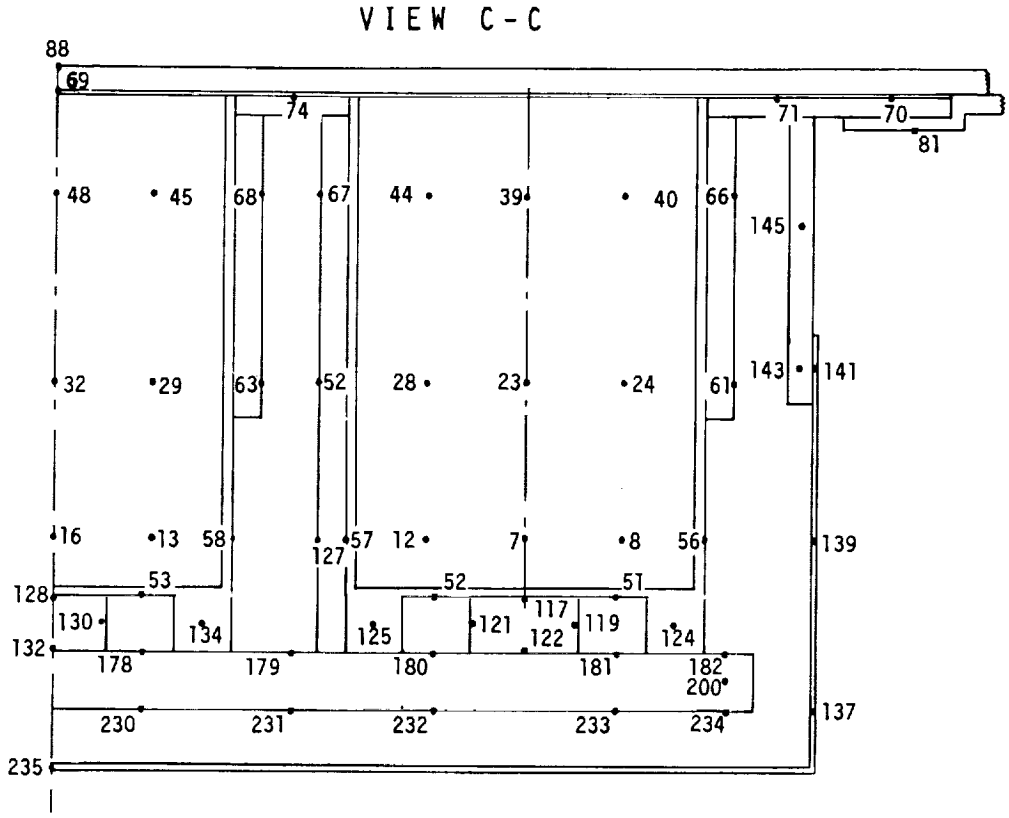

FIGURE 8 ANTENNA THERMAL MODEL NODAL DISTRIBUTION - ANTENNA CROSS-SECTION LOOKING AFT

vehicle in orbit sees the Sun is determined by the beta angle, β, and the altitude. This angle is defined as the angle between the orbit plane and the Earth/Sun line and depends on: (1) the orbit inclination angle, i, (2) the longitude of the ascending node, Ω, and (3) the time of year. From figure 10 it can be shown that the beta angle reduces to the inclination angle when the solar declination angle, δ, is zero and the ascending node angle, Ω, is 90.0, since the Sun line and the reference line then coincide. For small inclination angles, figure 10 shows part of the orbit path is shaded by the Earth. For a typical Space Shuttle Orbiter altitude of 500 km, beta angles greater than about 68.5° provide 100% of sunlight. However, as β increases the amount of thermal radiation received from the Earth decreases. Therefore, a high total flux condition is provided by an orbit in which the beta angle is near the minimum 100% Sun angle with the receiving surface normal to the Sun's rays. Conversely, a cold environment can be found in the same orbit by rotating the surface 180° such that no direct solar radiation is received.

Using the basic ground rule that any Orbiter solar inertial attitude may be maintained for up to 168 hours, a survey of the attitude and pointing timelines, contained in the Space Shuttle Baseline Reference Mission II - Options 1, 2, and 3, was conducted to find the extreme antenna environments. No appropriate maximum or minimum heating conditions were found because the frequent attitude changes in these typical missions did not allow adequate

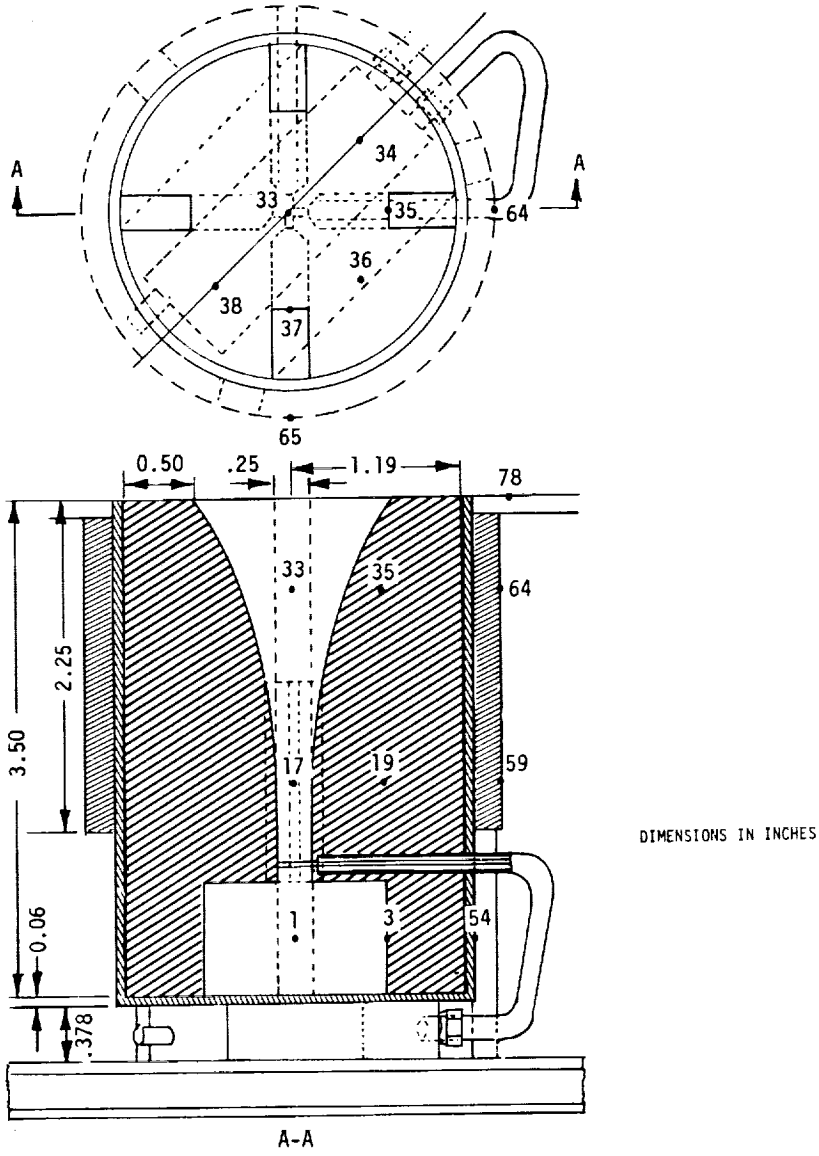

FIGURE 9 ANTENNA THERMAL MODEL - RADIATING ELEMENT NODAL DISTRIBUTION

time for complete heat soak to equilibrium. Therefore, an orbit, which met the above requirements, was chosen from Option 1. The vehicle was then rotated into the proper solar inertial attitudes to maximize or minimize the direct solar heating on the TPS surfaces over both the upper and lower antennas. In addition to these extreme cases, an orbit near the end of Option 1, in which thermal conditioning was occurring was also chosen for analysis. Table I shows the orbits and attitudes analyzed during this program. The orbital location parameters are shown in figure 10 while the local and body axis systems for the Sun oriented coordinate system are shown in figure 11.

Figure 12 shows the total absorbed heat flux histories for the hot and cold orbits (i.e., antenna heating maximized or minimized) while tables II

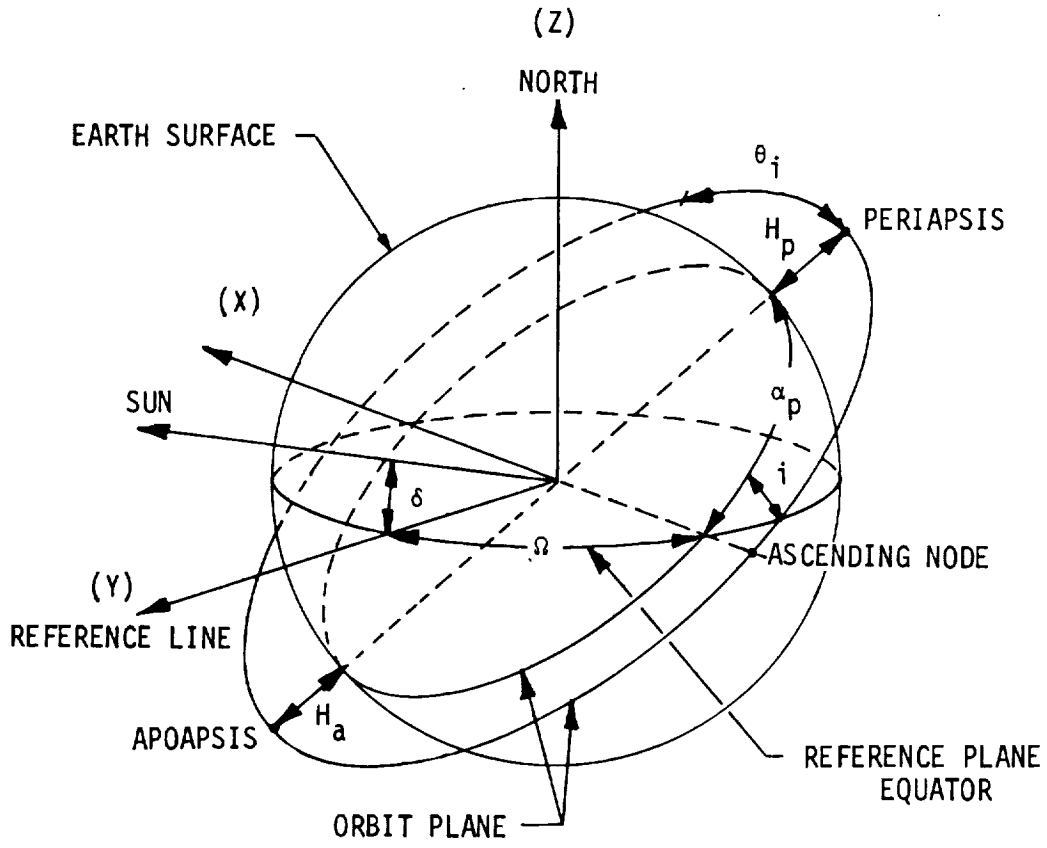

β = i when δ = 0.0 and Ω = 90.0

FIGURE 10 ELEMENTS OF ORBITAL MOTION

TABLE I

SPACECRAFT ORBITS AND ATTITUDES ANALYZED

CONDITION	OPTION 1 TIME (SEC)	β DEG	ϕ DEG	ψ DEG	ω DEG	% TIME IN SUN	COMMENTS
HOT LOWER ANTENNA	192 000	75.2	0	0	27	100	3 AXIS SOLAR INERTIAL
COLD LOWER ANTENNA	192 000	75.2	0	0	127	100	3 AXIS SOLAR INERTIAL
HOT UPPER ANTENNA	192 000	75.2	0	0	127	100	3 AXIS SOLAR INERTIAL
COLD UPPER ANTENNA	192 000	75.2	91	-3.8	75.6	100	3 AXIS SOLAR INERTIAL
THERMAL CONDITIONING	537 660	72.6	NA	0	NA	100	$\dot{\phi}$ = 0.5 DEGREE/SECOND $\dot{\omega}$ = 0.5 DEGREE/SECOND

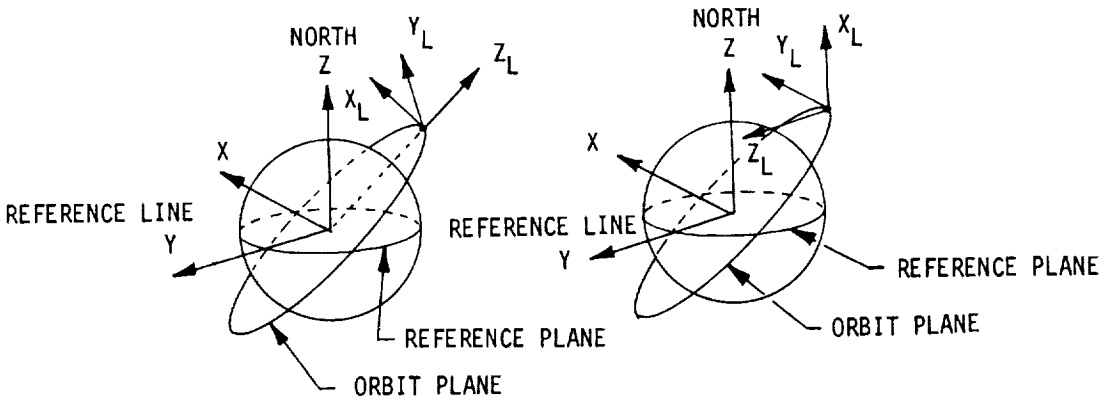

EARTH ORIENTED

X_L = ORBITAL PLANE COMPONENT IN DIRECTION OF MOTION

Y_L = PERPENDICULAR TO ORBIT PLANE (RIGHT-HANDED)

Z_L = LOCAL ZENITH (AWAY FROM EARTH)

SUN ORIENTED

X_L = PARALLEL TO NORTH POLE OF REFERENCE PLANE

Y_L = FORMS RIGHT-HANDED SET

Z_L = PARALLEL TO REFERENCE LINE

A. ORBIT LOCAL COORDINATE SYSTEM

ROTATE LOCAL COORDINATE SYSTEM INTO VEHICLE BODY AXIS SYSTEM.

ϕ : ROTATE ABOUT Z_L, $Y_L \rightarrow X_L$ IS POSITIVE

ψ : ROTATE ABOUT Y_L, $X_L \rightarrow Z_L$ IS POSITIVE

ω : ROTATE ABOUT X_L, $Y_L \rightarrow Z_L$ IS POSITIVE

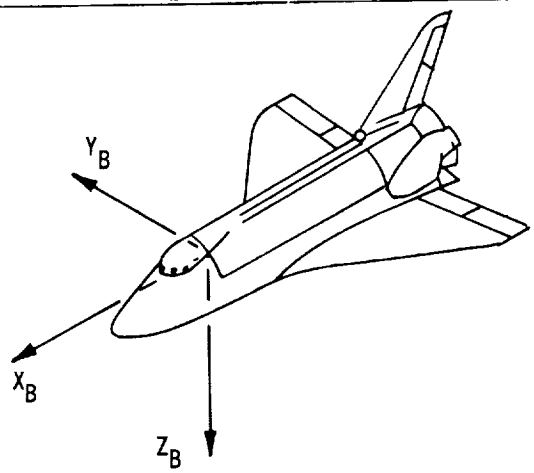

B. SPACECRAFT BODY AXIS SYSTEM

FIGURE 11 ELEMENTS OF SPACECRAFT ORBITAL ATTITUDES

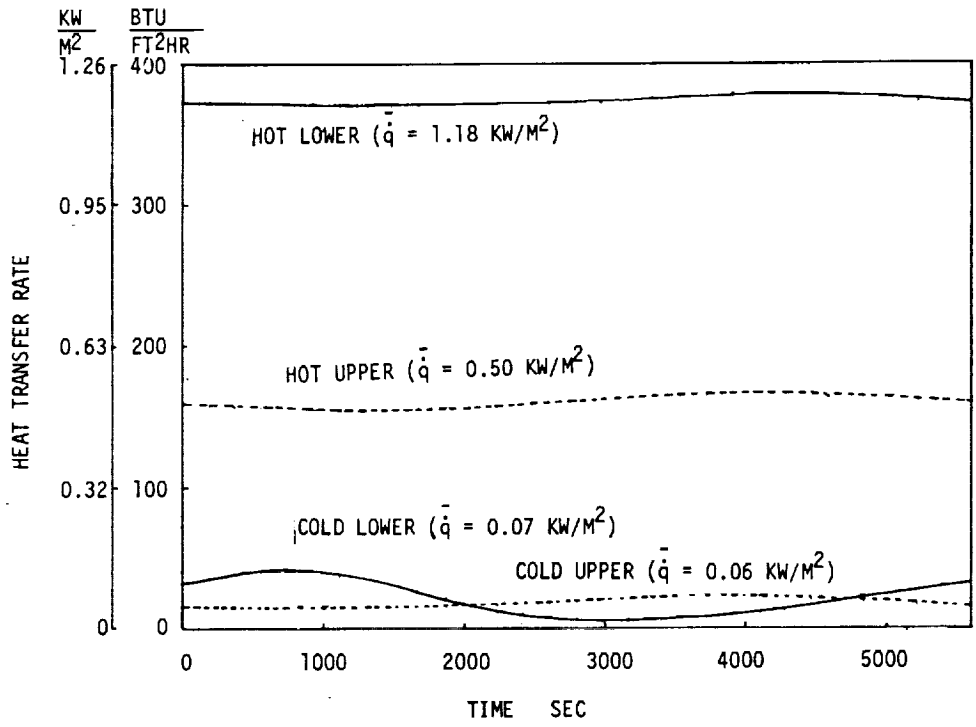

FIGURE 12 ANTENNA MAX/MIN ORBITAL ABSORBED HEATING HISTORIES

and III indicate the individual irradiation at each antenna location. The absorbed flux differs from the irradiation due to the absorptivity of the TPS surface coating. The total hemispherical emissivity of the TPS coating is 0.8. However, the solar absorptivity, α_s, of the lower antenna TPS coating is 0.8 while that of the upper is 0.32. Therefore, during the hot orbits when the principal flux is solar, a much higher percentage of the irradiation is absorbed at the lower antenna location than at the upper. For the cold orbits the solar flux at the antenna is composed only of Earth reflected radiation and its magnitude is comparable to that of the Earth emitted radiation.

Figures 13 and 14 illustrate the total absorbed flux during thermal conditioning. In contrast with the hot and cold environments, the heat rates shown in these figures are highly variable. This is due to the rotation of the spacecraft which results in the antenna surfaces facing the Sun periodically even though the entire orbit is in sunlight as shown in table I.

Exterior boundary condition during entry. - During entry the principal mode of heat transfer to the TPS surface over the antenna is convection due to aerodynamic heating. Figures 15 and 16 show the entry TPS surface and bondline temperatures for the upper and lower locations specified for this program by NASA. (Note that the TPS bondline is between the SIP and skin. Later reference will be made to an RSI bondline which is between the RSI and the SIP.) Figure 17 indicates the corresponding TPS pressures during the deorbit trajectory. These temperatures were determined by applying a local heating rate to a one-dimensional model of the vehicle TPS and skin, as shown on

TABLE II

LOWER ANTENNA MAX/MIN INCIDENT HEAT FLUX

HOT LOWER ANTENNA (+Y); (ϕ, ψ, ω) = (0.0, 0.0, 27.0)

TIME	SOLAR	ALBEDO	PLANET	SUMMED FLUX
AVERAGES----	.44091E+03	.36775E+01	.21954E+02	.46654E+03
.19200E+06	.44091E+03	.35099E+01	.20994E+02	.46541E+03
.19219E+06	.44091E+03	.50618E+01	.19277E+02	.46525E+03
.19237E+06	.44091E+03	.62401E+01	.17694E+02	.46484E+03
.19256E+06	.44091E+03	.70538E+01	.16251E+02	.46422E+03
.19275E+06	.44091E+03	.75671E+01	.15049E+02	.46353E+03
.19293E+06	.44091E+03	.78501E+01	.14112E+02	.46287E+03
.19312E+06	.44091E+03	.79771E+01	.13471E+02	.46236E+03
.19331E+06	.44091E+03	.80202E+01	.13173E+02	.46210E+03
.19349E+06	.44091E+03	.80208E+01	.13253E+02	.46218E+03
.19368E+06	.44091E+03	.79692E+01	.13702E+02	.46258E+03
.19387E+06	.44091E+03	.78078E+01	.14477E+02	.46320E+03
.19405E+06	.44091E+03	.74590E+01	.15531E+02	.46390E+03
.19424E+06	.44091E+03	.68532E+01	.16852E+02	.46462E+03
.19442E+06	.44091E+03	.59155E+01	.18384E+02	.46521E+03
.19461E+06	.44091E+03	.45951E+01	.20004E+02	.46551E+03
.19480E+06	.44091E+03	.29077E+01	.21829E+02	.46565E+03
.19498E+06	.44091E+03	.13355E+01	.23886E+02	.46613E+03
.19517E+06	.44091E+03	.56049E+00	.25874E+02	.46734E+03
.19535E+06	.44091E+03	.23108E+00	.27641E+02	.46878E+03
.19554E+06	.44091E+03	.94827E-01	.29153E+02	.47016E+03
.19573E+06	.44091E+03	.41820E-01	.30316E+02	.47127E+03
.19591E+06	.44091E+03	.22567E-01	.31065E+02	.47200E+03
.19610E+06	.44091E+03	.17525E-01	.31388E+02	.47232E+03
.19628E+06	.44091E+03	.18694E-01	.31294E+02	.47222E+03
.19647E+06	.44091E+03	.26506E-01	.30782E+02	.47172E+03
.19666E+06	.44091E+03	.59193E-01	.29848E+02	.47082E+03
.19684E+06	.44091E+03	.13544E+00	.28522E+02	.46957E+03
.19703E+06	.44091E+03	.32438E+00	.26892E+02	.46813E+03
.19722E+06	.44091E+03	.77069E+00	.25035E+02	.46672E+03
.19740E+06	.44091E+03	.18221E+01	.22977E+02	.46571E+03
.19759E+05	.44091E+03	.35099E+01	.20994E+02	.46541E+03

COLD LOWER ANTENNA (-Y); (ϕ, ψ, ω) = (0.0, 0.0, 127.0)

TIME	SOLAR	ALBEDO	PLANET	SUMMED FLUX
AVERAGES----	0.	.27495E+01	.23263E+02	.26012E+02
.19200E+06	0.	.18844E+00	.40001E+02	.40189E+02
.19219E+06	0.	.18324E+01	.41580E+02	.43413E+02
.19237E+06	0.	.46652E+01	.42170E+02	.46835E+02
.19256E+06	0.	.76011E+01	.41850E+02	.49451E+02
.19275E+06	0.	.93260E+01	.40580E+02	.50506E+02
.19293E+06	0.	.11219E+02	.38329E+02	.49548E+02
.19312E+06	0.	.11332E+02	.35199E+02	.46532E+02
.19331E+06	0.	.10412E+02	.31522E+02	.41934E+02
.19349E+06	0.	.89097E+01	.27957E+02	.36866E+02
.19368E+06	0.	.69676E+01	.24315E+02	.31283E+02
.19387E+06	0.	.48751E+01	.20692E+02	.25567E+02
.19405E+06	0.	.28774E+01	.17133E+02	.20011E+02
.19424E+06	0.	.12765E+01	.13918E+02	.15194E+02
.19442E+06	0.	.31190E+00	.11548E+02	.11860E+02
.19461E+06	0.	.48703E-02	.98728E+01	.98777E+01
.19480E+06	0.	0.	.85145E+01	.85145E+01
.19498E+06	0.	0.	.76353E+01	.76353E+01
.19517E+06	0.	0.	.72417E+01	.72417E+01
.19535E+06	0.	0.	.74578E+01	.74578E+01
.19554E+06	0.	0.	.82264E+01	.82264E+01
.19573E+06	0.	0.	.94323E+01	.94323E+01
.19591E+06	0.	0.	.11013E+02	.11013E+02
.19610E+06	0.	0.	.13123E+02	.13123E+02
.19628E+06	0.	0.	.16144E+02	.16144E+02
.19647E+06	0.	0.	.19599E+02	.19599E+02
.19666E+06	0.	0.	.23278E+02	.23278E+02
.19684E+06	0.	0.	.26911E+02	.26911E+02
.19703E+06	0.	0.	.30462E+02	.30462E+02
.19722E+06	0.	0.	.34143E+02	.34143E+02
.19740E+06	0.	0.	.37516E+02	.37516E+02
.19759E+05	0.	.18844E+00	.40001E+02	.40189E+02

TABLE III

UPPER ANTENNA MAX/MIN INCIDENT HEAT FLUX

HOT UPPER ANTENNA (+Y); (ϕ, ψ, ω) = (0.0, 0.0, 127.0)

TIME	SOLAR	ALBEDO	PLANET	SUMMED FLUX
AVERAGES----	.44091E+03	.36775E+01	.21954E+02	.46654E+03
.19200E+06	.44091E+03	.35116E+01	.21012E+02	.46543E+03
.19219E+06	.44091E+03	.50650E+01	.19293E+02	.46577E+03
.19237E+06	.44091E+03	.62444E+01	.17709E+02	.46486E+03
.19256E+06	.44091E+03	.70587E+01	.16264E+02	.46423E+03
.19275E+06	.44091E+03	.75717E+01	.15059E+02	.46354E+03
.19293E+06	.44091E+03	.78540E+01	.14120E+02	.46288E+03
.19312E+06	.44091E+03	.79796E+01	.13476E+02	.46237E+03
.19331E+06	.44091E+03	.80209E+01	.13175E+02	.46211E+03
.19349E+06	.44091E+03	.80196E+01	.13250E+02	.46218E+03
.19368E+06	.44091E+03	.79661E+01	.13696E+02	.46257E+03
.19387E+06	.44091E+03	.78036E+01	.14468E+02	.46318E+03
.19405E+06	.44091E+03	.74542E+01	.15520E+02	.46388E+03
.19424E+06	.44091E+03	.68484E+01	.16838E+02	.46460E+03
.19442E+06	.44091E+03	.59115E+01	.18369E+02	.46519E+03
.19461E+06	.44091E+03	.45924E+01	.19988E+02	.46549E+03
.19480E+06	.44091E+03	.29065E+01	.21810E+02	.46563E+03
.19498E+06	.44091E+03	.13352E+01	.23865E+02	.46611E+03
.19517E+06	.44091E+03	.56040E+00	.25855E+02	.46733E+03
.19535E+06	.44091E+03	.23106E+00	.27625E+02	.46877E+03
.19554E+06	.44091E+03	.94821E-01	.29140E+02	.47014E+03
.19573E+06	.44091E+03	.41818E-01	.30306E+02	.47126E+03
.19591E+06	.44091E+03	.22566E-01	.31060E+02	.47199E+03
.19610E+06	.44091E+03	.17525E-01	.31387E+02	.47231E+03
.19628E+06	.44091E+03	.18694E-01	.31296E+02	.47223E+03
.19647E+06	.44091E+03	.26507E-01	.30789E+02	.47173E+03
.19666E+06	.44091E+03	.59196E-01	.29859E+02	.47083E+03
.19684E+06	.44091E+03	.13545E+00	.28536E+02	.46958E+03
.19703E+06	.44091E+03	.32442E+00	.26909E+02	.46814E+03
.19722E+06	.44091E+03	.77083E+00	.25054E+02	.46674E+03
.19740E+06	.44091E+03	.18226E+01	.22997E+02	.46573E+03
.19759E+06	.44091E+03	.35116E+01	.21012E+02	.46543E+03

COLD UPPER ANTENNA (-Y); (ϕ, ψ, ω) = (9.10, -3.8, 75.6)

TIME	SOLAR	ALBEDO	PLANET	SUMMED FLUX
AVERAGES----	0.	.13590E+01	.21899E+02	.23258E+02
.19200E+06	0.	.25184E-01	.19601E+02	.19626E+02
.19219E+06	0.	.36889E+00	.18694E+02	.19063E+02
.19237E+06	0.	.11860E+01	.17916E+02	.19102E+02
.19256E+06	0.	.21491E+01	.17339E+02	.19488E+02
.19275E+06	0.	.30467E+01	.16948E+02	.19995E+02
.19293E+06	0.	.37884E+01	.16754E+02	.20543E+02
.19312E+06	0.	.43384E+01	.16762E+02	.21101E+02
.19331E+06	0.	.46785E+01	.16973E+02	.21651E+02
.19349E+06	0.	.47856E+01	.17384E+02	.22170E+02
.19368E+06	0.	.46334E+01	.17988E+02	.22621E+02
.19387E+06	0.	.41991E+01	.18764E+02	.22963E+02
.19405E+06	0.	.34607E+01	.19689E+02	.23149E+02
.19424E+06	0.	.24469E+01	.20715E+02	.23162E+02
.19442E+06	0.	.12857E+01	.21806E+02	.23092E+02
.19461E+06	0.	.35420E+00	.22914E+02	.23269E+02
.19480E+06	0.	.17469E-03	.24012E+02	.24013E+02
.19498E+06	0.	0.	.25024E+02	.25024E+02
.19517E+06	0.	0.	.25888E+02	.25888E+02
.19535E+06	0.	0.	.26600E+02	.26600E+02
.19554E+06	0.	0.	.27100E+02	.27100E+02
.19573E+06	0.	0.	.27351E+02	.27351E+02
.19591E+06	0.	0.	.27340E+02	.27340E+02
.19610E+06	0.	0.	.27069E+02	.27069E+02
.19628E+06	0.	0.	.26557E+02	.26557E+02
.19647E+06	0.	0.	.25838E+02	.25838E+02
.19666E+06	0.	0.	.24948E+02	.24948E+02
.19684E+06	0.	0.	.23935E+02	.23935E+02
.19703E+06	0.	0.	.22839E+02	.22839E+02
.19722E+06	0.	0.	.21716E+02	.21716E+02
.19740E+06	0.	0.	.20613E+02	.20613E+02
.19759E+06	0.	.25184E-01	.19601E+02	.19626E+02

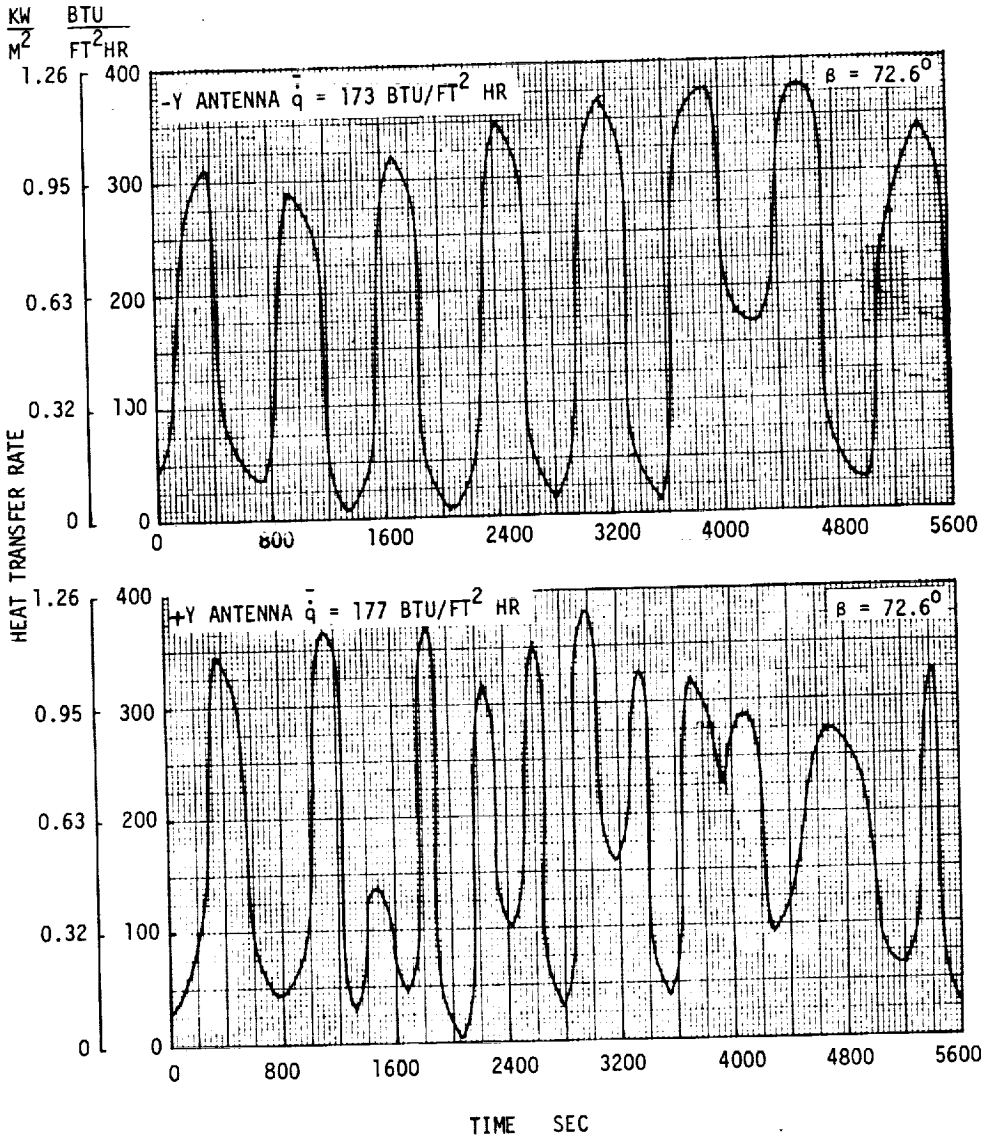

FIGURE 13 LOWER ANTENNA TOTAL ABSORBED HEATING DURING THERMAL CONDITIONING

figures 15 and 16 for a specified RSI thickness such that a maximum bondline temperature of 177°C (350°F) was attained. This type of analysis neglects heat leaks to the skin structural support and the effects of the interface with the vehicle interior. Consequently, the calculated bondline temperatures are higher than would be actually realized in the spacecraft.

The temperatures given on these curves correspond to those at locations where the RSI thicknesses are 8.23 cm (3.24 in.) and 0.84 cm (0.33 in.) for the lower and upper surfaces, respectively. The actual RSI thicknesses above the lower and upper array antennas are 3.99 cm (1.57 in.) and 0.61 cm (0.24 in.), respectively. These values correspond to TPS thicknesses of 4.45 cm (1.75 in.) and 1.07 cm (0.42 in.). Because of the differences in

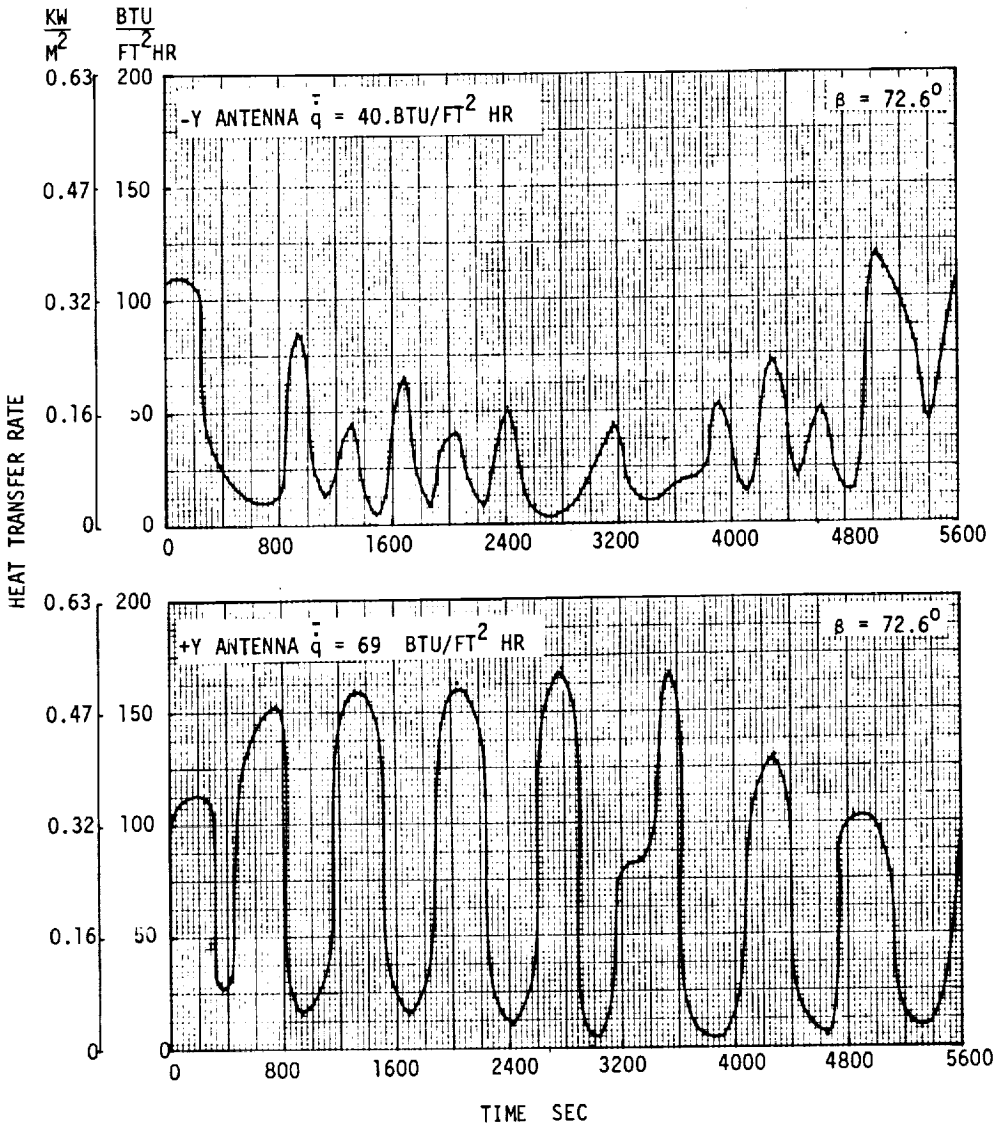

FIGURE 14 UPPER ANTENNA TOTAL ABSORBED HEATING DURING THERMAL CONDITIONING

insulation thickness use of the surface temperatures shown in figures 15 and 16 would yield bondline temperatures considerably in excess of 177°C (350°F). Therefore, it was necessary to scale the local heat transfer rates.

A one dimensional model, similar to that discussed above, was constructed and the surface temperatures shown in figures 15 and 16 were input into an inverse heat transfer program using the 8.23 cm (3.24 in.) and 0.84 cm (0.33 in.) RSI thicknesses. The resultant bondline temperature histories compared very well with those specified by NASA indicating that the NASA and MDAC-E models were equivalent. This program also supplies the convective heating rates corresponding to the impressed surface temperatures.

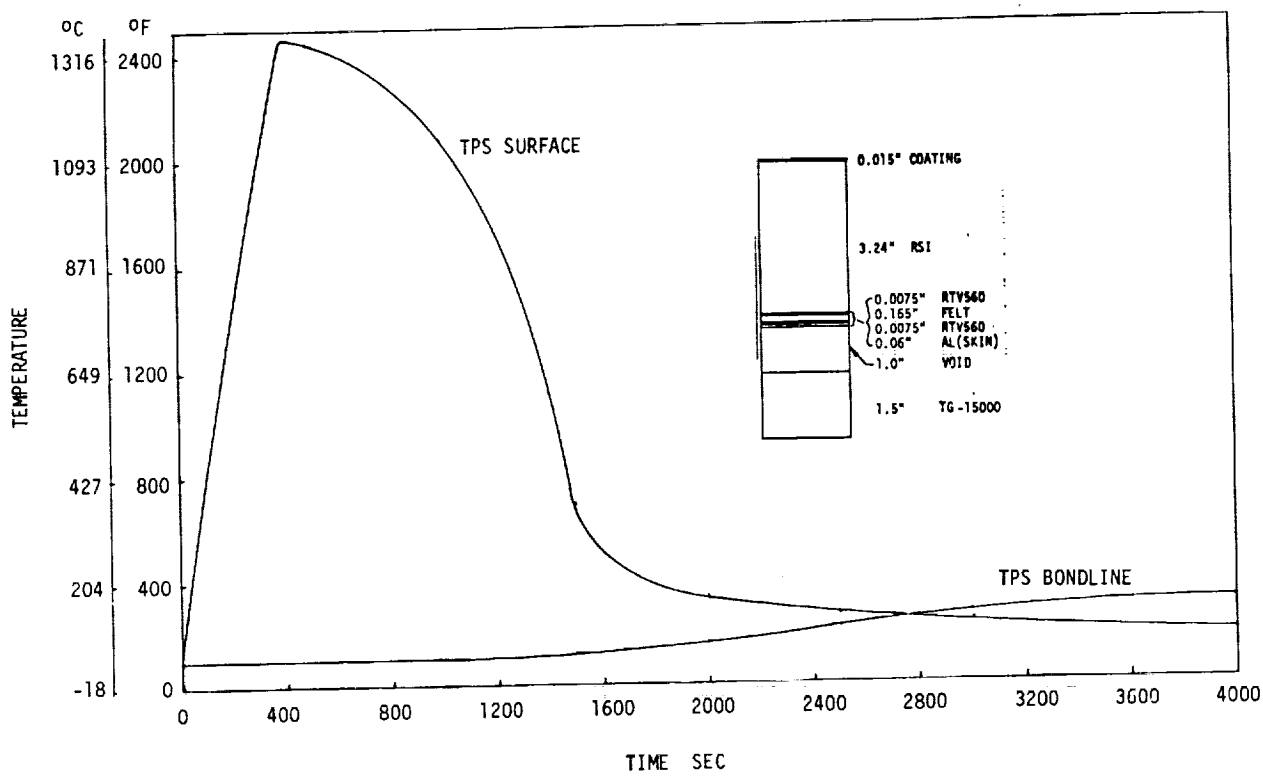

FIGURE 15 LOWER ANTENNA REGION TPS TEMPERATURES DURING ENTRY

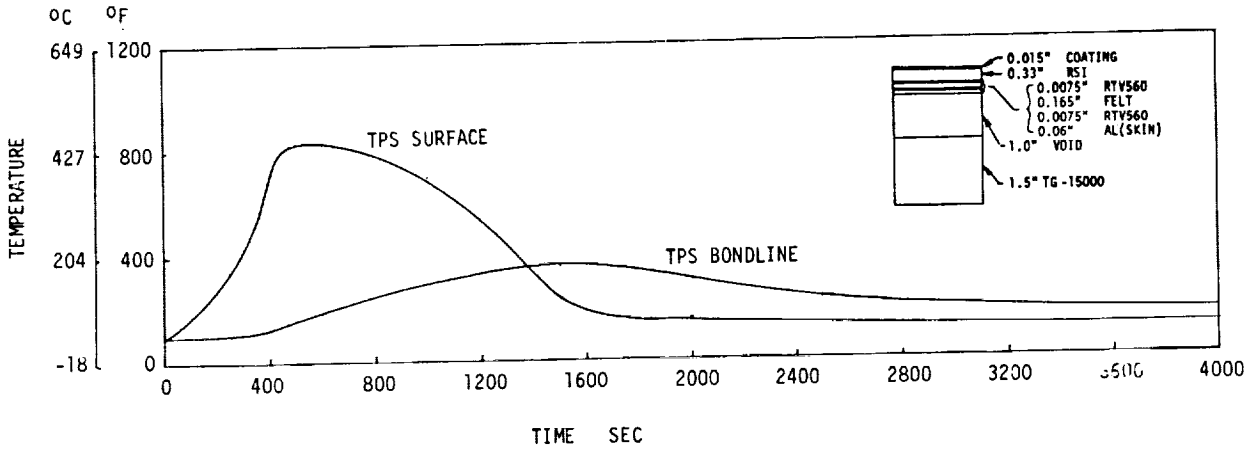

FIGURE 16 UPPER ANTENNA REGION TPS TEMPERATURES DURING ENTRY

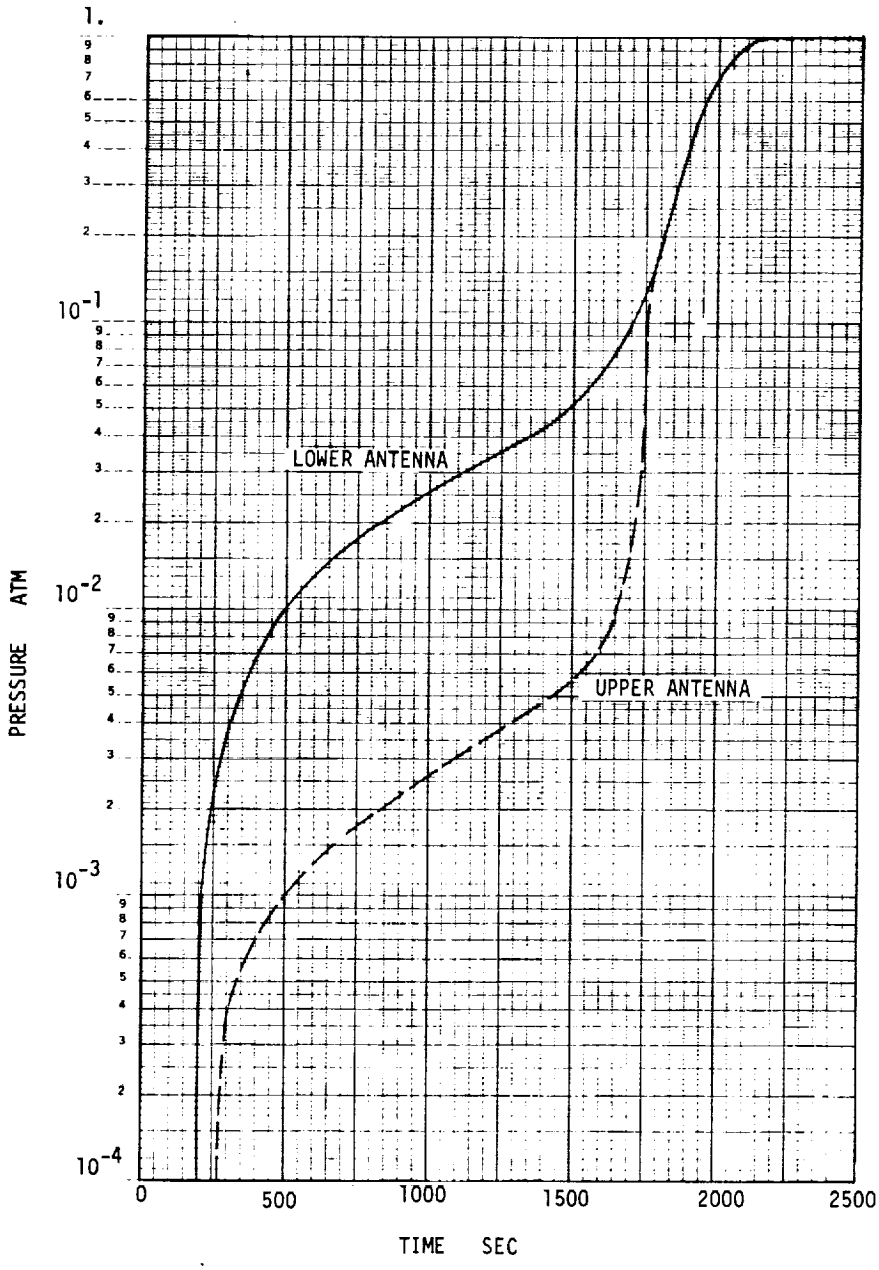

FIGURE 17 ANTENNA TPS SURFACE PRESSURE DURING ENTRY

The maximum heat fluxes for the upper and lower arrays were 13.13 and 316.13 kW/m^2 (4160 and 100 200 BTU/ft^2 hr), respectively during the trajectory. The RSI thicknesses were then changed to the actual values and the one dimensional model was run using a parametric application of a constant scale factor on the heating histories. This analysis indicated that heat transfer multipliers of 0.86 and 0.25 were required to maintain maximum TPS bondline temperatures at 177°C (350°F) for the upper and lower antenna locations, respectively. The calculated heating histories are shown in figure 18 and were used for all of the entry thermal analyses during this program.

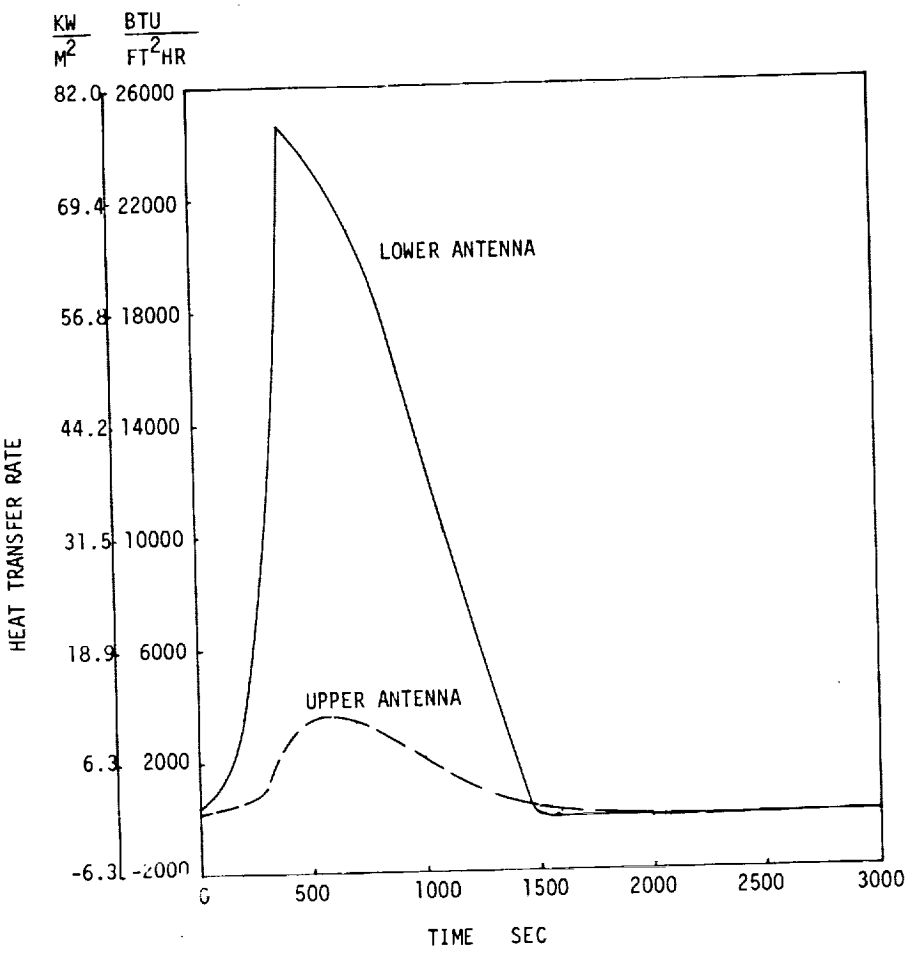

FIGURE 18 CALCULATED ANTENNA REGION TPS SURFACE CONVECTIVE HEAT TRANSFER RATES DURING ENTRY

The majority of the aerodynamic heat convection is reradiated by the TPS surface to space and to the atmosphere during entry. Prior to 1700 sec the antenna radiated to the space environment and the assumed sink temperature was 1.7 K (3°R). After this time when the vehicle is in the lower atmosphere a sink temperature of 300 K (540°R) was used.

Thermal Response

The boundary conditions and heat inputs discussed in the previous section were used as inputs to determine the transient thermal response of the antenna in orbit and during entry.

Orbital temperatures. - The response of the antenna to variations in the external surface heat flux is slow in orbital flight, due to the large mass

of the antenna, the TPS thickness and the isothermal spacecraft interior boundary condition. Therefore, large temperature gradients in the antenna during orbital flight are amsll.

The maximum and minimum orbital temperatures of the antenna components and their surroundings were calculated using the ANTENA thermal model with the extreme heating conditions shown on figure 12. The antenna was soaked at these conditions until the equilibrium temperatures were attained. The equilibrium temperatures for various antenna and TPS components are tabulated in table IV for the hot and cold extremes at both upper and lower antenna locations. Although the TPS surface temperature over the lower antenna varied between -66 and 128°C (-86 and 262°F) the calculated extremes within the antenna are only -24 and 82°C (-12 and 180°F). The corresponding TPS bondline temperatures are -25 and 82°C (-13 and 180°F). The limits of the antenna temperature are approximately equal to the TPS bondline limits. The TPS surface temperature range over the upper antenna is -89 to 53°C (-102 to 128°F) while the antenna temperature range is -57 to 47°C (-70 to 117°F). The upper antenna is more responsive to the absorbed heat than the lower because of the thinner TPS. However, as was explained in this section under Thermal Model, the fraction of the irradiation absorbed is smaller for the upper TPS due to its lower solar absorptivity.

Figures 19 thru 22 show the orbital temperature histories of the TPS and internal insulation at the upper and lower antenna locations in the extreme hot and cold environments. From an initial temperature of 38°C (100°F) about eight orbits are required to reach equilibrium at the lower antenna in the hot environment and about fourteen in the cold environment. By comparison, about five orbits are required to reach equilibrium at the upper antenna for both hot and cold conditions. The cabin wall temperature was assumed to be 33°C (92°F) in all four of these analyses. Except for the outer portion of the TPS, very little temperature change occurs during an individual orbit in any component of the antenna. Therefore, the antenna temperature variations are not illustrated. However, the antenna temperatures calculated in these analyses were close to or between the values in figures 19 thru 22 labeled TPS bondline and TG-15000.

To assess the impact of the interior isothermal wall boundary condition on the antenna temperature, two cases were analyzed with hot and cold cabin walls. The first case consisted of the upper antenna in the cold orbit with a 17°C (62°F) wall and the second of the lower antenna in the hot orbit with a 50°C (122°F) wall. Table V summarizes these results. At the upper antenna, lowering the cabin temperature changed the antenna temperature from -56 to -63°C (-70 to -82°F). At the lower antenna, the increase in cabin temperature resulted in an increase of the antenna equilibrium temperature of 8°C (14°F) to 89°C (193°F). Comparison of the equilibrium temperatures shown on tables IV and V shows that the interior boundary condition significantly affects the antenna temperature.

Another parameter which can change the antenna temperature is the power dissipated in the radiating elements by operation. To evaluate this effect an input power of fifty watts and an 85% element efficiency were assumed. Thus, 7.5 watts were dissipated in the radiating elements. To maximize the effect

TABLE IV

ANTENNA AND TPS TEMPERATURES
FOR HOT AND COLD ORBITAL ENVIRONMENTS

	UPPER ANTENNA		LOWER ANTENNA	
LOCATION	HOT	COLD	HOT	COLD
TPS SURFACE	128.	-102.	262.	-86.
RSI BONDLINE	124.	-96.	197.	-82.
TPS BONDLINE	118.	-70.	180.	-13.
TG-15000, OUTBOARD	116.	-47.	174.	-1.
ANTENNA COMPONENTS				
DUST COVER, SIDE	117.	-69.	179.	-12.
DUST COVER, BOTTOM	117.	-68.	178.	-11.
MOUNTING FLANGE	117.	-70.	179.	-12.
RADIATING ELEMENT WALL	117.	-70.	179.	-12.
RADIATING ELEMENT INSULATION	117.	-70.	179.	-12.
RADIATING ELEMENT RIDGES	117.	-70.	179.	-12.
CIRCUIT BOARD, OUTBOARD	117.	-70.	179.	-12.
CIRCUIT BOARD, INBOARD	117.	-70.	179.	-12.

1. TEMPERATURES IN °F
2. ANTENNA NOT TRANSMITTING
3. CABIN WALL TEMPERATURE, 92°F
4. VEHICLE ORIENTATION PER TABLE I.

of this heating, and since most of the power is fed to the center element, it was assumed that all of this energy was concentrated in the center element, evenly divided among the four ridges. Table VI shows the antenna equilibrium temperatures for continuous antenna operation in the cold upper and hot lower environments. Antenna operation results in a temperature increase of about 11°C (20°F) in each case. However, even with this internal heating, no large temperature gradients occur.

Temperatures of the upper and lower antennas during orbital thermal conditioning were also calculated. For these cases, the heating rates shown on figures 13 and 14 were impressed on the TPS surface and the cabin wall was assumed to be 33°C (92°F). Figure 23 shows the orbital variation of the equilibrium temperature of the lower RSI bondline and the antenna center element for the 559 W/m^2 (117 BTU/hr ft^2) heating case. Although the outer TPS temperatures vary considerably during the conditioning orbit, the antenna temperature level is essentially constant. The larger temperature variation at the upper antenna location is due to the thinner RSI. Table VII shows the corresponding maximum and minimum temperatures of the antenna components and TPS during orbital thermal conditioning. The lower antenna temperature is constant at 48°C (119°F) while the upper antenna temperature varies less than ± 1°C (± 2°F) from 3°C (37°F).

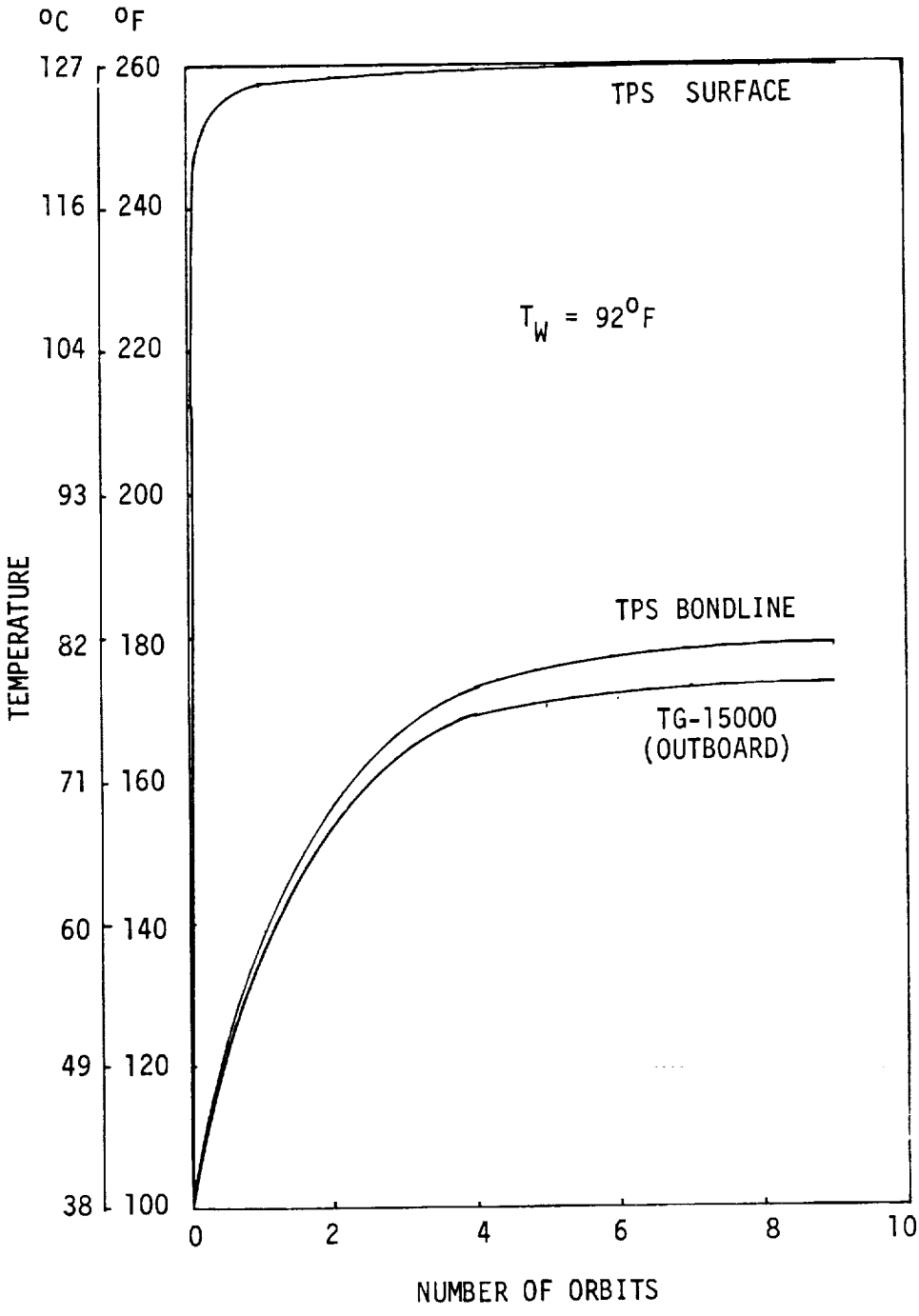

FIGURE 19 LOWER ANTENNA THERMAL RESPONSE - HOT ORBIT

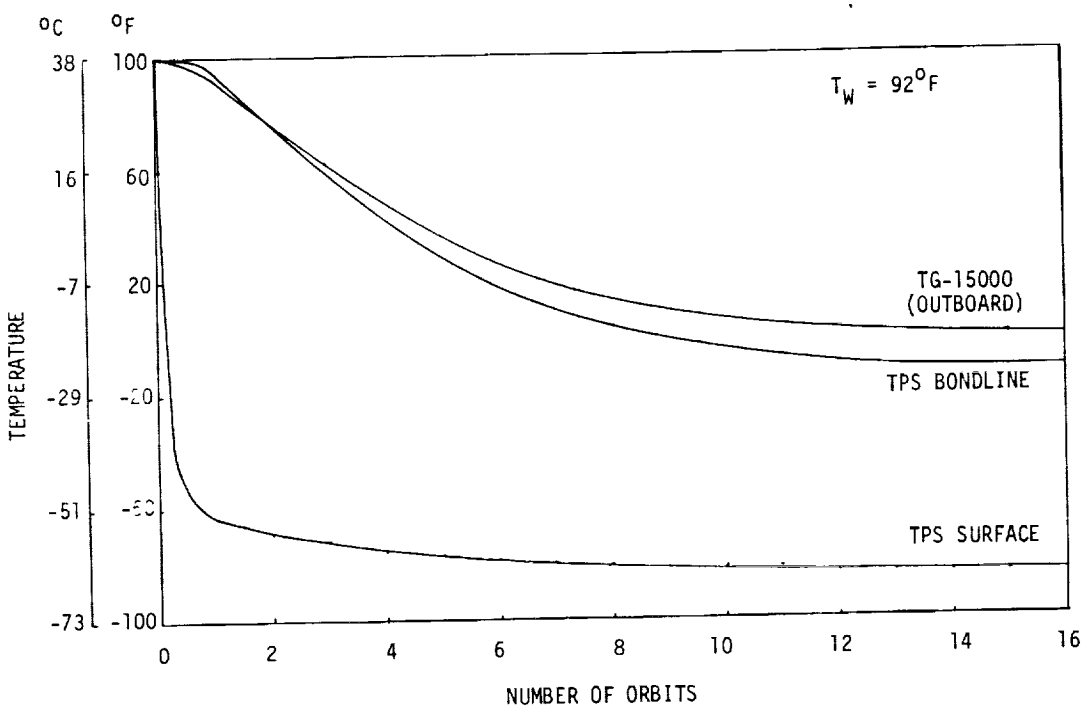

FIGURE 20 LOWER ANTENNA THERMAL RESPONSE - COLD ORBIT

Entry temperatures. - The TPS pressure and heat flux histories shown in figures 17 and 18 were used to determine the entry thermal response of the antenna. Four sets of initial conditions were used: the hot and cold orbital equilibrium temperatures for the upper and lower antennas as shown on table IV. The cabin wall temperature used for these calculations was 33°C (92°F).

Although entry from these extreme temperature environments is not contemplated, these analyses yield the maximum antenna temperature range. Entry from any other environment, such as that following the thermal conditioning orbit, will result in temperatures between these limits.

Table VIII presents the maximum temperature of each of the upper and lower antenna components following entry from the hot environment. These temperatures should be the maximum temperatures of the antennas for this trajectory. The maximum TPS bondline temperatures of the upper and lower antennas are 124 and 144°C (256 and 292°F), respectively. The maximum temperatures reached within the antenna are 100 and 128°C (212 and 262°F), respectively. The TPS bondline temperatures are less than the 177°C (350°F) maximum allowable due to structural heat leaks as was explained previously.

Figures 24 and 25 are the TPS temperature histories over the lower antenna during entry from the hot and cold environments. The initial temperature has little effect on the TPS surface temperature. However, the TPS bondline temperatures differ by about 69°C (125°F) after 4000 seconds. Due to heat soak effects, the maximum temperature occurs later in the trajectory for components farther from the surface. Therefore, the temperatures shown on

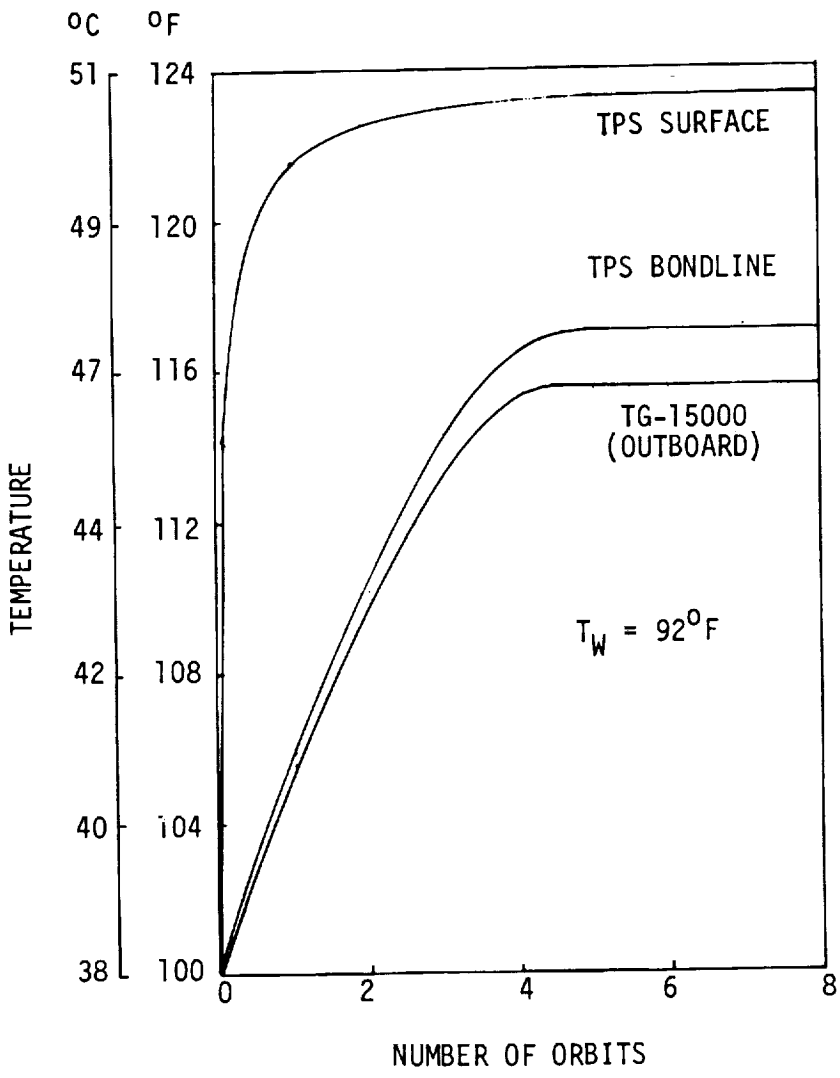

FIGURE 21 UPPER ANTENNA THERMAL RESPONSE - HOT ORBIT

table VIII are not concurrent. Also, due to the heat sink effect of the antenna the temperatures of the skin and TPS are not uniform laterally as shown by figure 26. Temperatures are shown at three locations on the RSI bondline for the initial cold and hot temperatures of the lower antenna. These locations are directly above the antenna and 28 and 58 cm (11 and 23 in.) from the antenna center (below nodes 324, 319 and 314 shown in figure 5). These locations were also selected for thermocouple, (T/C), installation in the thermal test fixture discussed later in this report. Due to the heat capacity of the antenna, the TPS temperature increases with distance from it. This variation is further illustrated on figure 27 in which isotherms on the RSI bondline surface are shown at the time of maximum RSI bondline temperature. The temperature increases with distance from the antenna but the rate of increase decreases with distance such that no effect of the antenna is found at large distances. The distortion of the isotherms from a circular shape is due to the

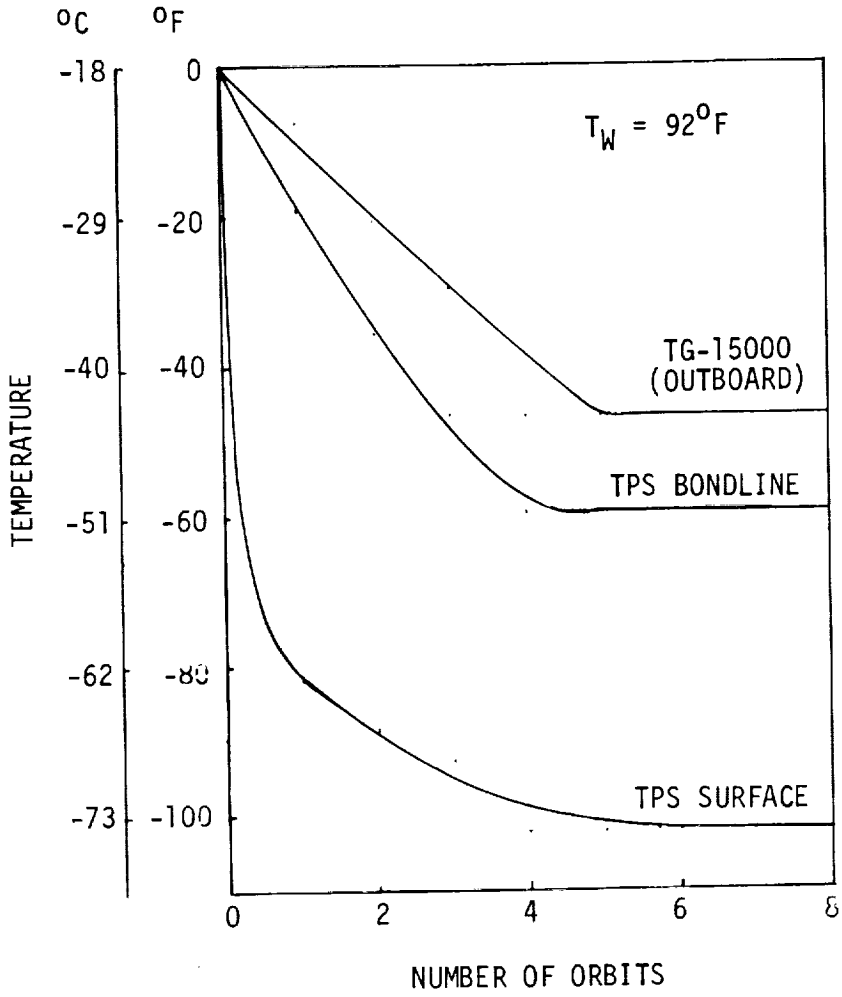

FIGURE 22 UPPER ANTENNA THERMAL RESPONSE - COLD ORBIT

preferential conduction path in the fore-and-aft direction as a result of the skin support stringers. Therefore the temperature gradient is smaller in the forward direction than it is laterally.

Figures 28 and 29 are the TPS temperature histories over the upper antenna during entry from the hot and cold environments. These temperatures are lower than those over the lower antenna but the response time of the interior of the TPS is shorter because of the thinner RSI. Also the effect of initial temperature is smaller because of the thinner RSI. The difference in the TPS bondline temperatures at 4000 sec is only about 33°C (60°F). Figures 30 and 31 show the time variation in temperature of three RSI bondline locations during entry while figure 27 shows the isotherms at the time of maximum temperature. The behavior of this surface is similar to that for the lower antenna bondline.

Figure 32 shows the temperature response inside the upper and lower antennas due to the entry heat flux for the different hot and cold initial conditions. These temperatures correspond to a location in the center of the

TABLE V

ANTENNA AND TPS TEMPERATURES WITH HOT AND COLD CABIN WALL

LOCATION	UPPER ANTENNA CABIN WALL = 62°F COLD ORBIT	LOWER ANTENNA CABIN WALL = 122°F HOT ORBIT
TPS SURFACE	-112.	263.
RSI BONDLINE	-95.	201.
TPS BONDLINE	-82.	193.
TG-15000, OUTBOARD	-62.	189.
ANTENNA COMPONENTS		
DUST COVER, SIDE	-81.	193.
DUST COVER, BOTTOM	-80.	192.
MOUNTING FLANGE	-82.	193.
RADIATING ELEMENT WALL	-82.	193.
RADIATING ELEMENT INSULATION	-82.	193.
RADIATING ELEMENT RIDGES	-82.	193.
CIRCUIT BOARD, OUTBOARD	-82.	193.
CIRCUIT BOARD, INBOARD	-82.	193.

1. TEMPERATURE IN °F
2. ANTENNA NOT TRANSMITTING
3. VEHICLE ORIENTATION PER TABLE I

TABLE VI

ANTENNA AND TPS TEMPERATURES WITH ANTENNA OPERATING

LOCATION	UPPER ANTENNA COLD ORBIT	LOWER ANTENNA HOT ORBIT
TPS SURFACE	-102.	263.
RSI BONDLINE	-76.	202.
TPS BONDLINE	-56.	198.
TG-15000, OUTBOARD	-37.	190.
ANTENNA COMPONENTS		
DUST COVER, SIDE	-54.	200.
DUST COVER, BOTTOM	-53.	196.
MOUNTING FLANGE	-54.	198.
RADIATING ELEMENT WALL	-51.	200.
RADIATING ELEMENT DIELECTRIC	-50.	200.
RADIATING ELEMENT RIDGES	-50.	200.
CIRCUIT BOARD, OUTBOARD	-53.	199.
CIRCUIT BOARD, INBOARD	-53.	198.

1. TEMPERATURES IN °F
2. CABIN WALL TEMPERATURE, 92°F
3. VEHICLE ORIENTATION PER TABLE I
4. POWER DISSIPATION = 1.875 WATT/RIDGE IN CENTER ELEMENT

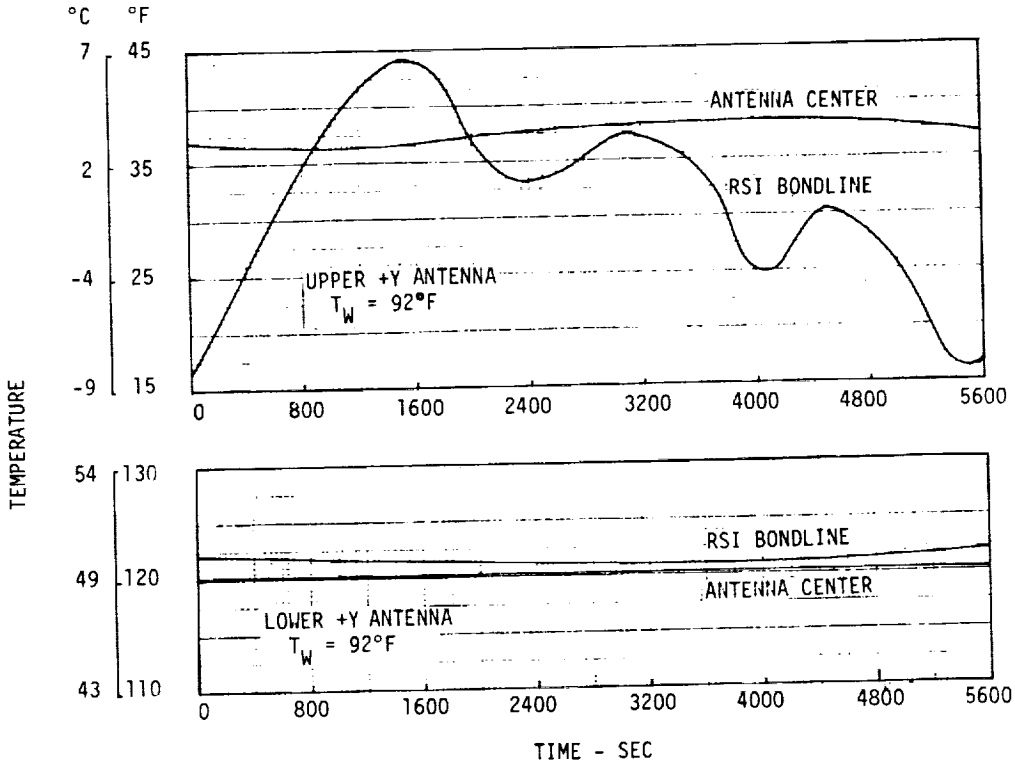

FIGURE 23 ANTENNA TEMPERATURES DURING ORBITAL THERMAL CONDITIONING

TABLE VII
ANTENNA AND TPS TEMPERATURES
DURING ORBITAL THERMAL CONDITIONING

	UPPER ANTENNA		LOWER ANTENNA	
LOCATION	MAX	MIN	MAX	MIN
TPS SURFACE	78.	-31.	198.	80.
RSI BONDLINE	45.	16.	123.	121.
TPS BONDLINE	38.	35.	119.	119.
TG-15000, OUTBOARD	43.	40.	118.	117.
ANTENNA COMPONENTS				
DUST COVER, SIDE	38.	36.	119.	118.
DUST COVER, BOTTOM	38.	36.	119.	119.
MOUNTING FLANGE	38.	36.	119.	119.
RADIATING ELEMENT WALL	38.	36.	119.	119.
RADIATING ELEMENT INSULATION	38.	36.	119.	119.
RADIATING ELEMENT RIDGES	38.	36.	119.	119.
CIRCUIT BOARD, OUTBOARD	38.	36.	119.	119.
CIRCUIT BOARD, INBOARD	38.	36.	119.	119.

1. TEMPERATURES IN °F
2. CABIN WALL TEMPERATURE, 92°F
3. LOWER +Y ANTENNA
   UPPER +Y ANTENNA
4. VEHICLE ATTITUDE PER TABLE I

TABLE VIII

ANTENNA AND TPS MAXIMUM ENTRY TEMPERATURES

LOCATION	UPPER ANTENNA	LOWER ANTENNA
TPS SURFACE	772.	1594.
RSI BONDLINE	389.	335.
TPS BONDLINE	256.	292.
TG-15000, OUTBOARD	225.	246.
ANTENNA COMPONENTS		
DUST COVER, SIDE	210.	261.
DUST COVER, BOTTOM	210.	257.
MOUNTING FLANGE	212.	262.
RADIATING ELEMENT WALL	206.	261.
RADIATING ELEMENT INSULATION	206.	261.
RADIATING ELEMENT RIDGES	206.	261.
CIRCUIT BOARD, OUTBOARD	206.	261.
CIRCUIT BOARD, INBOARD	203.	259.

1. TEMPERATURES IN °F
2. CABIN WALL TEMPERATURES, 92°F
3. ENTRY FROM MAXIMUM HOT CONDITIONS

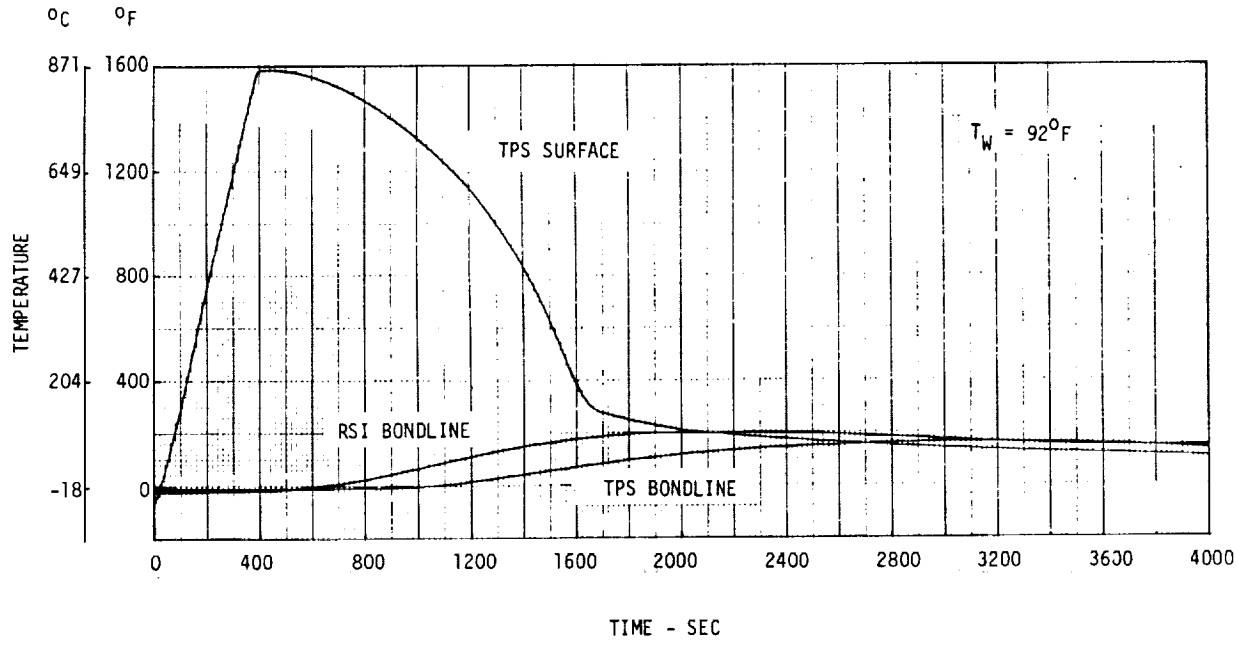

FIGURE 24 TPS TEMPERATURES DURING ENTRY AT LOWER ANTENNA - HOT ENVIRONMENT

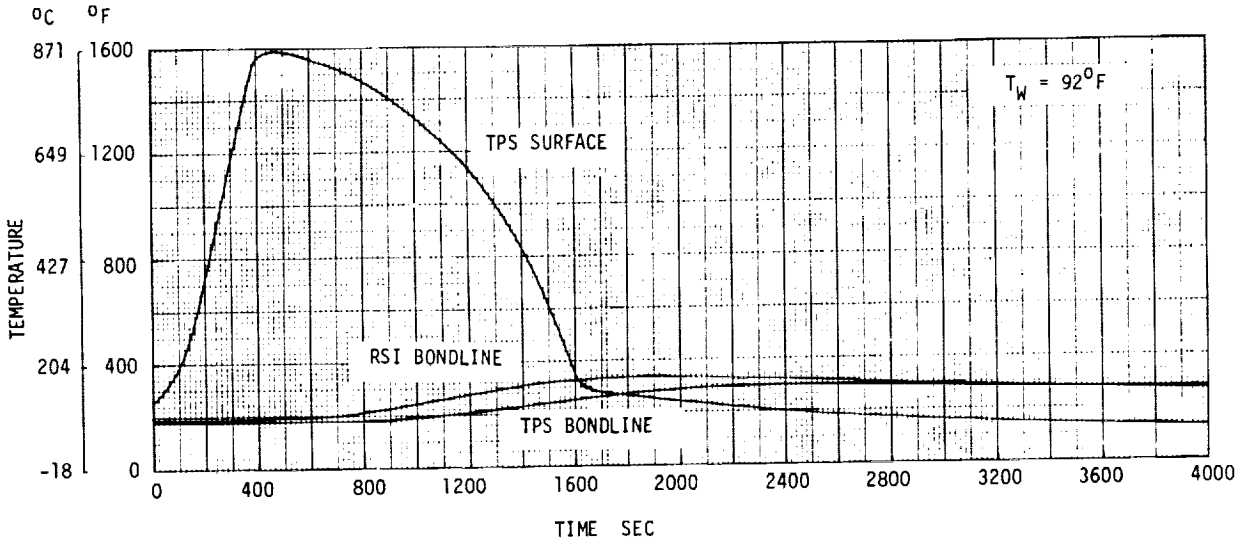

FIGURE 25 TPS TEMPERATURES DURING ENTRY AT LOWER ANTENNA - COLD ENVIRONMENT

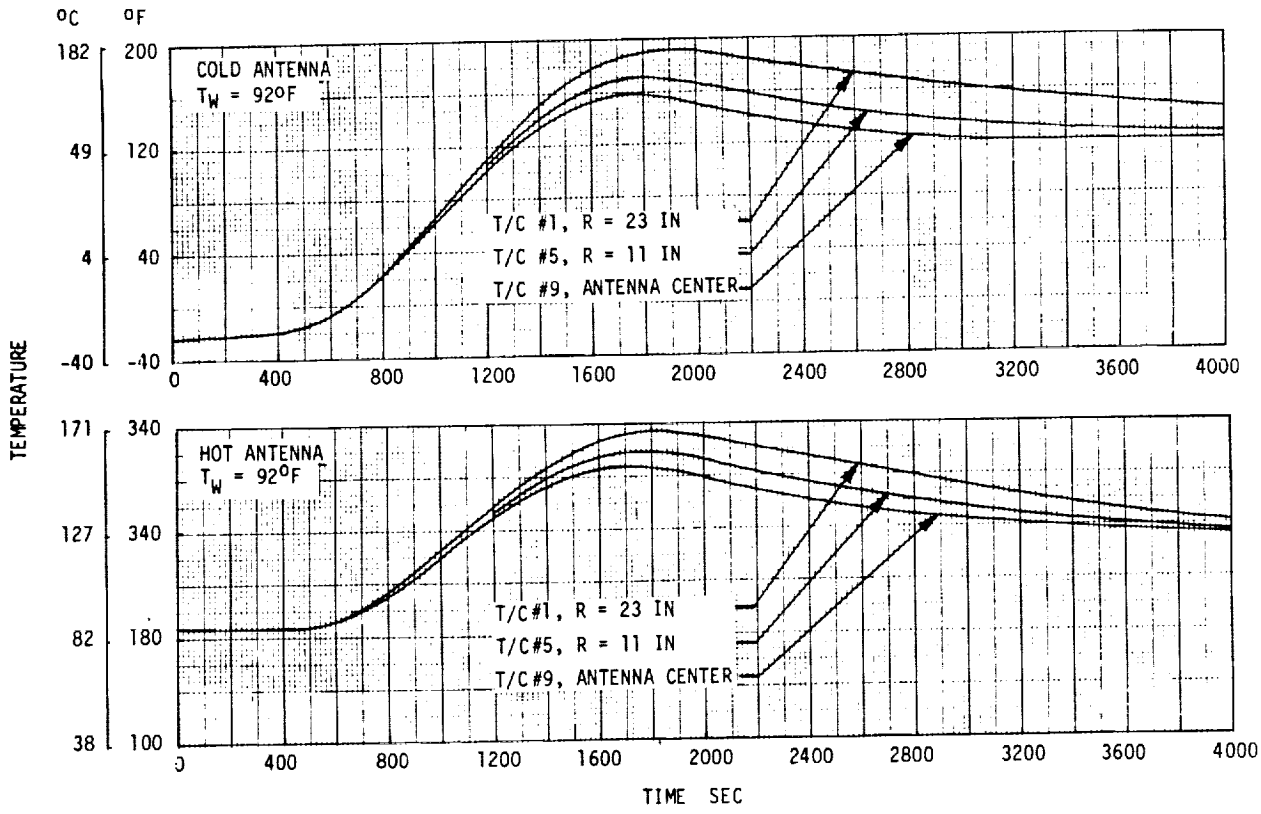

FIGURE 26 RSI BONDLINE TEMPERATURES DURING ENTRY AT LOWER ANTENNA

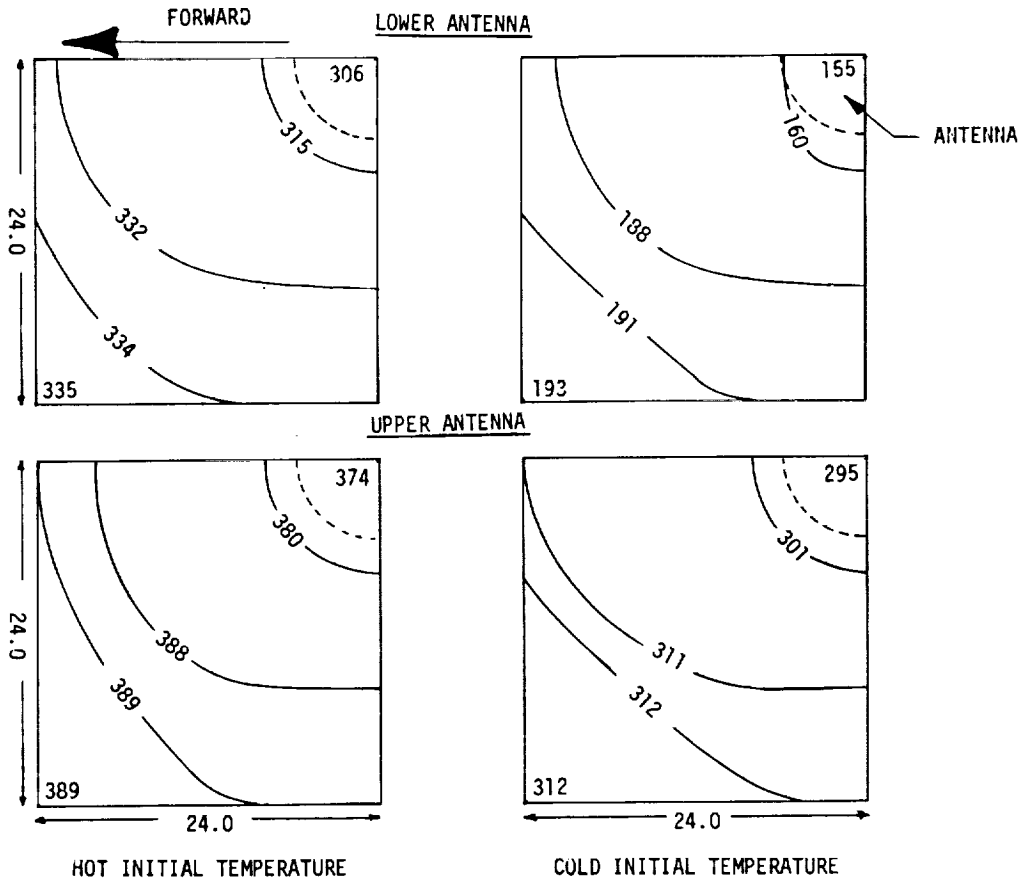

FIGURE 27 RSI BONDLINE ISOTHERMS AT MAXIMUM ENTRY TEMPERATURE

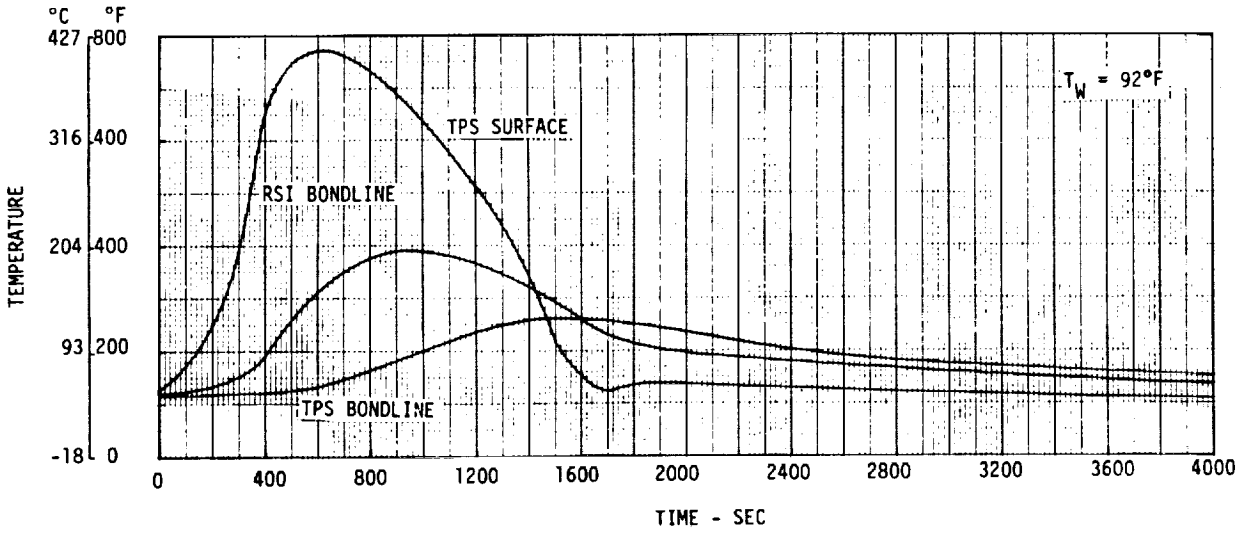

FIGURE 28 TPS TEMPERATURES DURING ENTRY AT UPPER ANTENNA - HOT ENVIRONMENT

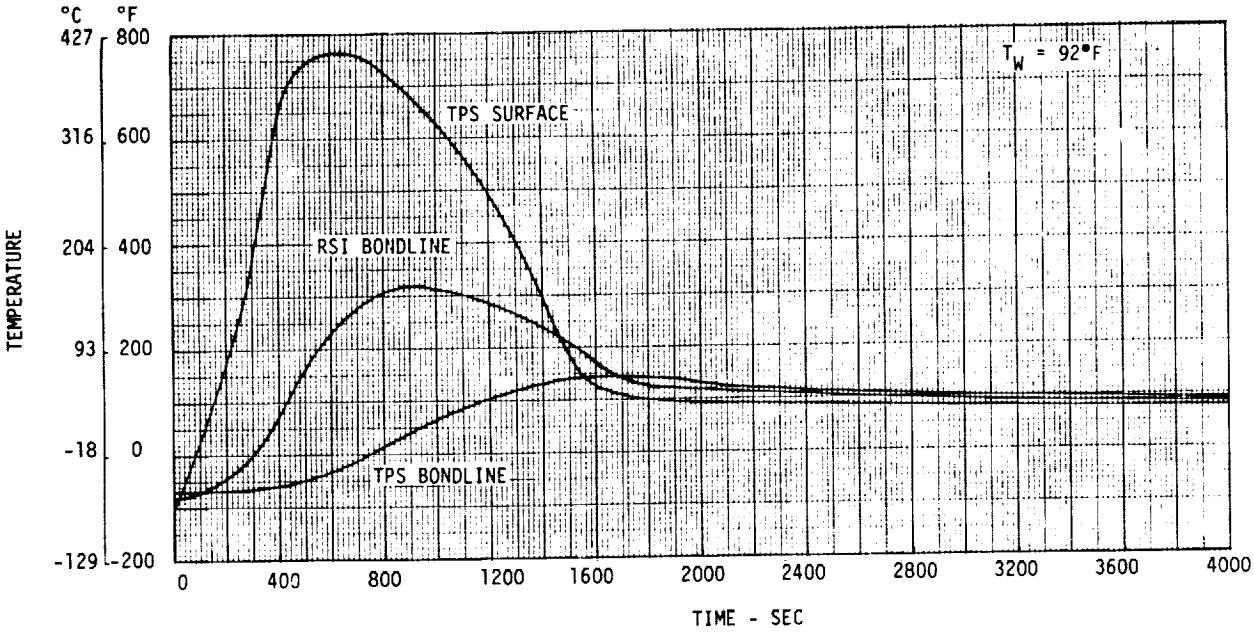

FIGURE 29 TPS TEMPERATURES DURING ENTRY AT UPPER ANTENNA - COLD ENVIRONMENT

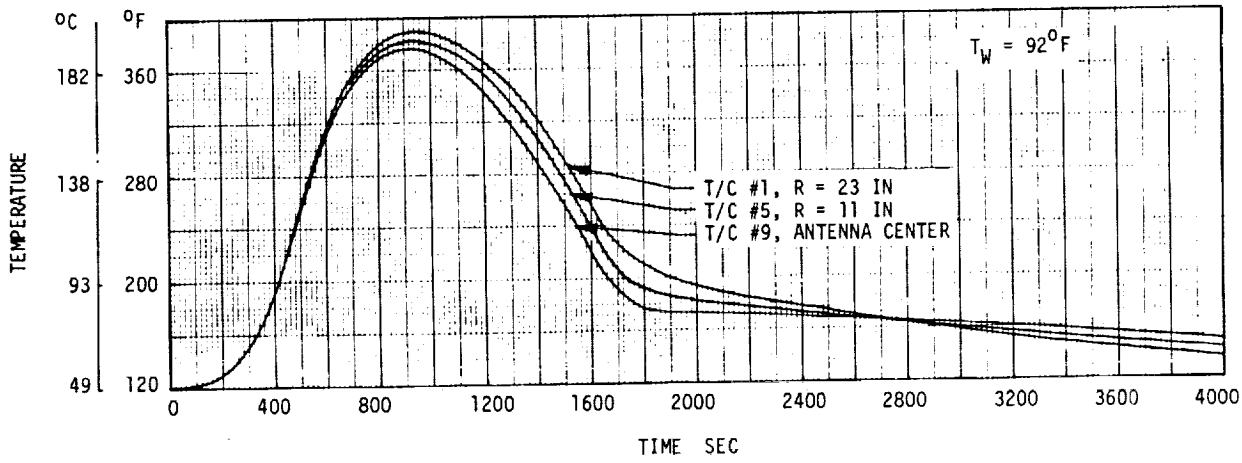

FIGURE 30 RSI BONDLINE TEMPERATURES DURING ENTRY AT UPPER ANTENNA - HOT ENVIRONMENT

antenna's center radiating element (node 32, figure 7). The upper antenna responds faster to heat flux variations but reaches a lower maximum temperature than the lower antenna.

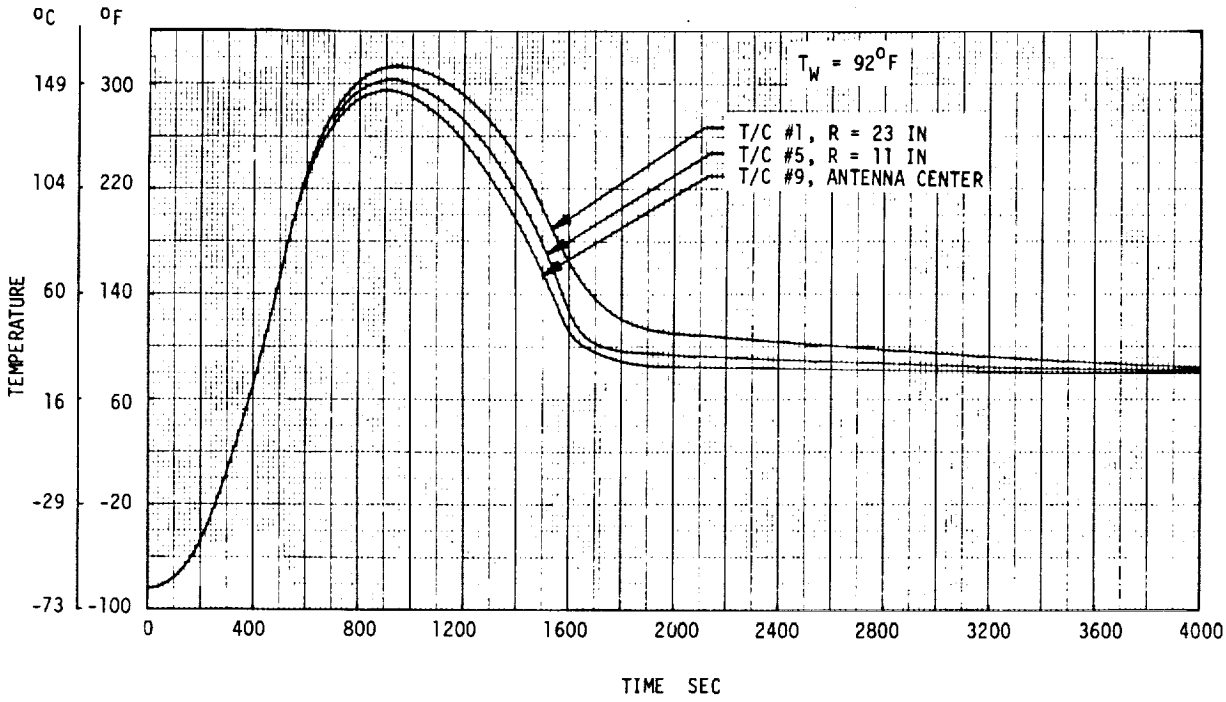

FIGURE 31 RSI BONDLINE TEMPERATURES DURING ENTRY AT UPPER ANTENNA - COLD ENVIRONMENT

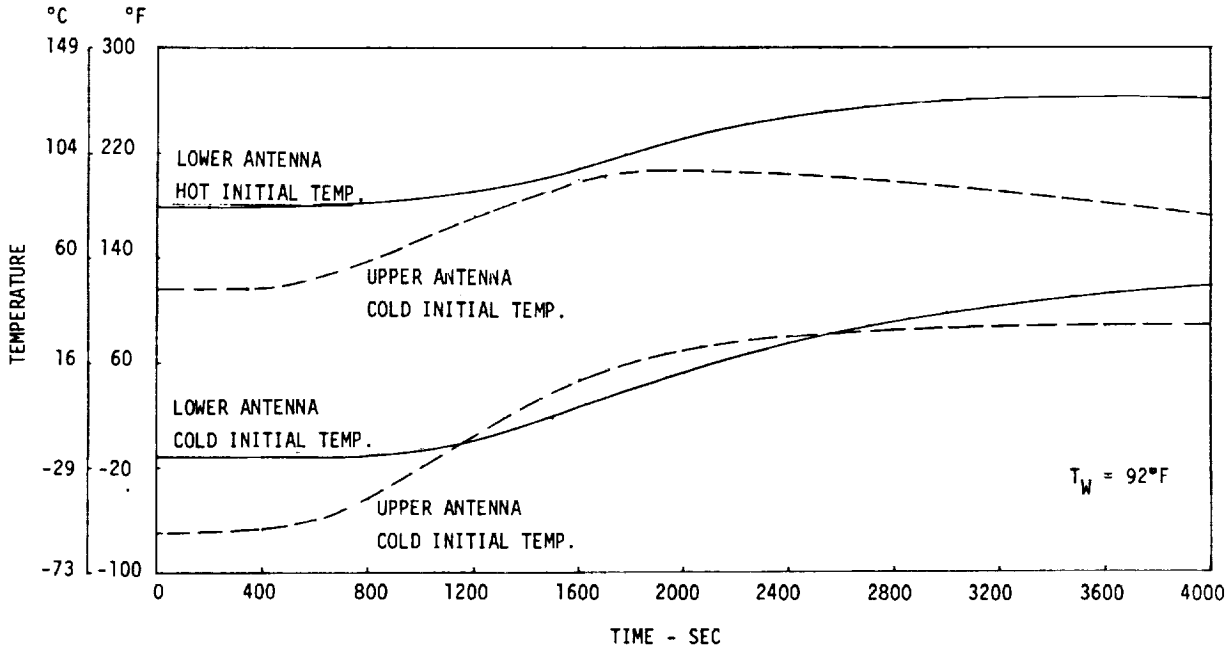

FIGURE 32 CENTER RADIATING ELEMENT TEMPERATURES DURING ENTRY

THIS PAGE INTENTIONALLY LEFT BLANK

THERMAL TEST FIXTURE

The Thermal Test Fixture task (Task 2.3.2) consisted of designing and fabricating a test fixture to be used to verify by thermal vacuum testing the thermal analyses and the thermal control plan obtained in Task 2.3.1 by evaluating the thermal response of the test fixture and the S-band antenna in simulated orbital and entry environments. The objectives of this task were: (1) to model a section of Space Shuttle Orbiter Structure with provisions for mounting the S-band antenna; (2) to minimize the effects of terminating the edges on the antenna's thermal response; (3) to provide a simulation of the interfaces with the space environment and the internal features of the Orbiter; and (4) to provide instrumentation for measuring the temperature histories at node points defined in the analytical thermal model. The details of the test fixture were reviewed with NASA prior to fabrication to ensure compatibility with NASA-JSC test facility requirements. This section discusses the design and fabrication approaches used to achieve these objectives.

Design

The thermal test fixture was designed to model the structure surrounding an S-band antenna so that both orbital and entry environments could be simulated and the thermal response of the antenna measured. The Orbiter features which could influence the antenna temperature and, thus, the test fixture design are: (1) the TPS over the antenna and surrounding skin; (2) the skin-stringer structure around the antenna; (3) the antenna mounting frame; (4) the internal insulation; (5) the crew cabin wall inboard of the internal insulation; and (6) the location of the antenna on the spacecraft. Other considerations which influence the test fixture design are: (1) test facility (vacuum chamber) size; (2) facility heating and cooling capabilities; and (3) instrumentation requirements.

One of the most important features considered was the exterior interface with the space and entry environments - the TPS. The TPS thicknesses at the upper and lower antenna locations (figure 1) are substantially different due to the difference in thermal environments as was discussed in the previous section, THERMAL ANALYSES - Thermal Model. This difference would require the construction of two thermal test fixtures or the necessity of having the capability of replacing the TPS in order to simulate the temperatures within both the upper and lower antennas. Also, as was shown in figures 24 and 28, the surface temperatures of the TPS are very high during entry. These temperature levels would require very large heating rates during testing. Therefore, since the primary purpose of the test fixture is to obtain the thermal response of the S-band antenna and since the thermal behavior of the RSI has been repeatedly verified by other tests, it was decided to eliminate the RSI from the test fixture and to control the SIP surface to simulate calculated orbital and entry temperature histories. Because of this design feature the same test fixture can be used to simulate either an upper or a lower antenna installation. In addition to eliminating the need for two test

fixtures, the heating rates and temperature limits required to simulate entry can be obtained with strip heaters at significantly lower input powers since the SIP temperature is much lower than the RSI surface temperature as shown in figures 24 and 28. The most significant difference between the thermal responses of the upper and lower antenna installations is the rate of temperature change. The upper antenna responds more rapidly because of the thinner RSI. However, the maximum and minimum temperatures are essentially the same. The temperature history of the RSI-SIP interface is one of the node temperatures calculated during the analysis of each environmental condition.

Inclusion of the SIP over the test fixture results in a significant simplification which should be noted. Thermal analyses show that the RSI bondline temperature is more uniform then the skin (TPS bondline) temperature due to the nonisotropic stringer conductance, (e.g., figure 27). However, since the SIP is essentially a thermal insulation material its surface temperature is difficult to measure and control accurately. This deficiency was overcome by including a thin sheet of stainless steel bonded on top of the SIP surface. This thin metal sheet provides a uniform lateral conductive path for the impressed heat and will allow for more accurate temperature control because of the fast response of the metal to heat input. The rapid control capability and the insulation provided by the SIP should result in less overshoot from the desired temperature history at the surface of the antenna and in the surrounding skin. The stainless steel skin over the SIP also provides a surface for attaching strip heaters which can be individually controlled in sectors to simulate solar or entry heating. To simulate space cooling the heaters can be turned off and the metallic surface permitted to radiate to the vacuum chamber shroud or to a low temperature sink directly over the test fixture surface.

Another design feature considered was the test fixture size. The surface dimensions should be large enough to prevent the edge conditions from affecting the temperature distribution at the antenna. Thermal analysis showed that a 1.23 x 1.23 m (4.0 x 4.0 ft) panel was sufficient to provide approximately adiabatic edges. This size is also compatible with the NASA-JSC test facility vacuum chambers.

A sketch of the final thermal test fixture design is shown in figure 33. The design is based on the external surface simulation technique discussed above. The skin thickness is an average of five different skin thicknesses used in the antenna region on the Orbiter structure. The stringer cross-section and thickness are based on an average of several different stringer sizes in the immediate area of the Orbiter antenna. A coating is required on the internal side of the structure to provide the correct thermal radiation emittance characteristics.

Since the antenna mount is designed for installation of the antenna from outside of the Orbiter it was necessary to provide a removable circular panel of SIP and stainless steel that could be bonded to the antenna after installation in the test fixture.

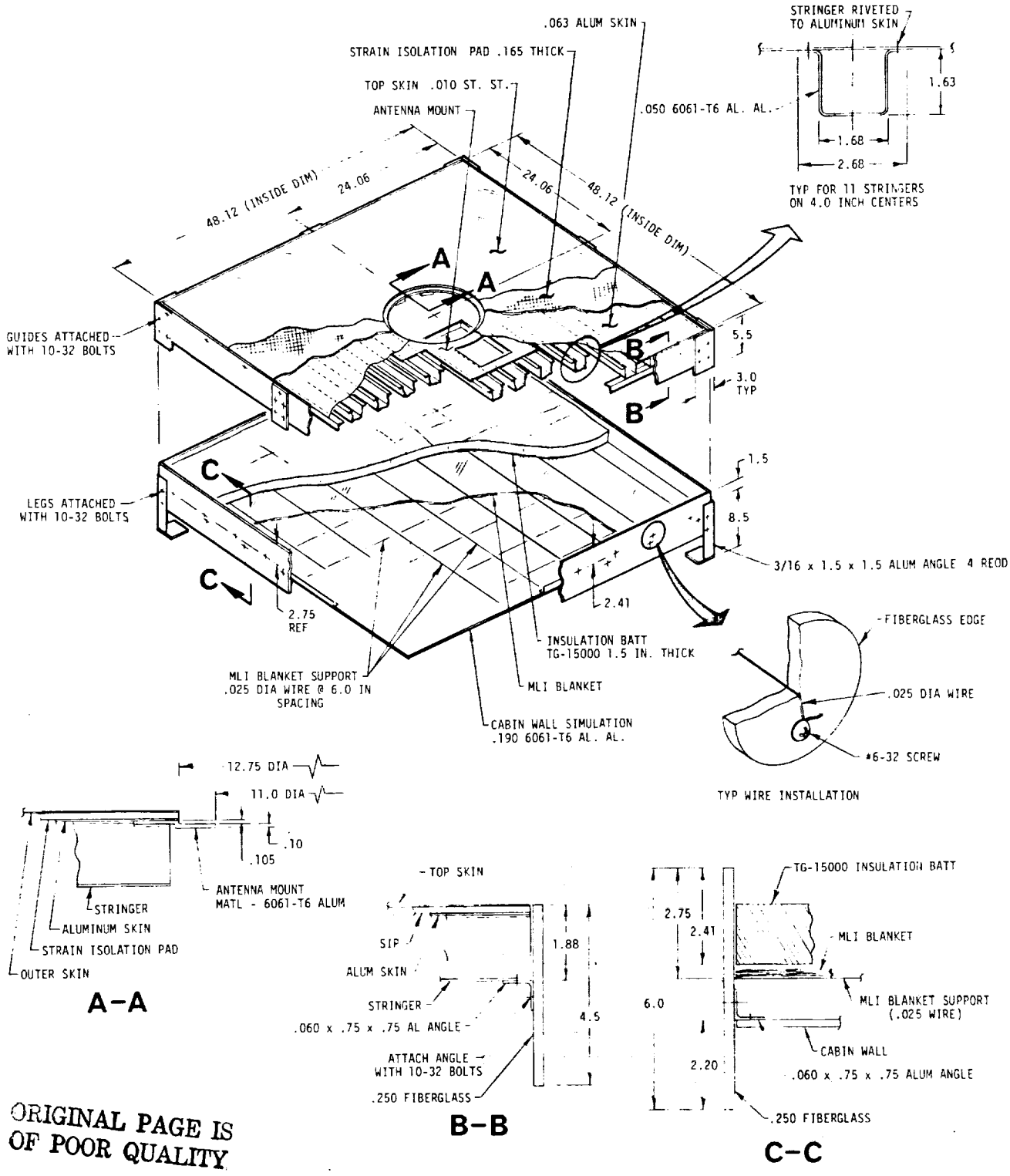

ORIGINAL PAGE IS
OF POOR QUALITY

DIMENSIONS IN INCHES

FIGURE 33 THERMAL TEST FIXTURE - DESIGN DETAILS

The simulated Orbiter structure, insulation and cabin wall panel are supported by a fiberglass frame. The frame was designed in two sections to permit easy access to the antenna following installation and to the internal insulation layers. The lower test fixture frame supports the TG-15000 insulation and MLI blanket over a panel which simulates the cabin wall.

During testing the test fixture must be surrounded on all four sides by at least 15 cm (6 in.) of min-K insulation or equivalent to provide adiabatic boundaries.

Instrumentation. - The thermal test fixture contains thirty-one 28-gage chromel-alumel thermocouples. An additional 17 thermocouples should be installed within the antenna. The thermocouples on the test fixture and those recommended on the antenna are tabulated in table IX. Figure 34 is a sketch of the thermocouple locations on the test fixture. A small hole is provided in the side of the test fixture frame for the thermocouple leads.

Temperature control. - It is recommended that thermocouples five through nine be designated as control points. Separation of the top surface into five zones (each quadrant and the center) will allow for more accurate temperature control of the test fixture surface. This zoning requires that heat be provided to each of the surface areas independently, by means of strip heaters, and that the temperature at thermocouples five through nine be used to regulate the heater power according to the predicted temperature history of these locations. Thus, locations one through four may vary slightly from the predicted temperature of the RSI bondline but the bondline temperature immediately over and around the antenna will have the correct input values.

Fabrication

The thermal test fixture was fabricated according to the design shown in figure 33, by the MDC Advanced Material Fabrication Facility. The test fixture is composed of two sections which can be separated for convenience. One section includes a skin-stringer structural panel and an antenna mounting frame. The other includes internal insulation and cabin wall simulations.

The basic frame (figure 35) was fabricated from 0.64 cm (0.25 in.) GSG fiberglass to minimize heat leaks between the upper and lower sections. The lower section includes an aluminum sheet to simulate the cabin wall. Two sets of orthogonal wires (figure 36) are used to support an MLI blanket ($\sim$0.84 cm (0.33 in.) thick) and a layer of TG-15000 (3.81 cm (1.5 in.) thick) parallel to and 2.54 cm (1.00 in.) above the aluminum plate. The orthogonal wire configuration permits the insulation layer to be installed or removed without dismantling the test fixture.

The structural section is composed of stringers and an antenna mounting fixture; both are riveted to a 1.23 x 1.23 m (4.00 x 4.00 ft) skin section. Figure 37 shows a bottom view of the skin-stringer panel. The stringer side of the panel was coated with a green epoxy primer (DeSoto 515-005 Super Koropon

TABLE IX

ANTENNA THERMAL TEST FIXTURE INSTRUMENTATION LOCATIONS

NUMBER	COMPONENT	LOCATION	
1	Top skin (9)	X=16, Y=16	Top
2		X=16, Y=-16	
3		X=-16, Y=-16	
4		X=-16, Y=-16	
5		X=8, Y=8	
6		X=8, Y=-8	
7		X=-8, Y=-8	
8		X=-8, Y=-8	
9		Center	
10	Al skin (16)	X=8, Y=-8	Top
11		X=8, Y=8	
12		X=-8, Y=8	
13		X=-8, Y=-8	
14		X=0, Y=-16	
15		X=16, Y=0	
16		X=0, Y=16	
17		X=-16, Y=0	
18		X=24, Y=-24	
19		X=24, Y=24	
20		X=-24, Y=24	
21		X=-24, Y=24	
22		X=16, Y=-16	
23		X=16, Y=16	
24		X=-16, Y=16	
25		X=-16, Y=-16	
26	TG-15000 (2)	X=12, Y=0	Top
27	TG-15000	X=-12, Y=0	
28	Cabin Wall (4)	X=12, Y=12	
29		X=12, Y=-12	
30		X=-12, Y=-12	
31		X=-12, Y=12	
32	F/G Antenna cover (1)	Center	Top
33	Antenna flange (2)	r=5.0, θ=22.5	Top
34	Antenna flange	r=5.0, θ=202.5	
35	Dust Cover flange (2)	z=-1.88, θ=22.5	Inside
36	Dust Cover flange	z=-1.88, θ=202.5	
37	Dust cover bottom (1)	Center	Outside
38	Circuit Board (1)	Center	Bottom
39	Center element wall(2)	z=-2.0, θ=45	
40	Center element wall	z=-2.0, θ=225	
41	+X element wall (2)	z=-2.0, θ=45	
42	+X element wall	z=-2.0, θ=225	
43	+Y element wall (2)	z=-2.0, θ=45	
44	+Y element wall	z=-2.0, θ=225	
45	-X element wall (2)	z=-2.0, θ=45	
46	-X element wall	z=-2.0, θ=225	
47	-Y element wall (2)	z=-2.0, θ=45	
48	-Y element wall	z=-2.0, θ=225	

1. Reference axes located at antenna center (top of element)
   - +X forward
   - +Z outboard (top)
   - +Y forms right-hand system

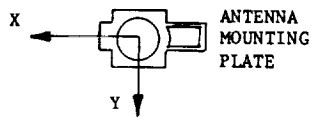

2. Angles (θ) defined as positive rotation +X → +Y
3. All thermocouples chromel-alumel 28 gage with 10 foot leads (from test fixture exit)

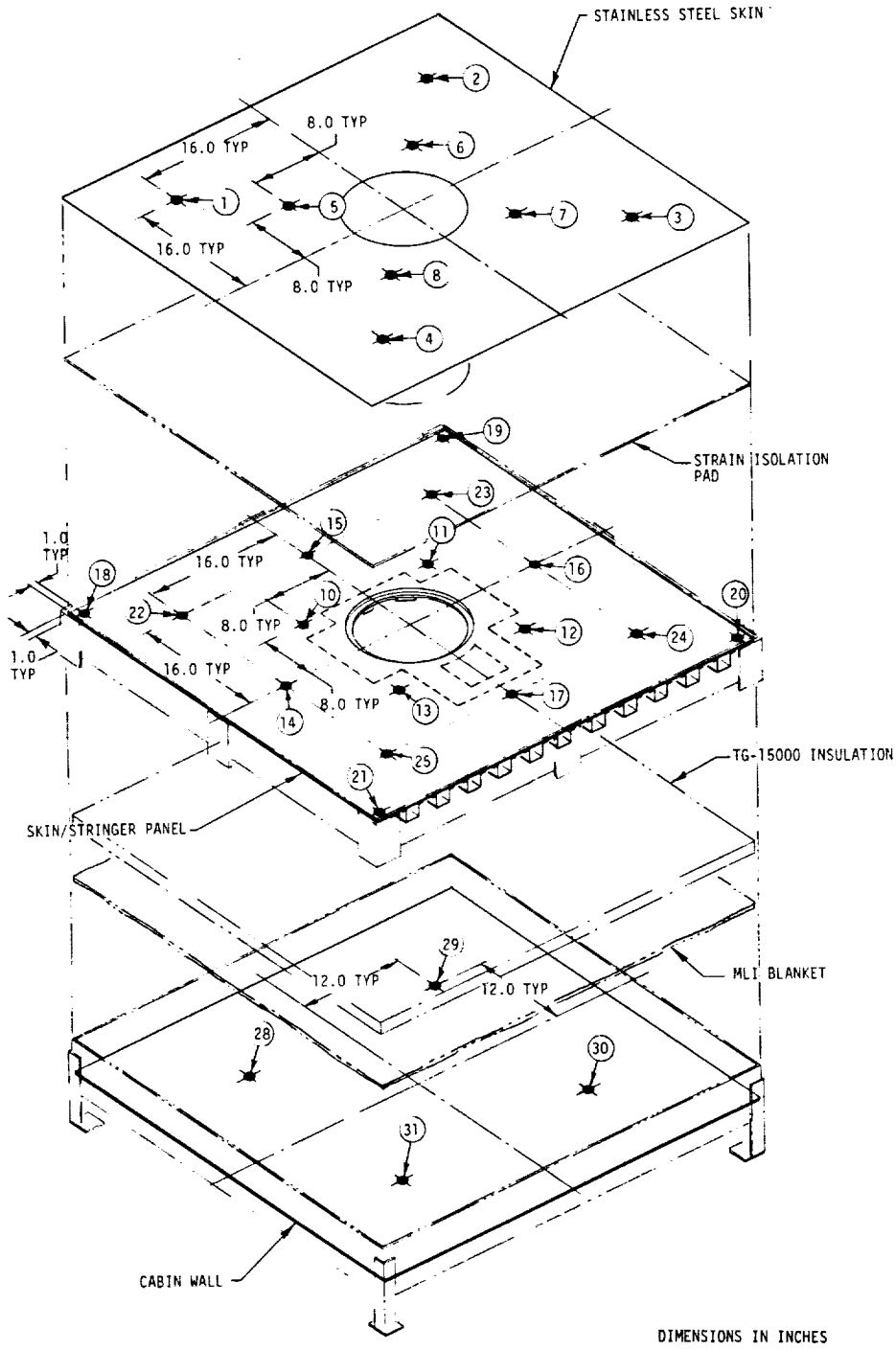

FIGURE 34 THERMOCOUPLE LOCATIONS

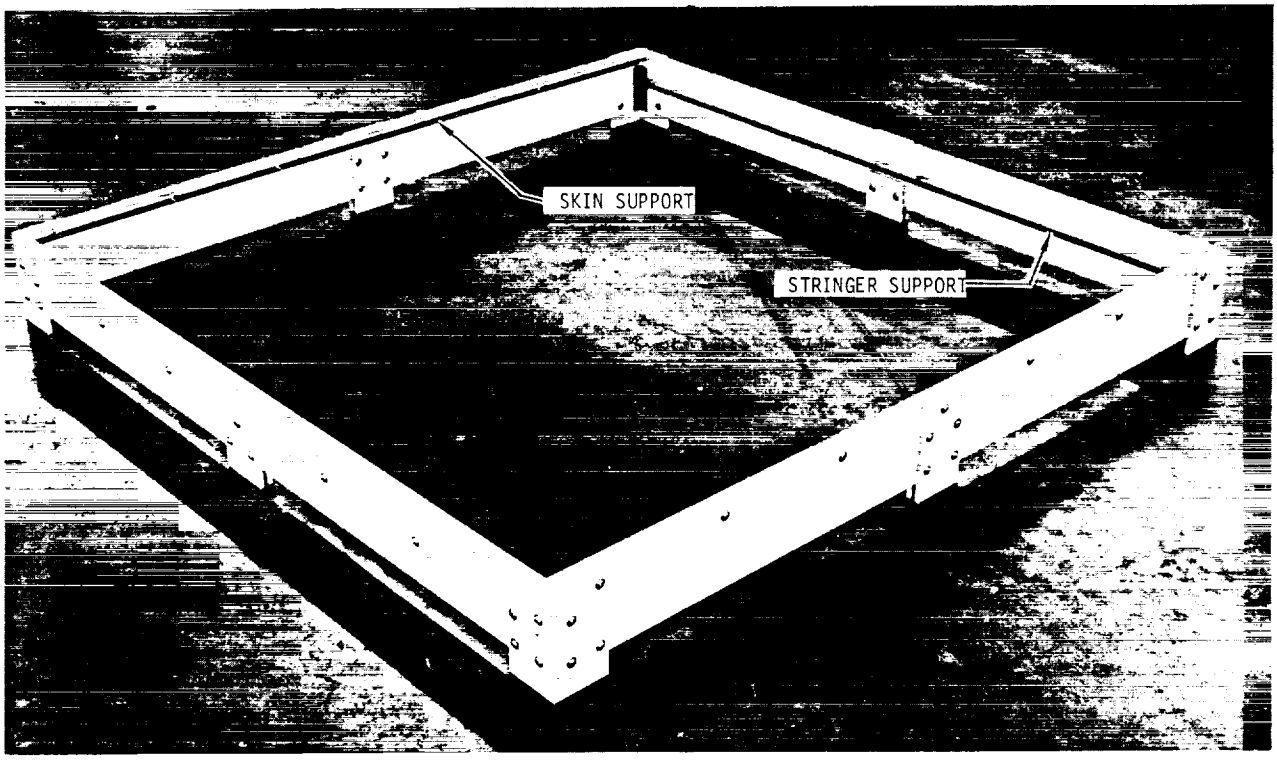

(a) UPPER SECTION

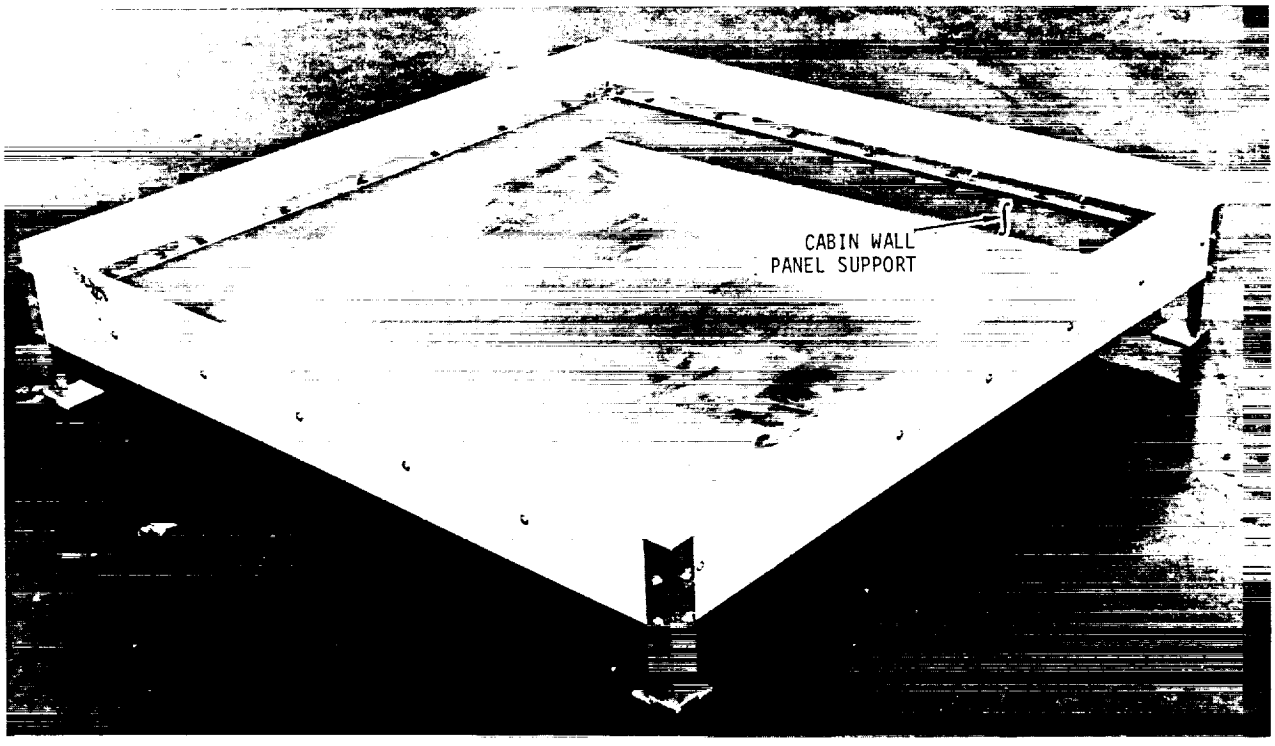

(b) LOWER SECTION

FIGURE 35 THERMAL TEST FIXTURE FRAME

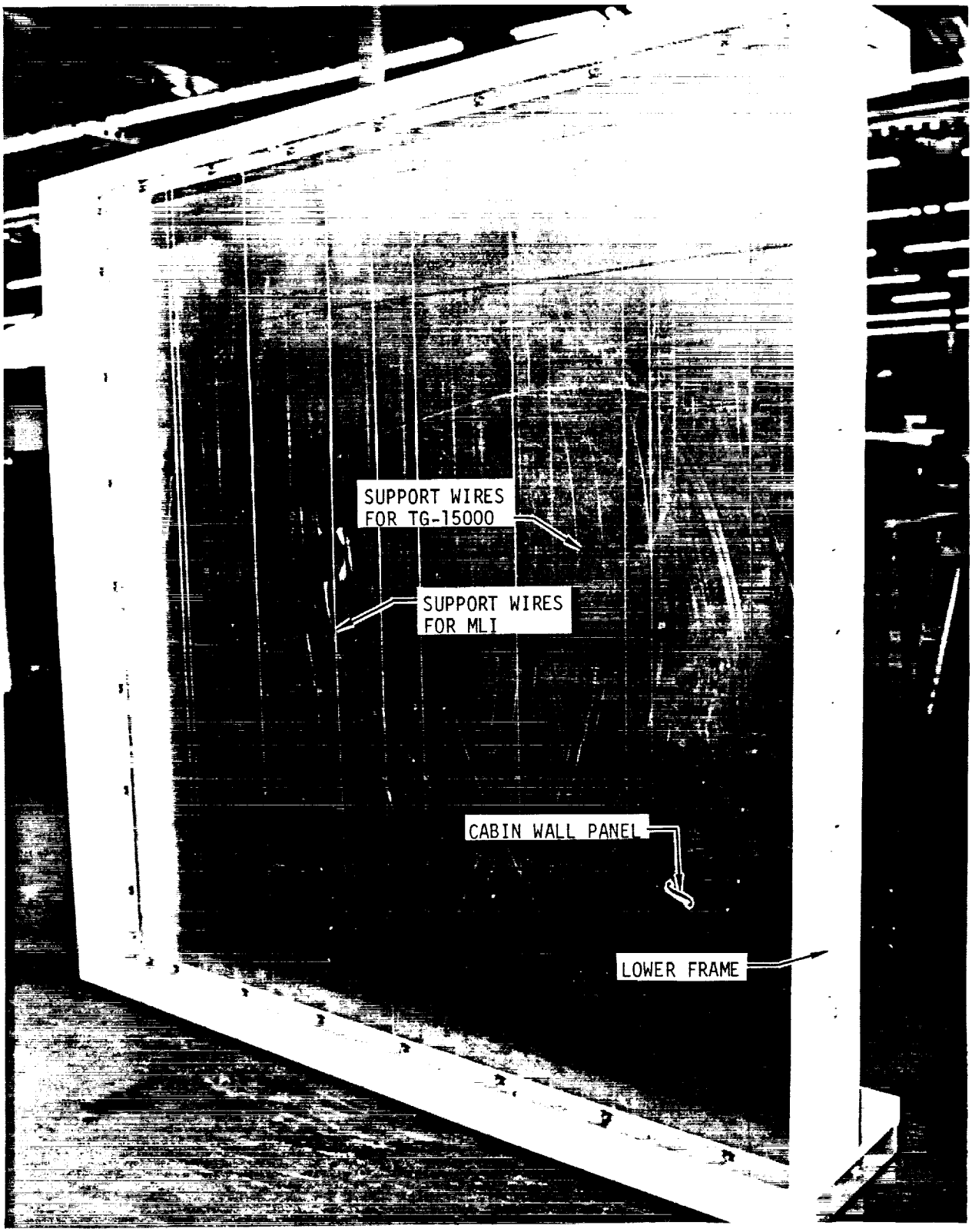

FIGURE 36 INTERNAL INSULATION SUPPORT

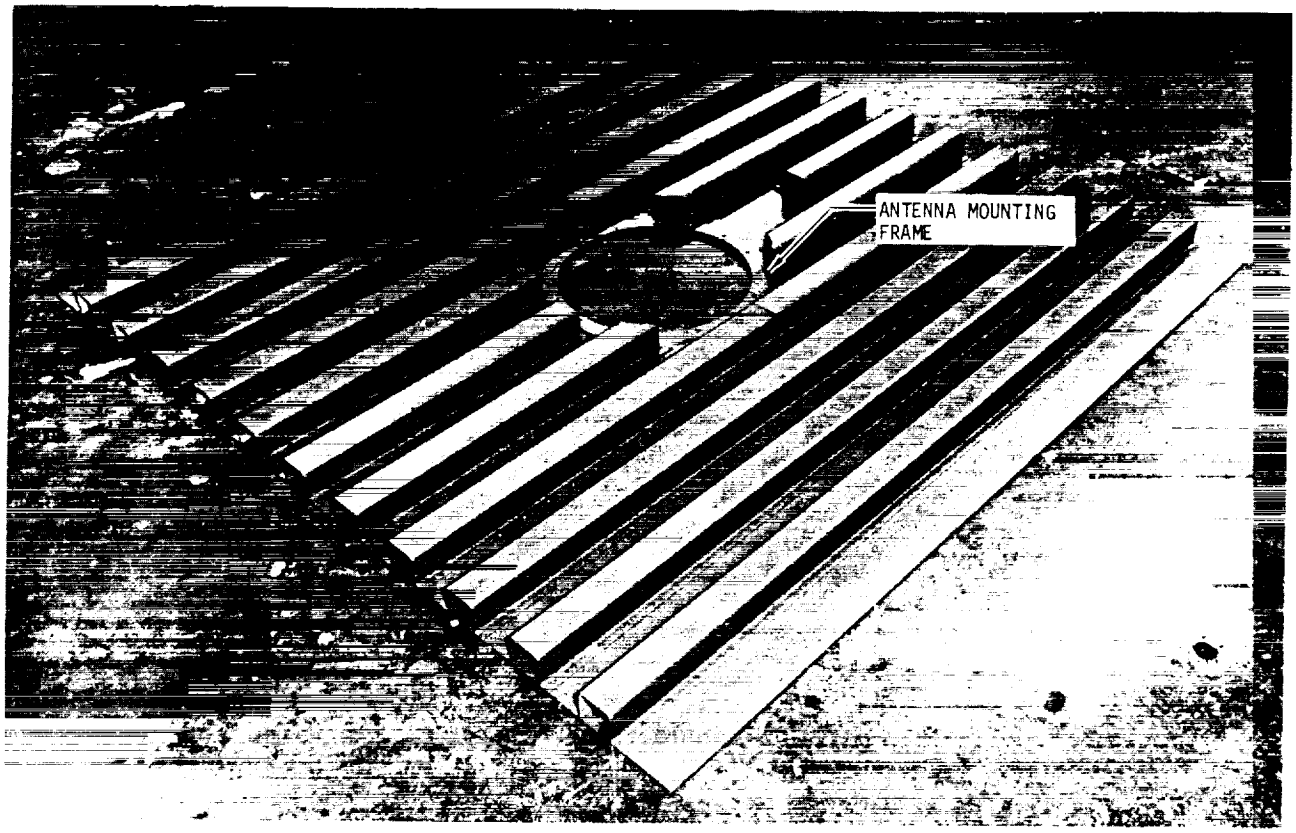

FIGURE 37 SKIN-STRINGER PANEL - BOTTOM VIEW

Fluid Resistant Primer) to provide the proper thermal emittance. This panel was attached to the angle brackets as shown in figure 35a. Figure 38 shows a top view of the skin-stringer panel attached to the test fixture framework. A layer of SIP (strain isolator pad) was bonded to the skin with RTV-560. A 0.254 mm (0.010) stainless steel sheet was bonded on top of the SIP with RTV-560 as shown in figure 39. A section was cut-out over the antenna through the SIP and stainless steel to permit installation of the antenna from the top. This circular section must be bonded to the antenna surface after installation to provide proper heat conduction during testing. The thin stainless steel surface serves as a conducting surface for heating the test fixture. Strip heaters can be bonded to this surface or it can be heated with quartz lamps and controlled to the RSI/SIP interface temperature.

The primary control thermocouples for the thermal test fixture are shown in figure 39. These thermocouples permit independent control of four areas surrounding the antenna and one directly over the antenna. Thermocouple instrumentation for monitoring the skin-stringer structural temperatures are shown in figure 40. The thermocouple leads were extended through holes in the stringers and skin and bonded to the skin surface. Figure 41 shows the control thermocouple installation on the panel used to simulate the cabin wall.

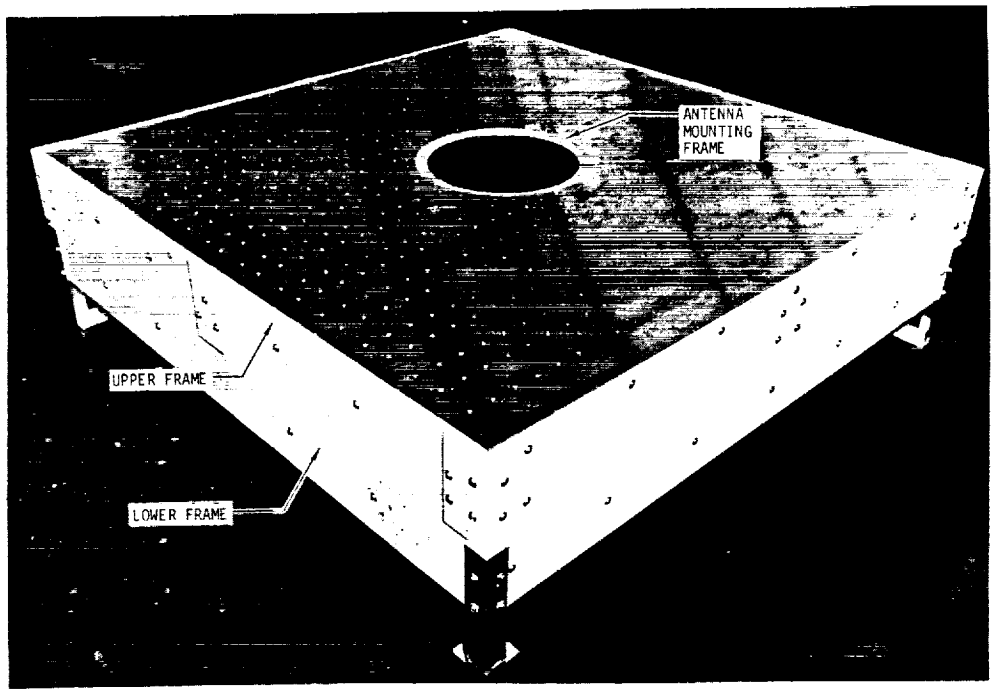

FIGURE 38 SKIN-STRINGER PANEL MOUNTED IN THERMAL TEST FIXTURE FRAME - TOP VIEW

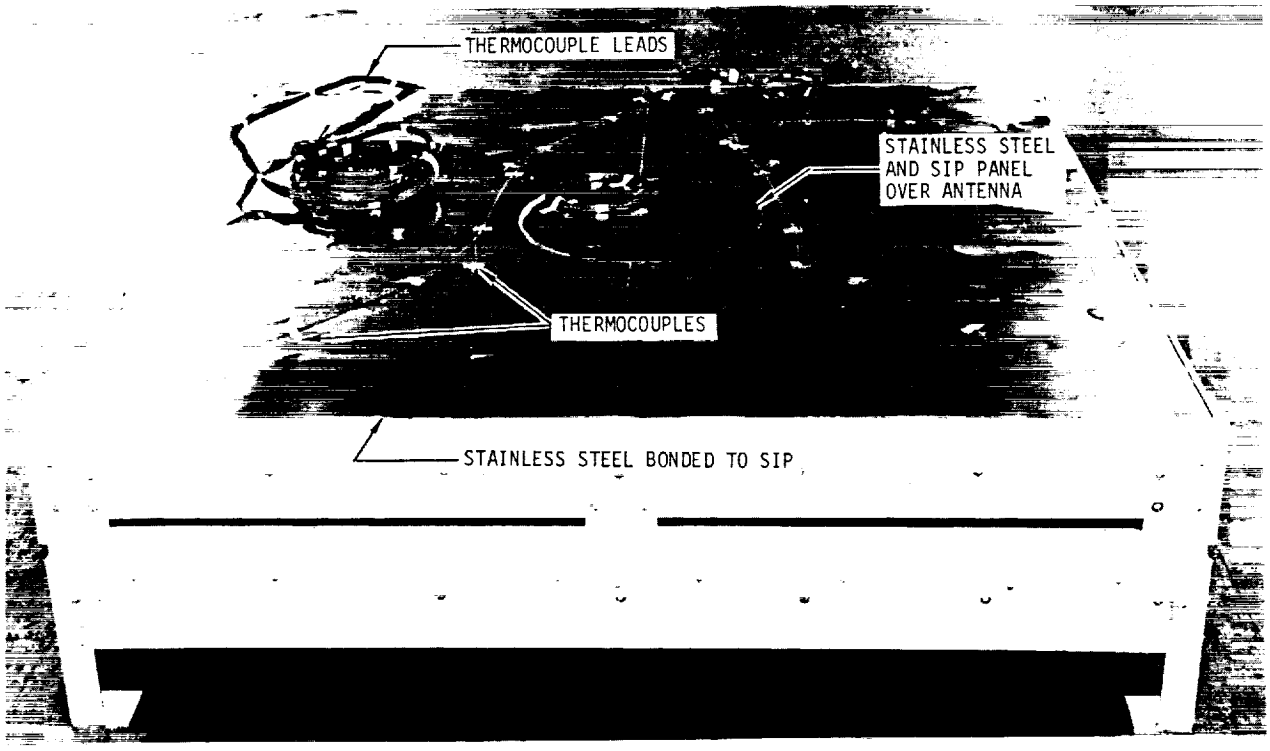

FIGURE 39 COMPLETED THERMAL TEST FIXTURE WITH SURFACE THERMOCOUPLES

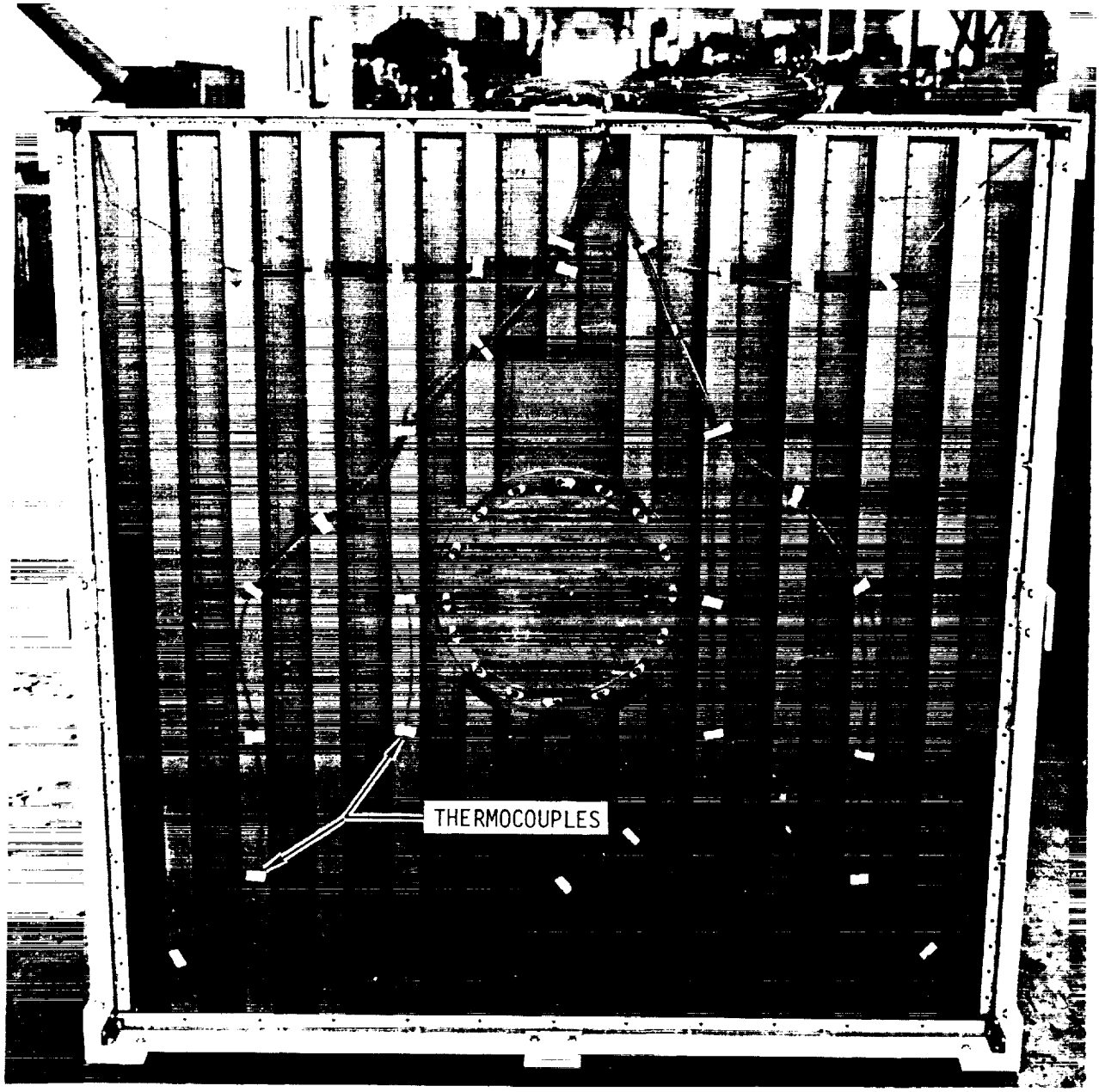

FIGURE 40 THERMOCOUPLE INSTALLATION ON SKIN-STRINGER PANEL

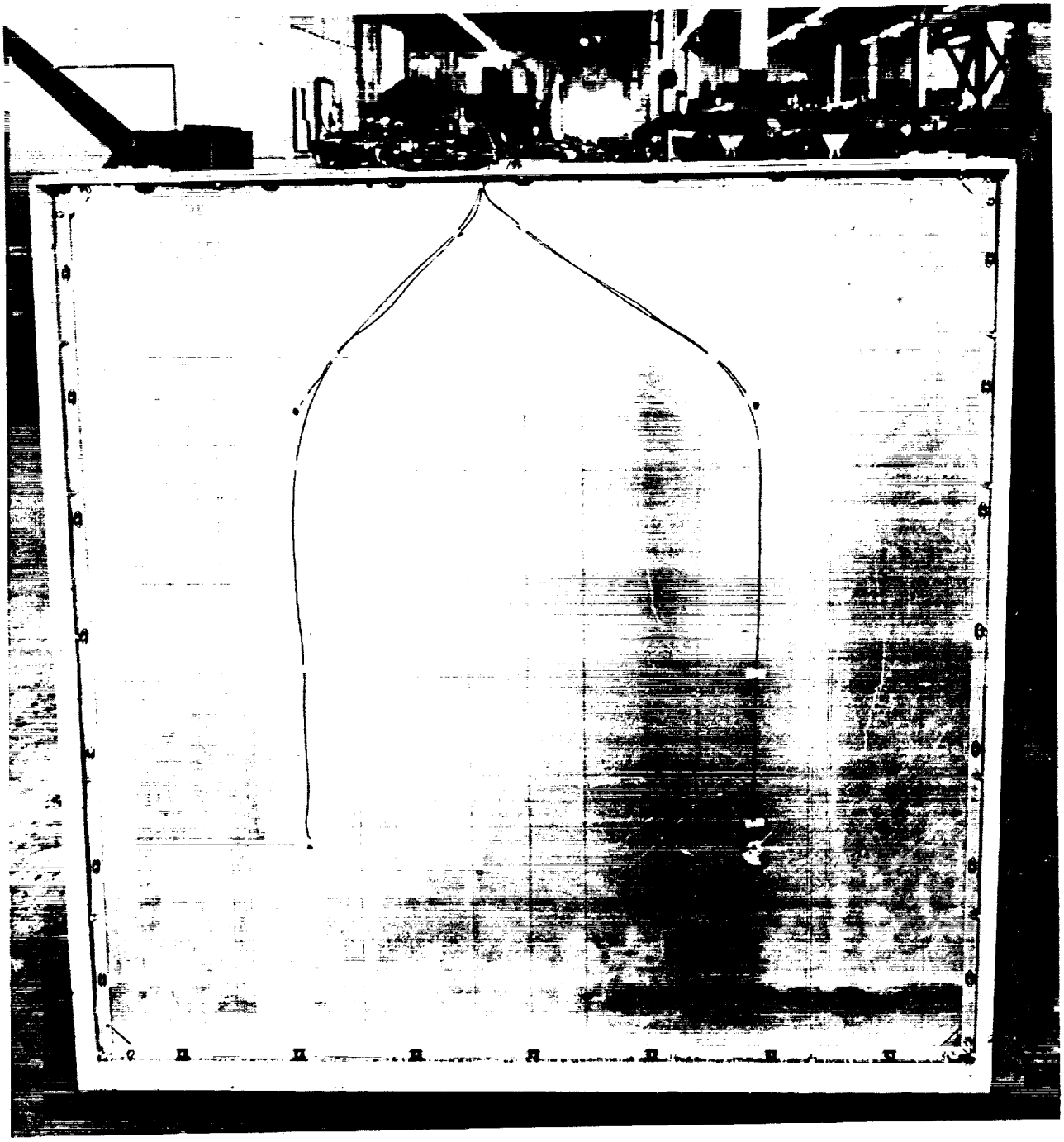

FIGURE 41 THERMOCOUPLE INSTALLATION ON CABIN WALL PANEL

ELECTRICAL TEST FIXTURES

The Electrical Test Fixtures task (Task 2.3.3) consisted of designing and fabricating two different electrical test fixtures to be used for evaluating the radiation pattern characteristics of an S-band antenna. The objectives of this task were to: (1) simulate sections of large and small radius spacecraft external surface (i.e., ground plane surface seen by the array antenna); (2) simulate the electrical characteristics of the thermal protection system (TPS) which is typically bonded to these surfaces; (3) select a size and/or edge configuration which minimizes the effects of the test fixture edges on the antenna radiation patterns; and (4) provide a mounting arbor configuration compatible with NASA-JSC antenna positioner requirements. This section discusses the design and fabrication approaches used to achieve these objectives.

Design

The electrical test fixtures were designed to simulate the surface areas surrounding two antenna locations on the Space Shuttle Orbiter. Simulation of the Orbiter TPS is the most significant problem associated with designing the test fixtures. In terms of antenna performance, the TPS on the Orbiter is similar to covering the antenna and the ground plane surrounding it with a dielectric sheet. The dielectric constant, loss tangent and thickness of the sheet cause transmission loss and support surface wave excitation which effect the radiation pattern and impedance of the antenna.

Figure 42 shows a sketch of the Orbiter and indicates the surface areas surrounding the two antenna locations used for this program along with the interface mold line (IML) (i.e., structural skin surface lines) shapes as a function of body station (X_0 = 505 through X_0 = 600). The antenna location on the upper body is at X_0 = 551.15, Y_0 = $\pm$70.70 and Z_0 = 472.50 (Orbiter coordinates in inches) and is in an area that has a large transverse surface radius. The antenna location on the lower body is near the lower chine at X_0 = 556, Y_0 = $\pm$95.62 and Z_0 = 294.65 and is in an area that has a small transverse surface radius. A right side configuration was arbitrarily selected for the two test fixtures. Since the Orbiter is symmetrical about the Y_0 = 0 plane, the test results will be equally applicable to the left side with the proper coordinate interpretation.

The TPS thickness dimensions differ significantly around the upper and lower body antenna locations. The upper body TPS is generally less than 1.27 cm (0.5 in.) and the TPS on the lower body varies from 3.58 cm (1.41 in.) to 7.52 cm (2.96 in.). Only the RSI thickness is varied to obtain the required TPS thickness.

The test fixture design approach is shown in figure 43. Plywood frames 1.27 cm (0.5 in.) thick with a maximum spacing of 50.8 cm (20 in.) provide the surface contour control. Aluminum "T" stringers tie the frames together and

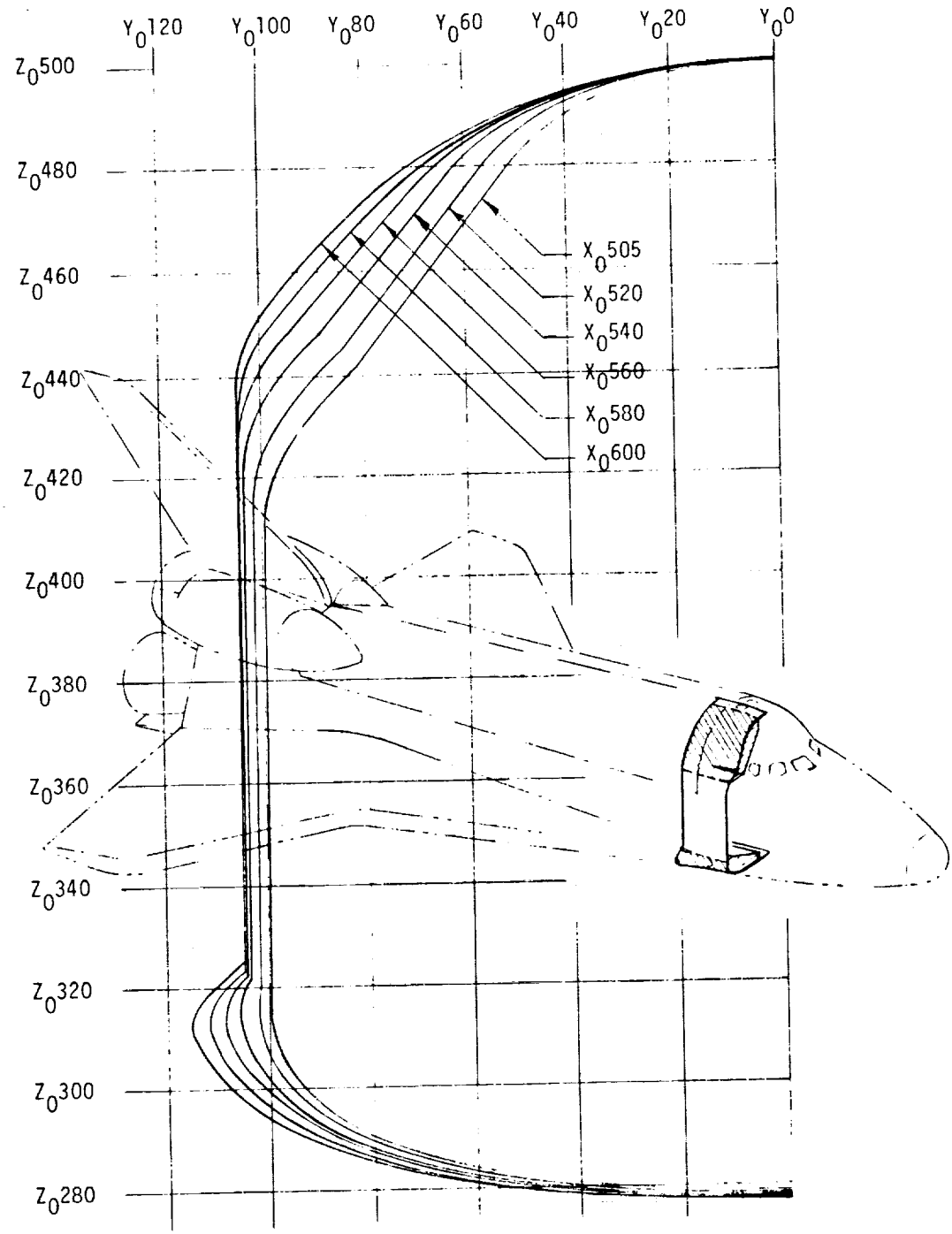

FIGURE 42 SPACE SHUTTLE ORBITER INTERFACE MOLDLINE CONTOURS

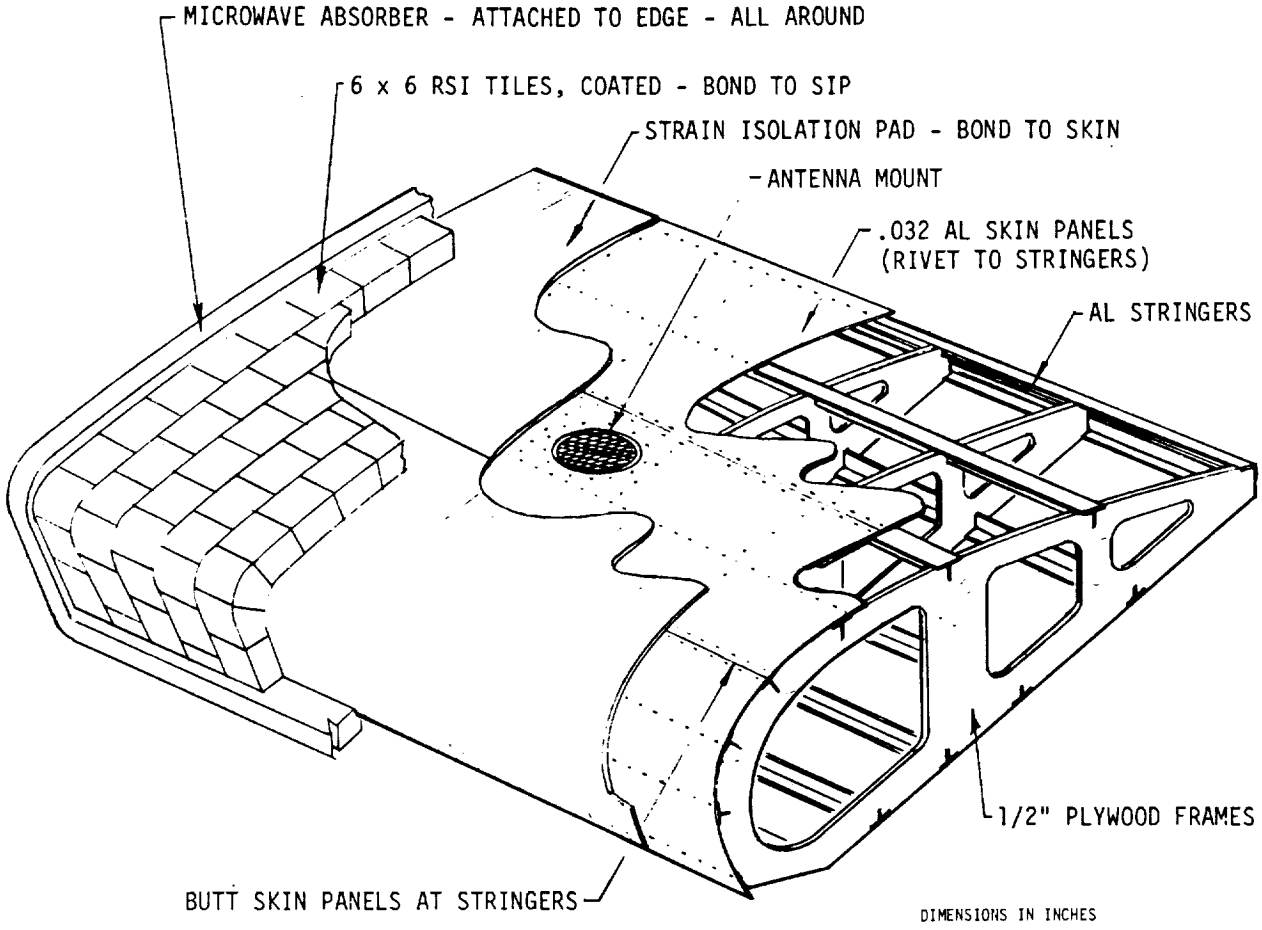

FIGURE 43 ELECTRICAL TEST FIXTURE - DESIGN DETAILS

provide intermediate support for an 0.813 mm (0.032 in.) aluminum skin. Simulated TPS is bonded to this skin to complete the simulation of the Orbiter surface configuration. Microwave absorber is attached to the test fixture edges to minimize the edge effects.

Size. - The size of the test fixtures was influenced by the cost and weight of the support structure required to maintain a rigid surface during antenna radiation pattern measurements and the requirement to minimize the edge effects on the test antenna radiation patterns. These factors resulted in the selection of a test fixture 2.44 m (8.0 ft) in length and a width based on the largest frame size which could be cut from a 1.22 x 2.44 m (4.0 x 8.0 ft) sheet of plywood. This approach also provides the largest test fixture that could be fabricated from standard material sizes within the budgeted cost. A larger test fixture would have increased both the weight and cost significantly due to the need for splicing and added bracing and the accompanying labor costs. Larger test fixtures would also have resulted in the need for longer transmission distances in order to obtain plane wave illumination.

The size cited above results in test fixture edges approximately 9 wavelengths (at the lowest S-band antenna frequency -2217.5 MHz) from the center of the antenna.

Surface contours. - The Orbiter IML from body stations X_0 = 505 to X_0 = 600 (figure 42) bracket the center of the respective antenna locations at X_0 = 551.15 and 556. Based on the frame size limits discussed in the preceding subsection, the large and small radius test fixture IML's are bounded by Y_0 = 30 and Z_0 = 440, and Y_0 = 30 and Z_0 = 320, respectively.

A simple cardboard model of each test fixture was constructed to aid in planning the frame configuration below the surface, the construction jig requirements and the overall test fixture details. These models showed that the use of the Orbiter body IML's would result in a compound surface curvature. However, a compound surface would require the use of form blocks to obtain a smooth skin. Since the use of form blocks would result in a significant construction cost increase, an alternate approach was used.

From the cardboard model, it was determined that a simply curved surface (i.e., one that can be covered with a flat sheet curved in only one direction) could be obtained that would not deviate from the IML's shown in figure 42 by more than 12.7 cm (5.0 in.) in one small region. In most locations the deviation would be less than 2.5 cm (1.0 in.). This is due to the fact the longitudinal radius of curvature is relatively large. By the use of the exact IML's for the frame contours adjacent to the antenna, the antenna aperture plane orientation can be held essentially coincident with that of an antenna normally installed in the Orbiter. The minor deviation from the exact Orbiter IML is expected to have no significant effect on the radiation patterns.

The test fixture frame contours were developed using a computer aided digital plotting machine. The Orbiter IML's adjacent to the antenna locations were used as control contours. Figure 44 shows the test fixture contours as developed. The variation in frame station selection results in antenna locations which are centered between the center frames of each test fixture. The maximum normal deviation from the true Orbiter IML is 2.7 cm (1.5 in.) and 1.3 cm (0.5 in.) for the large and small radius test fixtures, respectively. Full-scale frame lines were drawn individually on mylar for use in fabricating the respective frames. Figure 45 shows a trimetric view of each of the test fixture surfaces. These surfaces can be covered with flat skin sheets, thus, avoiding special tooling.

Interface definition: The coordinates of the test fixture forward and aft frames and the inboard and outboard edges are given in tables X thru XIII. These coordinates define the edge contours required on adjacent test fixtures in order to obtain a smooth transition between the test fixtures fabricated in this program. The coordinates are consistent with those shown in figures 44 and 45.

TPS simulation. - The TPS consists of two principal components and an adhesive as shown in figure 2. The RSI is fabricated in 15.2 x 15.2 cm (6.0 x 6.0 in.) tiles with the thickness dependent upon the location on the

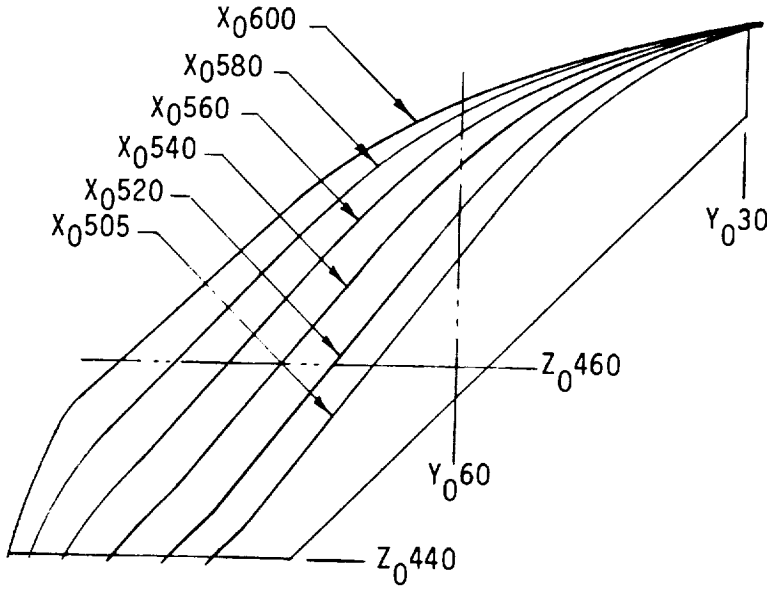

(a) LARGE RADIUS CURVATURE

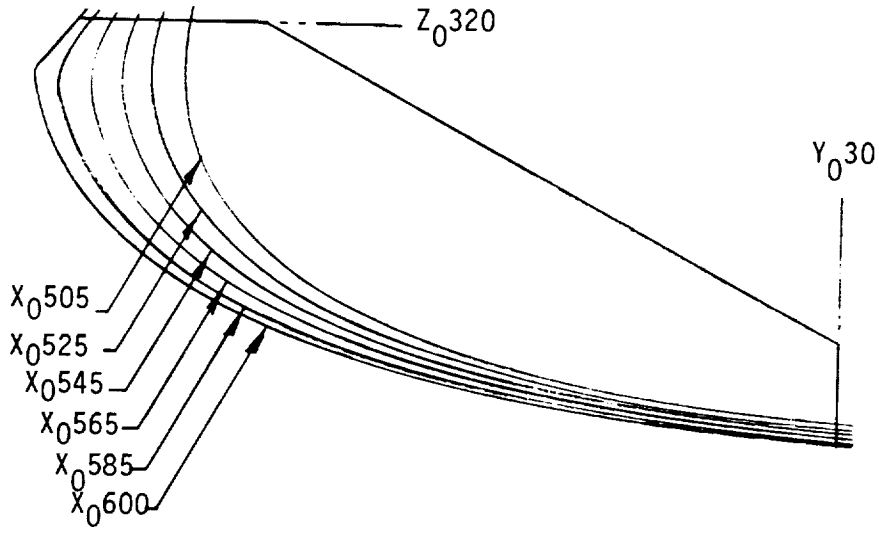

(b) SMALL RADIUS CURVATURE

FIGURE 44 ELECTRICAL TEST FIXTURE CONTOURS

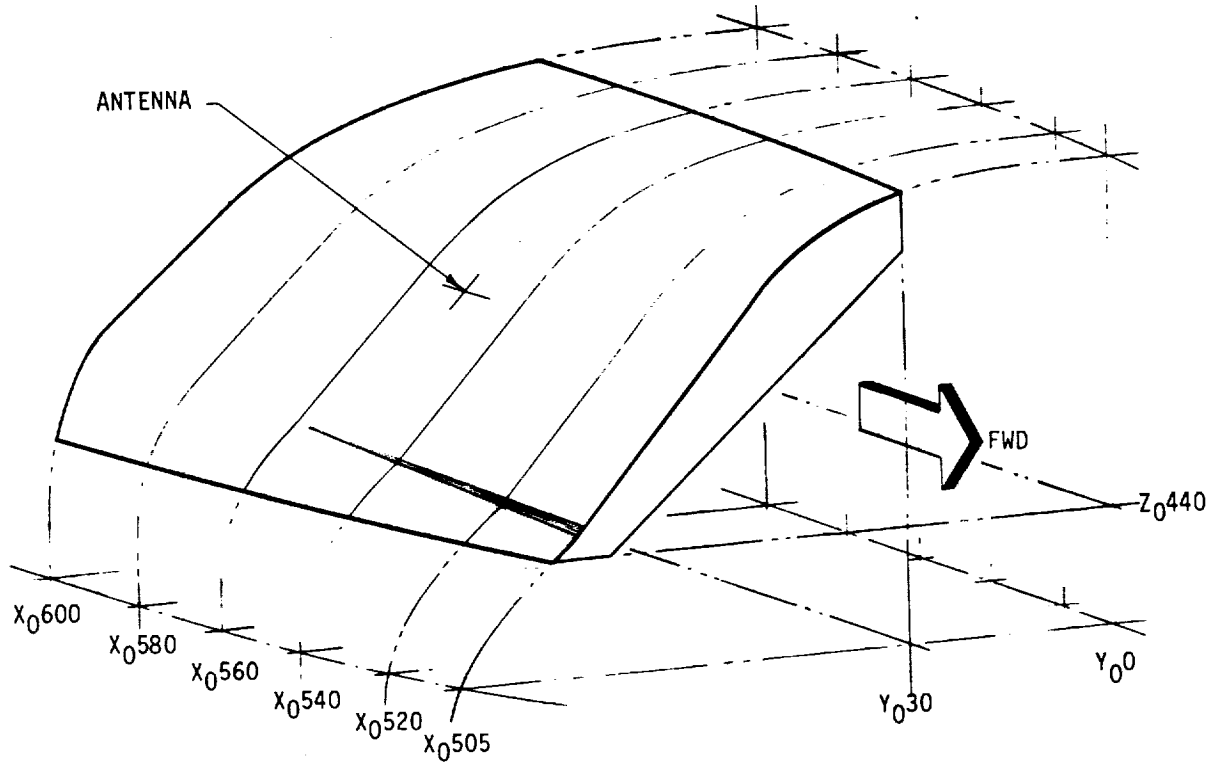

(a) LARGE RADIUS CURVATURE

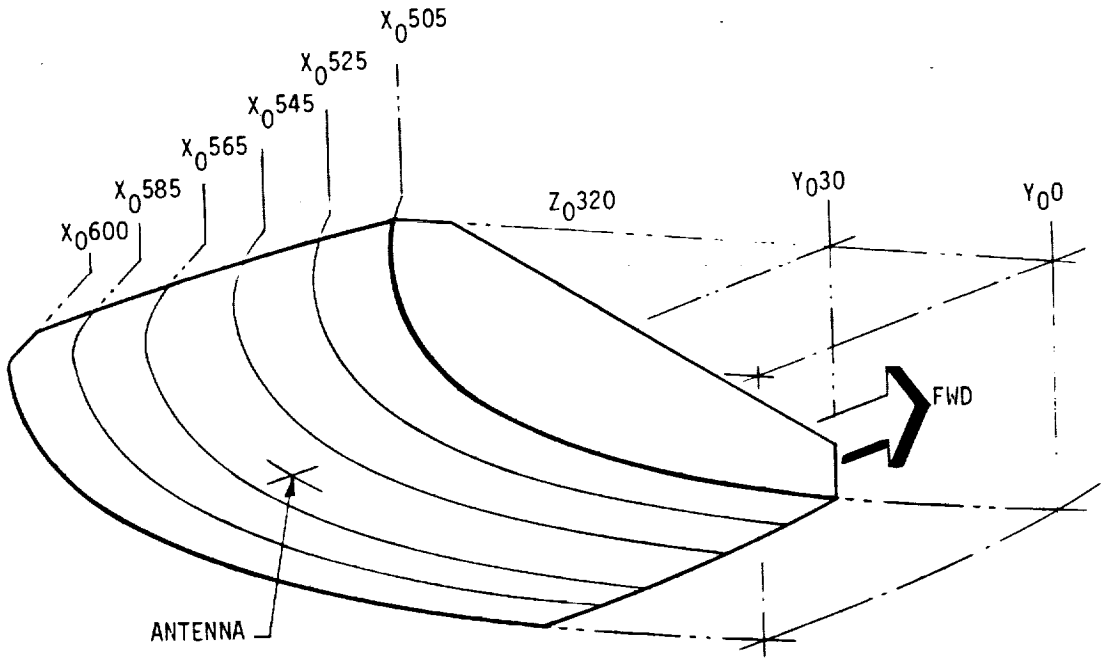

(b) SMALL RADIUS CURVATURE

FIGURE 45 ELECTRICAL TEST FIXTURE SURFACE CONTOURS - TRIMETRIC VIEW

TABLE X

LARGE RADIUS TEST FIXTURE FRAME COORDINATES

Forward Frame
X_0 = 505

Y_0	Z_0
26.200	279.476
29.379	279.678
32.544	279.910
35.695	280.174
38.833	280.472
41.955	280.805
45.060	281.177
48.148	281.589
51.217	282.046
54.266	282.549
57.293	283.104
60.296	283.715
63.273	284.385
66.221	285.123
69.138	285.933
72.021	286.824
74.864	287.806
77.663	288.891
80.413	290.091
83.105	291.425
85.729	292.916
88.274	294.594
90.721	296.497
93.046	298.685
95.212	301.243
97.159	304.311
98.775	308.150
99.476	310.960
99.855	314.166
99.811	317.259
99.370	320.246
98.537	323.129

Aft Frame
X_0 = 600

Y_0	Z_0
30.000	277.536
33.166	277.736
36.321	277.961
39.465	278.214
42.598	278.496
45.717	278.817
48.824	279.149
51.917	279.525
54.996	279.935
58.059	280.382
61.106	280.869
64.135	281.397
67.147	281.969
70.138	282.588
73.108	283.259
76.056	283.984
78.978	284.770
81.874	285.619
84.740	286.540
87.574	287.539
90.371	288.625
93.128	289.808
95.840	291.101
98.499	292.520
101.097	294.084
103.624	295.821
106.064	297.766
108.397	299.969
110.590	302.507
112.594	305.501
114.315	309.175
115.380	313.052
114.407	316.028
112.469	318.335
110.480	320.606
108.900	322.395

TABLE XI

LARGE RADIUS TEST FIXTURE
INBOARD AND OUTBOARD COORDINATES

	Y_0 = 30	Z_0 = 440
X_0	Z_0	Y_0
505	496.081	85.357
510	496.200	86.967
515	496.297	88.558
520	496.378	90.126
525	496.446	91.664
530	496.504	93.164
535	496.553	94.620
540	496.595	96.021
545	496.631	97.359
550	496.663	98.628
555	496.691	99.817
560	496.715	100.924
565	496.736	101.944
570	496.756	102.877
575	496.773	103.726
580	496.789	104.492
585	496.803	105.183
590	496.815	105.802
595	496.827	106.354
600	496.837	106.818

Orbiter. The tile pattern is offset 7.6 cm (3.0 in.) in one direction and aligned in the other. The gap width between tiles is nominally 1.27 $\pm$ .51 mm (0.050 $\pm$ 0.020 in.).

The RSI was simulated with ECCOFOAM PS-A because of the high cost and limited availability of the actual material. The RSI (LI-900) dielectric constant and loss tangent are approximately 1.15 and .0008, respectively (reference 1). The ECCOFOAM is a light weight artificial dielectric plastic foam material, manufactured by Emerson & Cuming, Inc. It can be obtained with dielectric constants ranging from 1.1 to 2.0. The loss tangents of this material are approximately 0.0005 for dielectric constants up to 1.6. ECCOFOAM is relatively easy to cut into the required tile shape. The borosilicate TPS surface coating was simulated with a silicon dispersion coating (Dow Corning 92-009) which has a dielectric constant of 2.75 and a loss tangent of 0.0023. The borosilicate has a dielectric constant of about 2.45 and a loss tangent of about 0.0065 at the S-band frequencies (reference 2) according to test data from the Massachusetts Institute of Technology Laboratory for Insulation Research. Therefore, the Dow Corning silicon is considered a suitable simulation for the borosilicate coating material.

TABLE XII

SMALL RADIUS TEST FIXTURE FRAME COORDINATES

Forward Frame
X_0 = 505

Y_0	Z_0
28.855	496.453
31.696	495.484
34.482	494.370
37.208	493.098
39.867	491.646
42.331	490.049
44.781	488.243
47.129	486.338
49.339	484.301
51.414	482.134
53.391	479.873
55.307	477.554
57.187	475.200
59.046	472.826
59.809	471.841
	Str Line
81.806	443.392
84.051	442.267
86.252	439.115
88.402	436.928

Aft Frame
X_0 = 600

Y_0	Z_0
29.004	497.022
31.979	496.456
34.938	495.846
37.882	495.188
40.808	494.478
43.716	493.713
46.603	492.889
49.470	492.001
52.313	491.043
55.130	490.009
57.920	488.893
60.680	487.687
63.407	486.384
66.098	484.973
68.749	483.443
71.356	481.782
72.850	480.751
75.249	478.931
77.510	476.959
79.712	474.920
81.896	472.863
84.074	470.798
86.248	468.730
88.421	466.661
88.800	466.300
	Str Line
100.100	455.704
101.861	453.190
103.243	450.517
104.458	447.773
105.531	444.970
106.424	442.091
106.832	439.700

TABLE XIII

SMALL RADIUS TEST FIXTURE
INBOARD AND OUTBOARD EDGE COORDINATES

	Y_0 = 30	Z_0 = 320
X_0	Z_0	Y_0
505	279.721	99.422
510	279.605	100.138
515	279.489	100.850
520	279.374	101.554
525	279.257	102.249
530	279.141	102.936
535	279.026	103.615
540	278.911	104.284
545	278.795	104.942
550	278.680	105.588
555	278.565	106.219
560	278.451	106.835
565	278.336	107.435
570	278.222	108.016
575	278.107	108.577
580	277.992	109.117
585	277.878	109.629
590	277.764	110.116
595	277.650	110.579
600	277.536	111.014

Simulated materials for the SIP (Nomex E Felt #2352 NRB) and RTV-560 were not necessary since both materials were readily available.

TPS thickness. - The TPS thickness variation on the Orbiter upper body is relatively small. Table XIV shows the total required Orbiter TPS thicknesses as a function of X_0 and Y_0 coordinates. The TPS RSI tile thicknesses were obtained by subtracting 0.160 in. (a standard allowance used for the SIP and bondline thicknesses) from these values. A review of the TPS thickness requirements resulted in the choice of 1.041 cm (0.410 in.) for the TPS thickness on the large radius test fixture. This choice results in a tile thickness of 0.64 cm (0.25 in.). It was also decided that a uniform TPS thickness could be used over the entire test fixture since the TPS thickness variation was very small over most of the area included in the test fixture design.

The TPS thickness variation on the Orbiter lower body is considerably larger than that on the upper body. Table XV shows the total required TPS thickness on the lower body as a function of X_0 and Y_0 coordinates. These TPS

TABLE XIV

TOTAL TPS THICKNESS-ORBITER UPPER BODY

	X_0						
Y_0	505	520	540	551.15	560	580	600
30	0.9214	0.4001	0.3817		0.3726	0.3699	0.3695
35	0.9256	0.4259	0.3967		0.3768	0.3700	0.3693
40	0.8003	0.4376	0.4123		0.3824	0.3718	0.3699
45	0.5714	0.4255	0.4243		0.3902	0.3758	0.3725
50	0.3671	0.3879	0.4284		0.4003	0.3840	0.3785
55	0.3600	0.3512	0.4217		0.4126	0.3969	0.3882
60	0.3600	0.3600	0.4102	0.4253	0.4253	0.4128	0.4006
65	0.3600	0.3599	0.4036		0.4342	0.4264	0.4126
70	0.3600	0.3600	0.3978	0.4134	0.4243	0.4320	0.4188
75	0.3600	0.3600	0.3978		0.4156	0.4254	0.4259
80	0.3600	0.3601	0.4006	0.4141	0.4189	0.4222	0.4304
85	0.4715	0.4505	0.4052		0.4310	0.4339	0.4447
90	0.5300	0.4953	0.4690		0.4496	0.4609	0.4768
95	0.6263	0.5662	0.5209		0.5007	0.5021	0.5295
100		0.7033	0.6090		0.5703	0.5681	0.6100

Notes: (1) These values obtained from Rockwell International.
(2) TPS thickness values are in inches.
(3) Subtract 0.160 from numbers in table to obtain RSI thickness.

thicknesses vary from a minimum of 3.58 cm (1.41 in.) to a maximum of 7.52 cm (2.96 in.). As a result of discussions between MDAC and NASA-JSC, a decision was made to approximate the TPS surface contours on the small radius test fixture with areas of constant thickness except over the antenna where the thickness would be contoured. This approach was necessary in order to keep the number of different tile thicknesses to a reasonably small number during fabrication. In areas where the thickness variation is small, a thickness step size of 4.06 mm (.160 in.) was selected. In areas outboard of buttline $Y_0 = 80$, where the thickness increased approximately 6 mm (1/4 in.) for every 15 cm (6 in.), a thickness step size of 6.6 mm (0.26 in.) was selected. This approach results in a TPS surface within $\pm$2.03 mm ($\pm$0.080 in.) and $\pm$3.30 mm ($\pm$0.130 in.) of the true surface.

Surface wave considerations: The material thickness for the onset of surface waves propagation (reference 3) is given by

$$\frac{d}{\lambda_o} = \frac{n}{4\sqrt{\varepsilon_r - 1}} \qquad n = 0, 1, 2, 3,$$

TABLE XV

TOTAL TPS THICKNESS-ORBITER LOWER BODY

	X_0						
Y_0	505	525	545	556	565	585	600
30	1.7198	1.7029	1.6831		1.6750	1.6676	1.6496
35	1.7247	1.6960	1.6638		1.6480	1.6370	1.6172
40	1.7318	1.6893	1.6430		1.6187	1.6040	1.5828
45	1.7417	1.6836	1.6217		1.5881	1.5698	1.5473
50	1.7556	1.6797	1.6007		1.5573	1.5356	1.5121
55	1.7745	1.6790	1.5813		1.5277	1.5028	1.4790
60	1.8004	1.6830	1.5654		1.5012	1.4735	1.4499
65	1.8356	1.6940	1.5552		1.4803	1.4501	1.4274
70	1.8836	1.7153	1.5540		1.4682	1.4359	1.4147
75	1.9497	1.7517	1.5667		1.4694	1.4351	1.4159
80	2.0418	1.8106	1.6000		1.4904	1.4536	1.4365
82	2.0886	1.8428	1.6214	1.5458	1.5064	1.4680	1.4516
84	2.1426	1.8814	1.6486	1.5693	1.5276	1.4874	1.4716
86	2.2051	1.9277	1.6829	1.5993	1.5553	1.5125	1.4970
88	2.2777	1.9832	1.7255	1.6372	1.5904	1.5443	1.5285
90	2.3623	2.0500	1.7784	1.6845	1.6343	1.5836	1.5670
92	2.4612	2.1306	1.8435	1.7431	1.6886	1.6317	1.6136
94	2.5763	2.2280	1.9235	1.8153	1.7555	1.6902	1.6691
96	2.7080	2.3462	2.0221	1.9041	1.8372	1.7605	1.7354
98		2.4895	2.1437	2.0131	1.9371	1.8447	1.8127
99.8	2.96						
100		2.6618	2.2937	2.1469	2.0588	1.9453	1.9039
102			2.478	2.3108	2.2067	2.0647	2.0102
103.1		2.96					
104						2.2059	2.1337
105			2.82		2.49	2.29	2.20
106.4			2.96				
107					2.71	2.46	2.35
109						2.66	2.52
109.7					2.96		
111						2.86	2.71
113						2.96	2.88
115.4							2.96

Notes: (1) These values obtained from Rockwell International.

(2) TPS thickness values are in inches.

(3) Subtract 0.160 from numbers in table to obtain RSI thickness.

where

d = thickness of dielectric coating
λ_o = free-space wavelength
ε_r = relative dielectric constant
n = order of surface wave mode.

Even TM_n modes (i.e., polarization perpendicular to ground plane) and odd TE_n modes (i.e., polarization parallel to ground plane) can exist. Since the antennas to be tested on the respective test fixtures are circularly polarized, both perpendicular and parallel polarization must be considered. From the above expression, it is obvious that surface waves for polarization perpendicular to the ground plane (TM_o mode) can always exist. However, for polarization parallel to the ground plane the thickness required for surface wave propagation is finite and is determined by the dielectric constant of the ground plane cover material.

The TPS thickness for the onset of the TE_1 surface wave mode is 0.645 wavelengths, assuming a TPS dielectric constant of 1.15 and an operating frequency of 2252.5 MHz (center transmit frequency specified by RFP). The TPS thickness in wavelengths (d/λ) on the small radius test fixture ranges from 0.269 to 0.565, and therefore, only the TM_o surface wave mode can be excited. Figure 46 shows a plot of the TM_o propagation velocity relative to free-space, c/v (also propagation phase constant relative to free-space, β/k), for a lossless dielectric ($\varepsilon_r = 1.15$) of thickness d/λ on a lossless ground plane. Since the SIP dielectric constant ($\varepsilon_r = 1.25$ (reference 2)) is only slightly greater than that of the RSI and the SIP layer is very thin (4.06 mm (0.160 in.)), the effect of the SIP on the c/v ratio is negligible. The propagation velocity and phase constant of free-space are represented by c (speed of light) and k ($2\pi/\lambda$), respectively. Using figure 46, it can be shown that the surface wave propagation velocity will be within 0.2% of that expected for a true surface contour when the steps in TPS tile thickness are 6.6 mm (0.26 in.) or less. Therefore, the approach described above for approximating the TPS thickness requirements on the small radius test fixture is considered technically sound.

Edge effects. - A microwave absorber was added to the test fixture edges (figure 47) to minimize the effects of surface waves and skin currents which radiate from sharp discontinuities and interact with the basic antenna radiation pattern. The absorber selected is Emerson & Cuming AN 77 which has good absorption characteristics (reflectivity $\leq$ 20 dB) down to frequencies of 1.2 GHz.

This technique has been used by MDAC in the past with good results. Figure 48 shows the patterns of a flat spiral antenna measured at 3.0 GHz on a ground plane 56 cm (26 in.) in diameter (which is about 6.6 wavelengths in diameter). The pattern with the polarization perpendicular to the ground plane shows significant ripple due to the ground plane edge. A change in ground plane size changes the frequency of ripple. The pattern with the polarization parallel to the ground plane shows no significant edge effect. By adding a

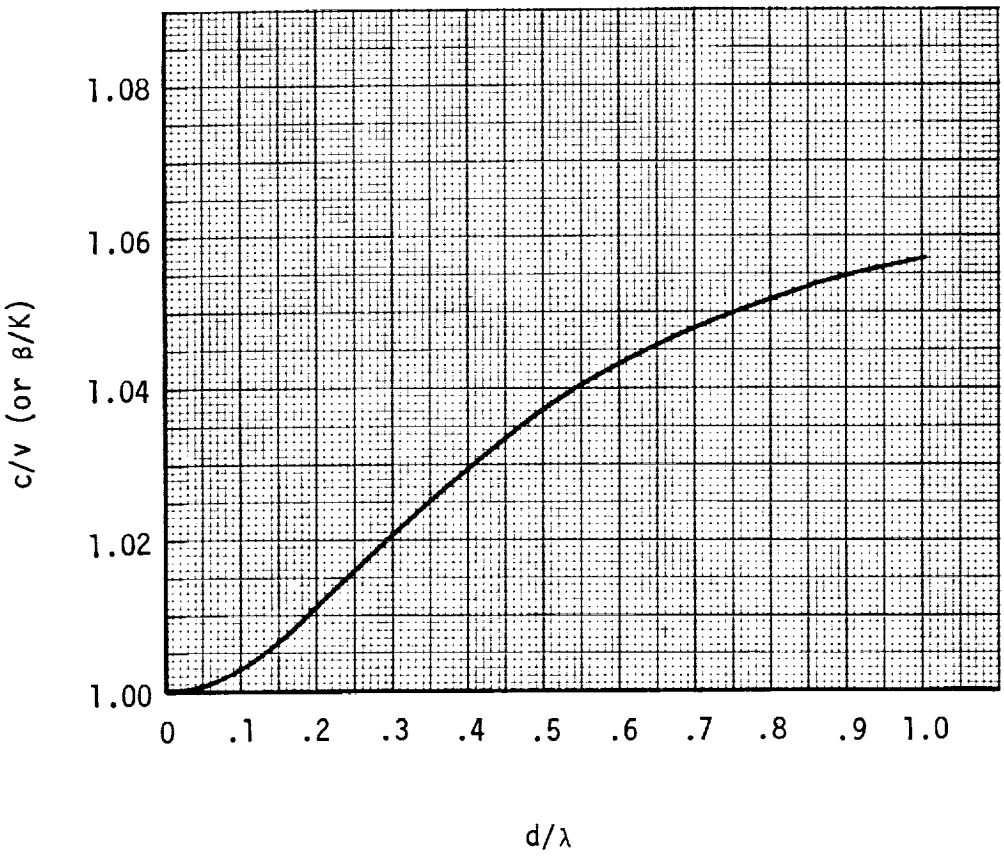

FIGURE 46 PROPAGATION VELOCITY RATIO (ϵ_r = 1.15)

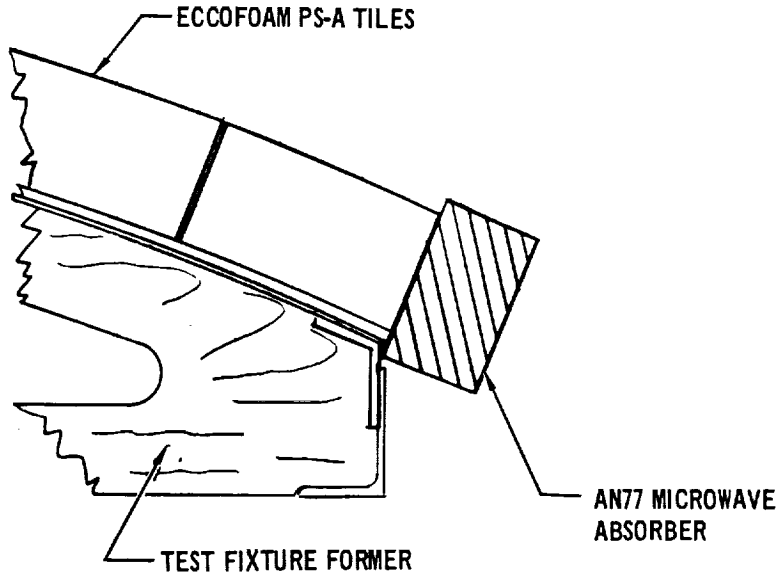

FIGURE 47 MICROWAVE ABSORBER CONFIGURATION FOR MINIMIZING EDGE RADIATION

(a) Polarization Parallel to Ground Plane

(b) Polarization Perpendicular to Ground Plane

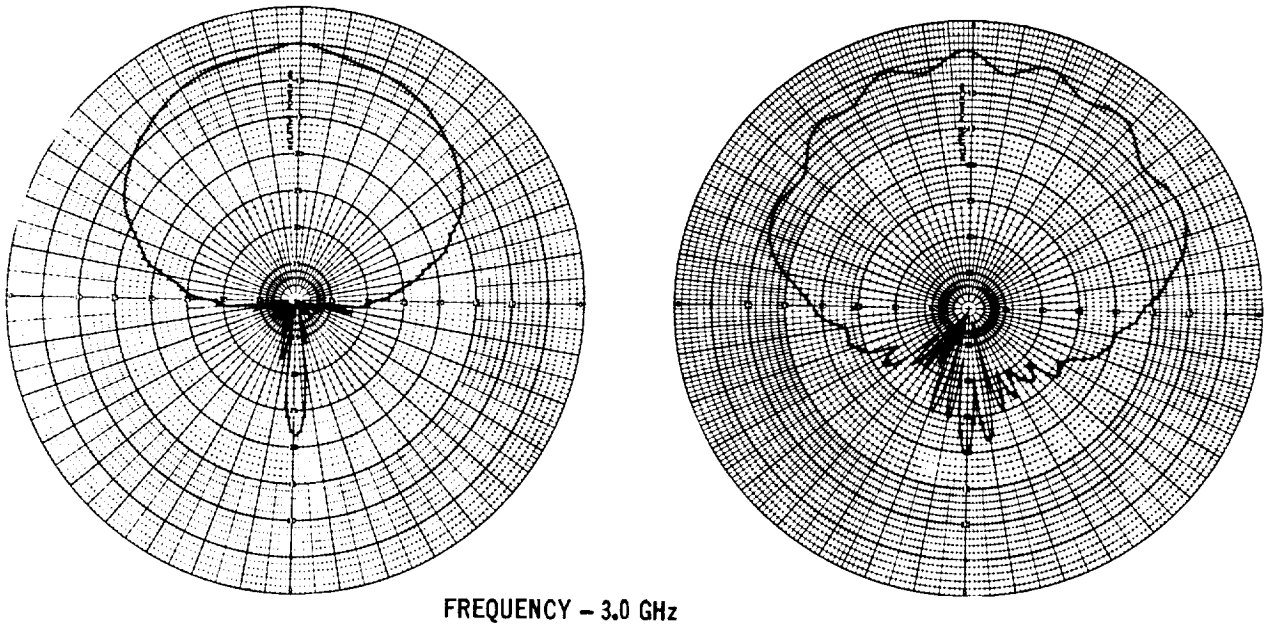

FREQUENCY – 3.0 GHz
GROUND PLANE DIAMETER – 26 IN.

FIGURE 48 EFFECTS OF GROUND PLANE EDGE ON S-BAND SPIRAL ANTENNA PATTERN

strip of Emerson & Cuming AN 75 microwave absorber 3 in. wide around the edges of the ground plane, the pattern with the polarization perpendicular was significantly improved as shown in figure 49.

Mounting provisions. - The mounting approach selected was one in which arbor plates are attached to the forward and aft ends of the test fixtures (figure 50) to permit rotation in rotisseire fashion. The extension, which spans between the end frame and next inboard frame, eliminates bending loads on the end frame and, thus, ensures adequate support and stiffness during testing and handling. The arbor plate design mates with the standard Scientific Atlanta Series 5860 and 5870 antenna tower arbor plates.

Fabrication

The test fixtures were fabricated per the design approach discussed in the preceding subsection on Design. The fabrication processes for both the large and small radius test fixtures were straightforward and essentially the same with a few exceptions as will be noted.

Test fixture structure. - The test fixture structure consists of 1.27 cm (0.50 in.) thick plywood frames and 3.18 x 2.22 x .32 cm (1-1/4 x 7/8 x 1/8 in.) aluminum "T" stringers as shown in figure 51. The frames were constructed with the aid of full-scale mylar drawings of the developed contour lines which were

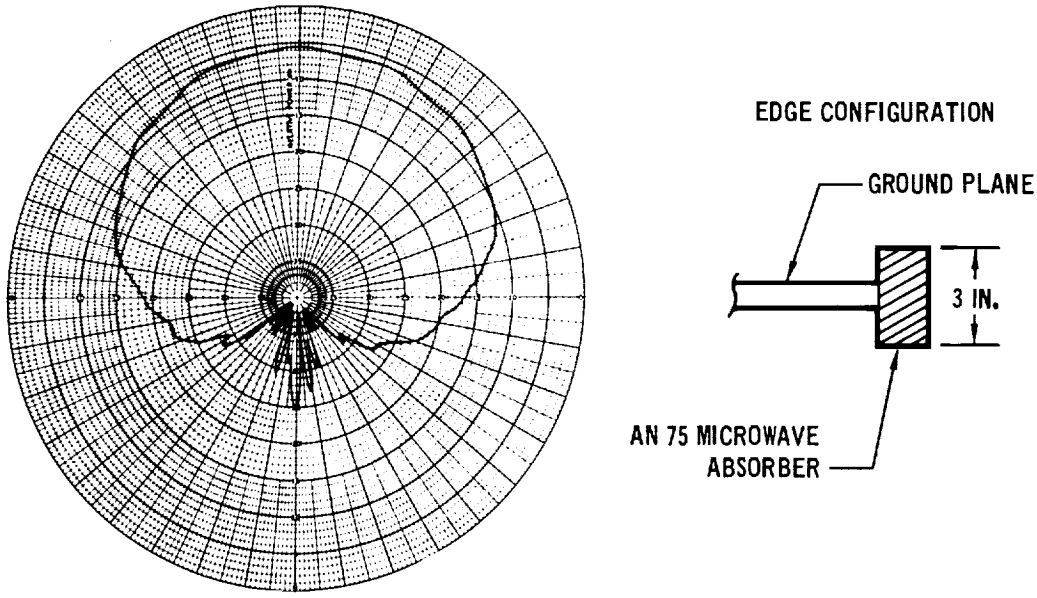

POLARIZATION – PERPENDICULAR TO GROUND PLANE
FREQUENCY – 3.0 GHz
GROUND PLANE DIAMETER – 26 IN.

FIGURE 49 EFFECTS OF ADDING MICROWAVE ABSORBER TO GROUND PLANE EDGE

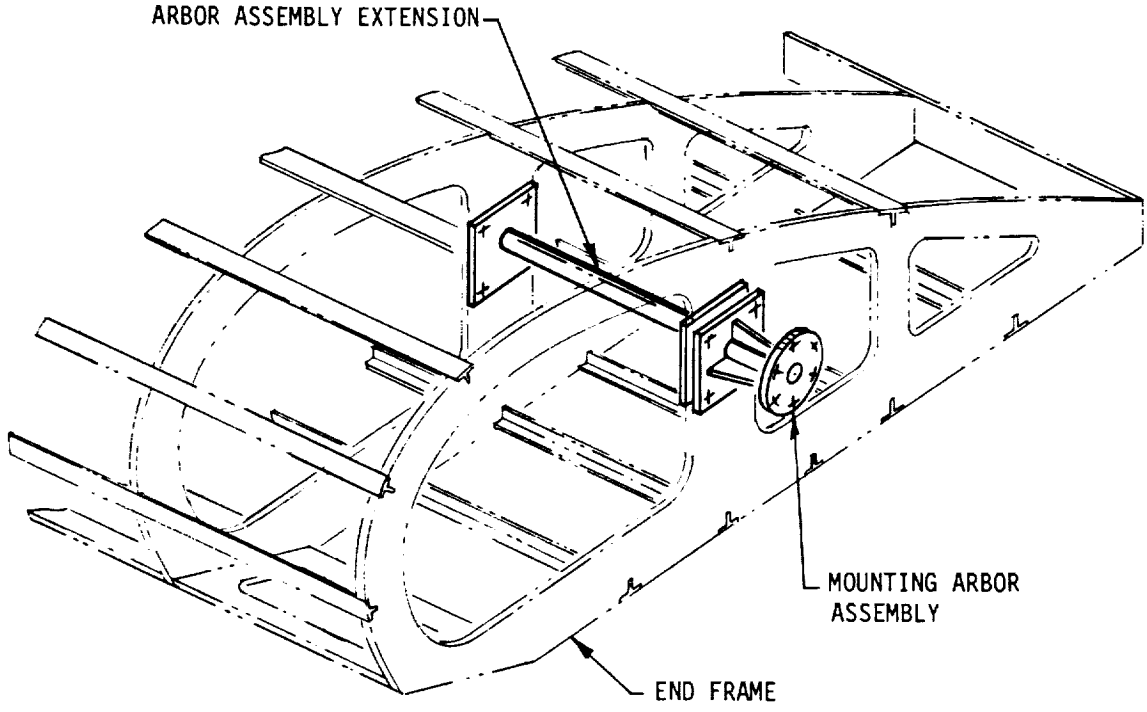

FIGURE 50 MOUNTING ARBOR ASSEMBLY

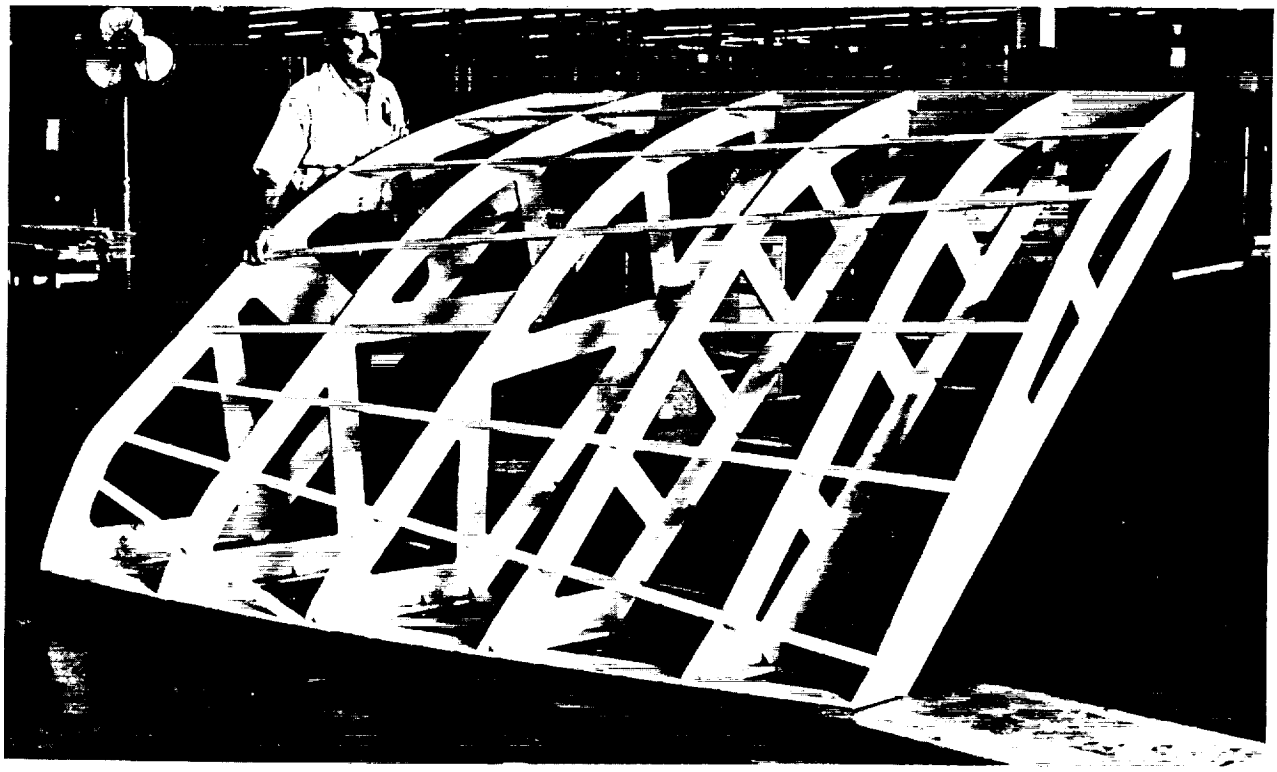

FIGURE 51 LARGE RADIUS TEST FIXTURE STRUCTURE

cut out and temporarily attached with rubber cement. Cut-outs were made in the frames to decrease their weight while maintaining the required strength and stiffness. Seven "T" stringers were arranged along straight line elements to provide uniform support for the skin. Plywood panels were used along the inboard buttline and the outboard waterline to tie the frame ends together and add stiffness to the structure. A 0.813 mm (0.032 in.) aluminum skin was attached to the framework using 3 mm (1/8 in.) brazier head (pull-through type) aluminum alloy Chobert rivets with a head height of 1.27 mm (0.050 in.). Figures 52 and 53 show the large and small radius test fixture structures with the skin attached. (Note: The skin distortions that appear in figure 52 are due to light reflections which greatly exaggerate small irregularities in flat surfaces.) A standard joint sealer (PR-1422, Class B-1/2 polysulfide, commonly used in airplane production) was used along the skin stringer and frame interfaces. This results in a more solid structure which will dampen skin motion and flutter when the test fixture is rotated during testing.

Antenna mounting frame. - Figure 52 also shows the antenna mounting frame. The skin around the antenna mount was backed by a 0.254 cm (0.100 in.) aluminum doubler plate which was contoured to match the skin contours and riveted to the skin near the frames and stringers. A sketch of the antenna mounting frame details is shown in figure 54. The back-side mounting approach was necessary because the TPS is continuous over the antenna and is essentially held in place over the antenna by the SIP. Conducting epoxy was used to avoid machining the complex surface to match the skin contours. Twenty, evenly-spaced, threaded holes, extending through the doubler plate and skin, were

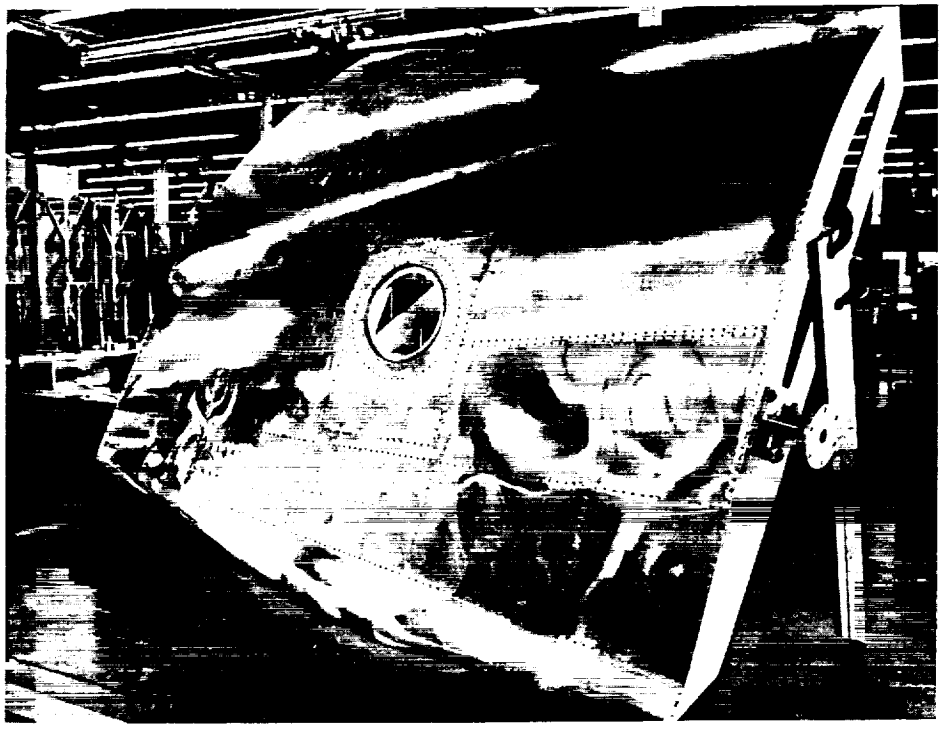

FIGURE 52 LARGE RADIUS TEST FIXTURE STRUCTURE WITH SKIN ATTACHED AND ANTENNA MOUNTING FRAME INSTALLED

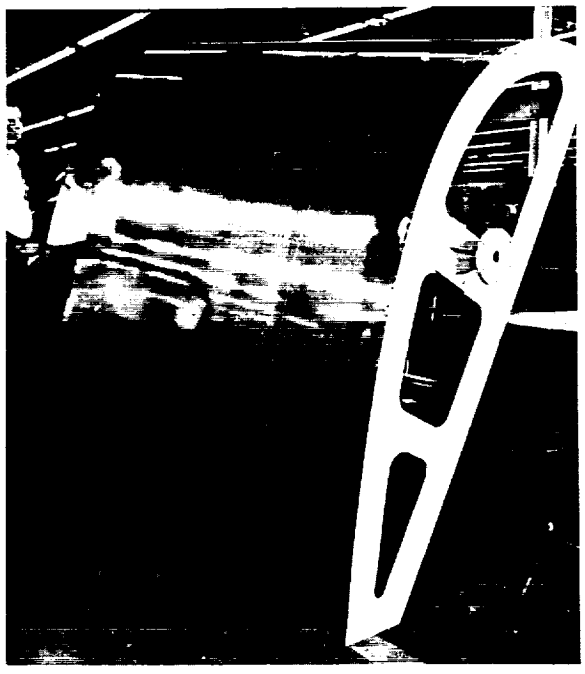

FIGURE 53 SMALL RADIUS TEST FIXTURE STRUCTURE WITH SKIN AND MOUNTING ARBOR ATTACHED

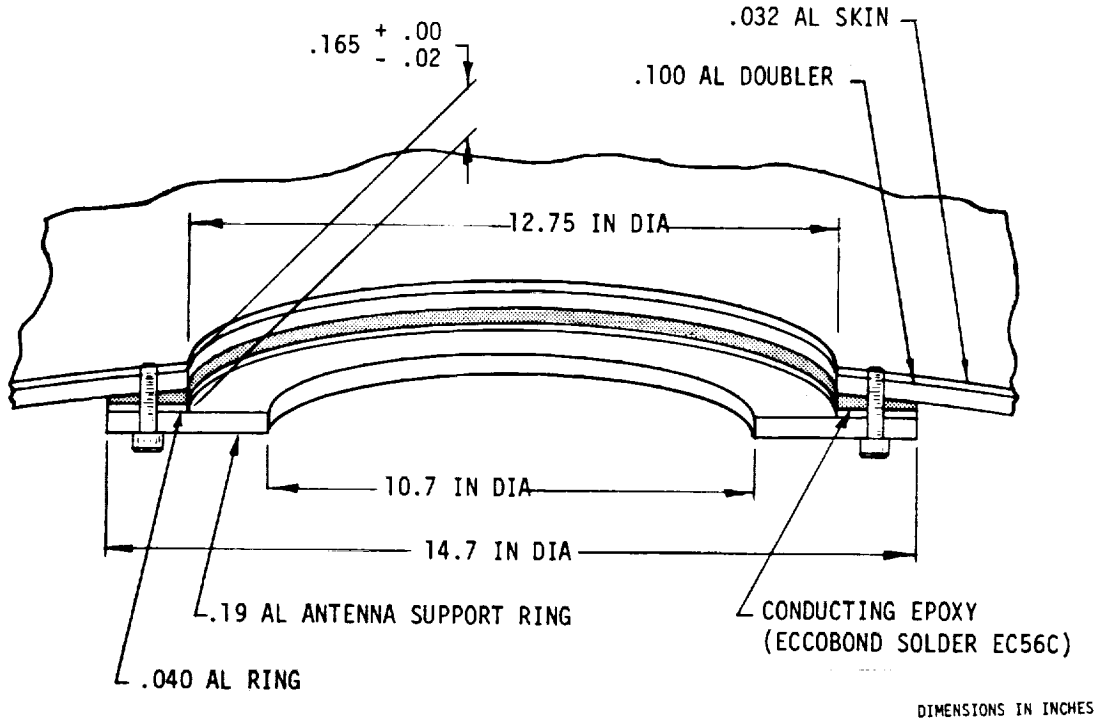

FIGURE 54 ANTENNA MOUNTING DETAILS

provided to attach the antenna support ring and antenna to the test fixture. The attachment screws were cut off so they would not extend above the skin surface and were color coded for convenience.

Test fixture interface continuity. - Copper tape 5.1 cm (2.0 in.) wide was attached to the skin and extended over the test fixture edge surfaces about 2.5 cm (1.0 in.) to provide a means for obtaining electrical continuity with an adjacent test fixture without disturbing the simulated TPS.

Simulated TPS attachment. - The SIP was bonded to the test fixture skin with RTV-560 adhesive as shown in figure 55. RTV was applied to the aluminum skin, primed with Dow Corning A4094 primer, and the SIP carefully laid in place. The RTV cannot be applied directly to the SIP because the SIP, which is a porous blanket, readily absorbs the RTV and the bond thickness cannot be controlled. Over the cut-out for the antenna, the SIP was supported by a dummy antenna mounting flange plate, which was formed to the skin surface contours with White Knight autobody putty.

TPS tile fabrication - large radius test fixture. - TPS tiles for the large radius test fixture were fabricated from 43 x 43 x 43 cm (17 x 17 x 17 in.) ECCOFOAM PS-A blocks. The blocks were first cut into 15.24 x 15.24 cm (6.00 x 6.00 in.) logs and then into tiles 6.35 mm (0.25 in.) thick. These tiles were layed out on the test fixture as shown in figure 56. Cardboard strips 1.27 mm (0.050 in.) thick were used to obtain the proper tile spacing. Where necessary, the thin ECCOFOAM tiles were molded to the curvature by using a small amount of heat while forcing them to the contour.

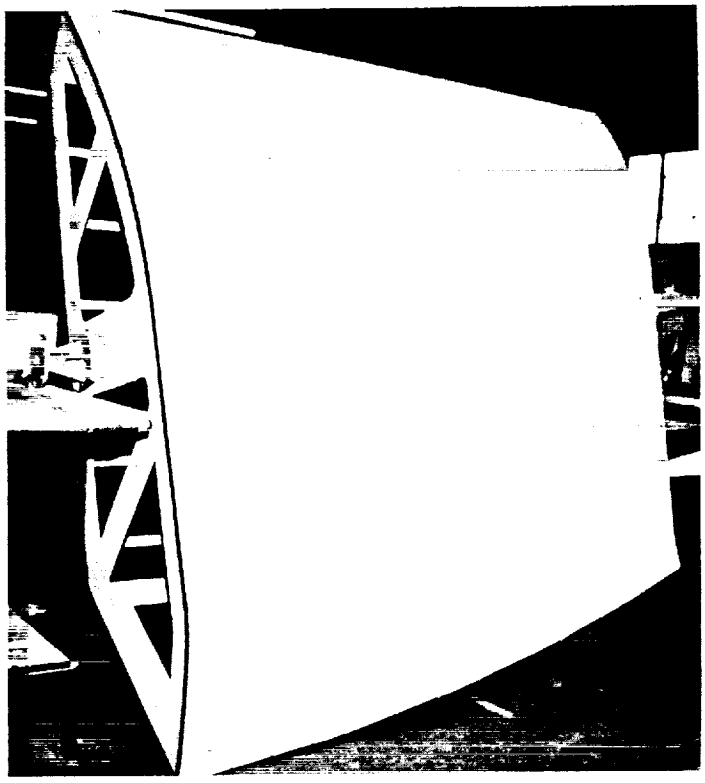

FIGURE 55 LARGE RADIUS TEST FIXTURE SKIN COVERED WITH NOMEX FELT (SIP)

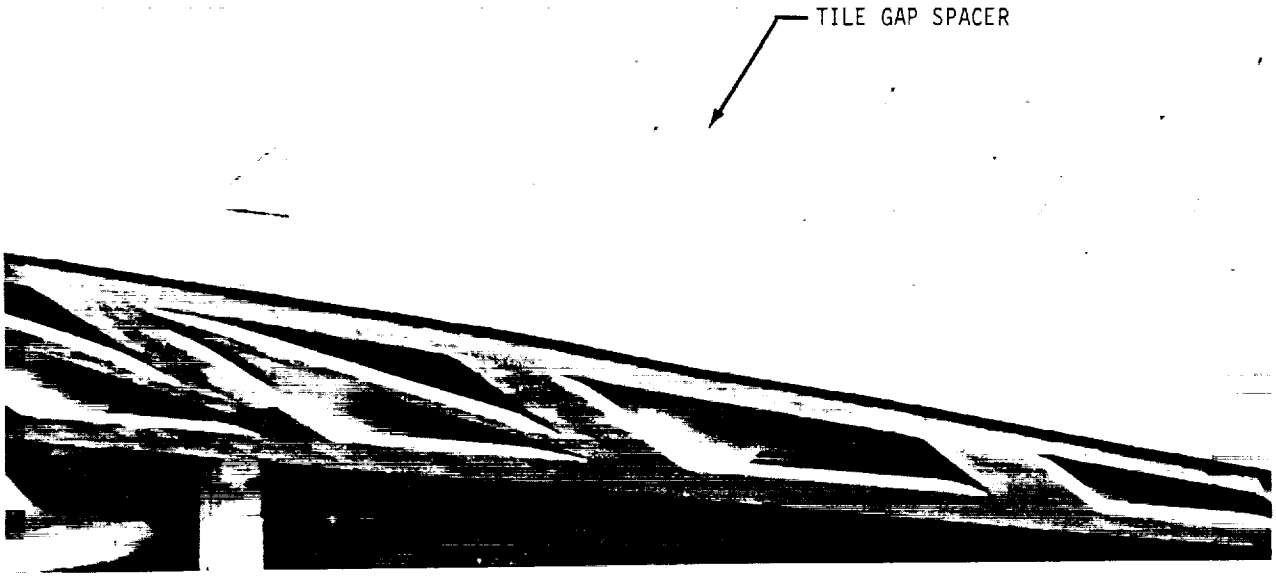

FIGURE 56 ECCOFOAM TILE LAY-OUT BEFORE BONDING

After the tile lay-out was completed, the tile edges were coated with Dow Corning 92-009 silicon. Preliminary tests showed that a Dow Corning A4094 primer applied to the ECCOFOAM PS-A surface would improve the bond strength 2-3 times. However, when the primer was applied to the thin tiles, they curled up as the primer cured and were unusable. Therefore, the tiles on the large radius test fixture were not primed before bonding.

Following cure of the edge coating, the tile surface was coated with RTV and placed on the SIP. A vacuum bag was used to apply a pressure of 6.9 N/m^2 (1 psi) on the tile surface during the cure cycle.

After the RTV cured, the tile surfaces were coated with Dow Corning 92-009 silicon. Three coats were required to obtain a coating thickness of 0.25 to 0.38 mm (0.010 to 0.015 in.). The silicon coating also tended to make the tiles curl slightly although preliminary test samples did not indicate such an effect. Further investigation showed that the curling was most prominent if the ECCOFOAM density was slightly low. Figure 57 shows a top view of the large radius test fixture after completion of bonding and surface coating. Figure 58 shows a photo of the completed large radius test fixture.

TPS tile fabrication - small radius test fixture. - The fabrication of the ECCOFOAM tiles for the small radius test fixture was considerably more difficult because of the variation in tile thickness and the smaller radius of curvature. From about the middle of the test fixture surface and outboard the curvature was such that two sides of the tiles had to be tapered to maintain a reasonable gap width. Further, the tiles thickness in each row decreased from body stations X_0 = 505 to X_0 = 600. The respective tile thickness as a function of location was determined by developing a flat pattern of the skin surface using the frame lines developed for the simply curved surface. Tile thickness contour plots (figure 59) were made on the flat pattern according to the thickness variation guidelines discussed in the previous section on Design. The respective contour lines bound the TPS thickness selected for each area except the area on the upper surface of the chine (or wing boot). In this region the TPS thickness rapidly decreases to about 2.5 cm (1.0 in.) at the right extremity of the flat pattern. These TPS thickness contours result in tile thicknesses of 3.40, 3.81, 4.22, 4.75, 5.41, 6.07, and 6.73 cm (1.34, 1.50, 1.66, 1.87, 2.13, 2.39, and 2.65 in.). A tile lay-out was made on the flat pattern to identify the tile requirements during fabrication. The tile thickness over the antenna and about 15 cm (6 in.) immediately surrounding it was contoured to conform to actual thickness requirements per table XV. The tile dimensions at the base were held to 15.24 x 15.24 cm (6.00 x 6.00 in.) and the transverse distance was increased as necessary to form a straight gap between tile rows.

The tiles over the antenna were bonded to the test fixture and then the surface was shaped to the required contour. This served as a base for the tile lay-out. The remaining tiles were fabricated and bonded to the SIP one row at a time. The tile edges were coated with silicon prior to bonding as discussed previously.

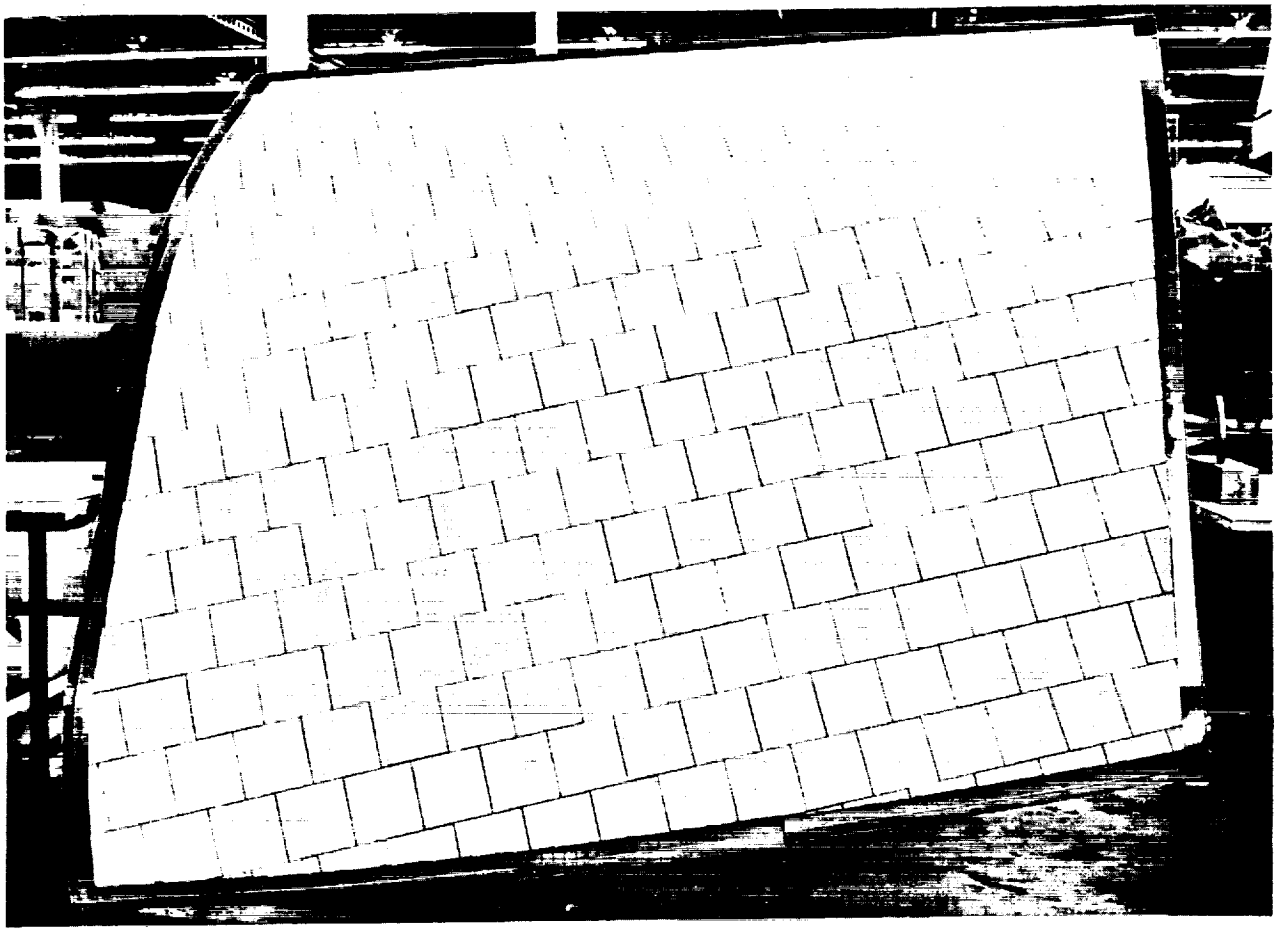

FIGURE 57 LARGE RADIUS TEST AFTER COMPLETION OF BONDING AND SURFACE COATING

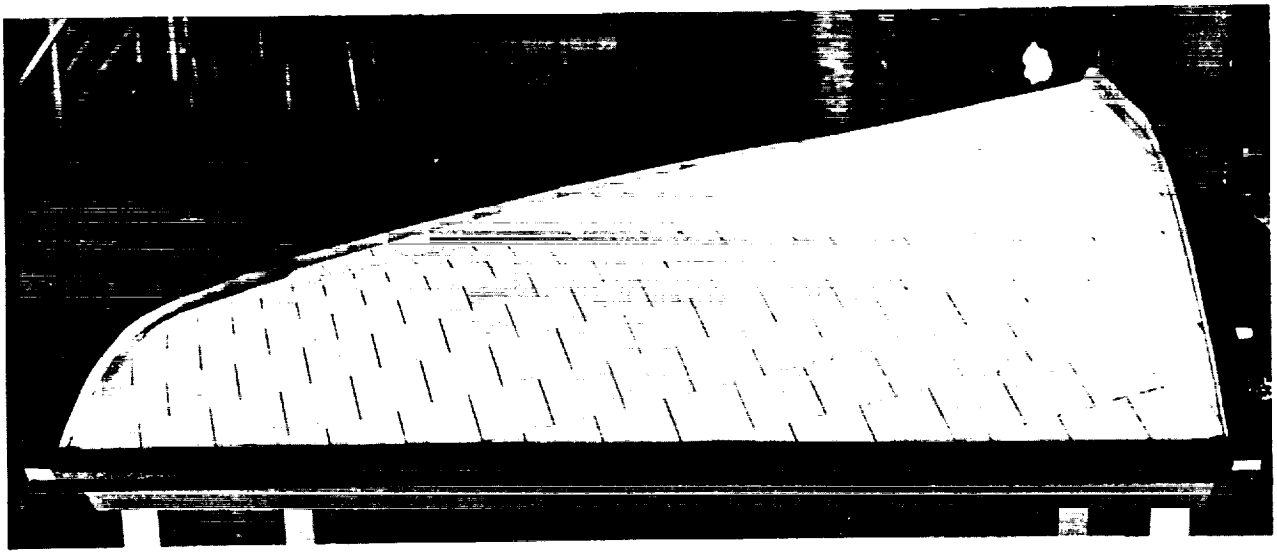

FIGURE 58 LARGE RADIUS ELECTRICAL TEST FIXTURE

FIGURE 59 TPS THICKNESS CONTOURS - SMALL RADIUS TEST FIXTURE

A thin coat of RTV-560 on the tile surface prior to bonding proved to be an excellent method of priming the tiles. After the tile was coated with RTV for bonding and put into place, force was applied to the tile surface. As before, cardboard gap spacers were used to maintain the proper gap spacing.

After the RTV cure cycle, when the gap spacers were removed it was observed that the gap spacing changed. This was attributed to the loading on the SIP during bonding. When the SIP is compressed, the expansion direction is not necessarily in the same direction as the applied compressive load. Therefore, when the load is removed, the SIP may spring back to its original shape with some sidewise movement. Figure 60 shows the small radius test fixture before all the tiles have been bonded in place. In some areas a variation in gap width can be seen. Figure 61 shows a photo of the completed small radius test fixture. The tile thickness contours can be seen.

Microwave absorber attachment. - Following the tile bonding and surface coating tasks, the Emerson & Cuming AN 77 microwave absorber was attached around the test fixture edges by means of a simple Z bracket as shown in figure 62. The absorber was bonded to the brackets and can be removed by removing the screws holding the brackets in place.

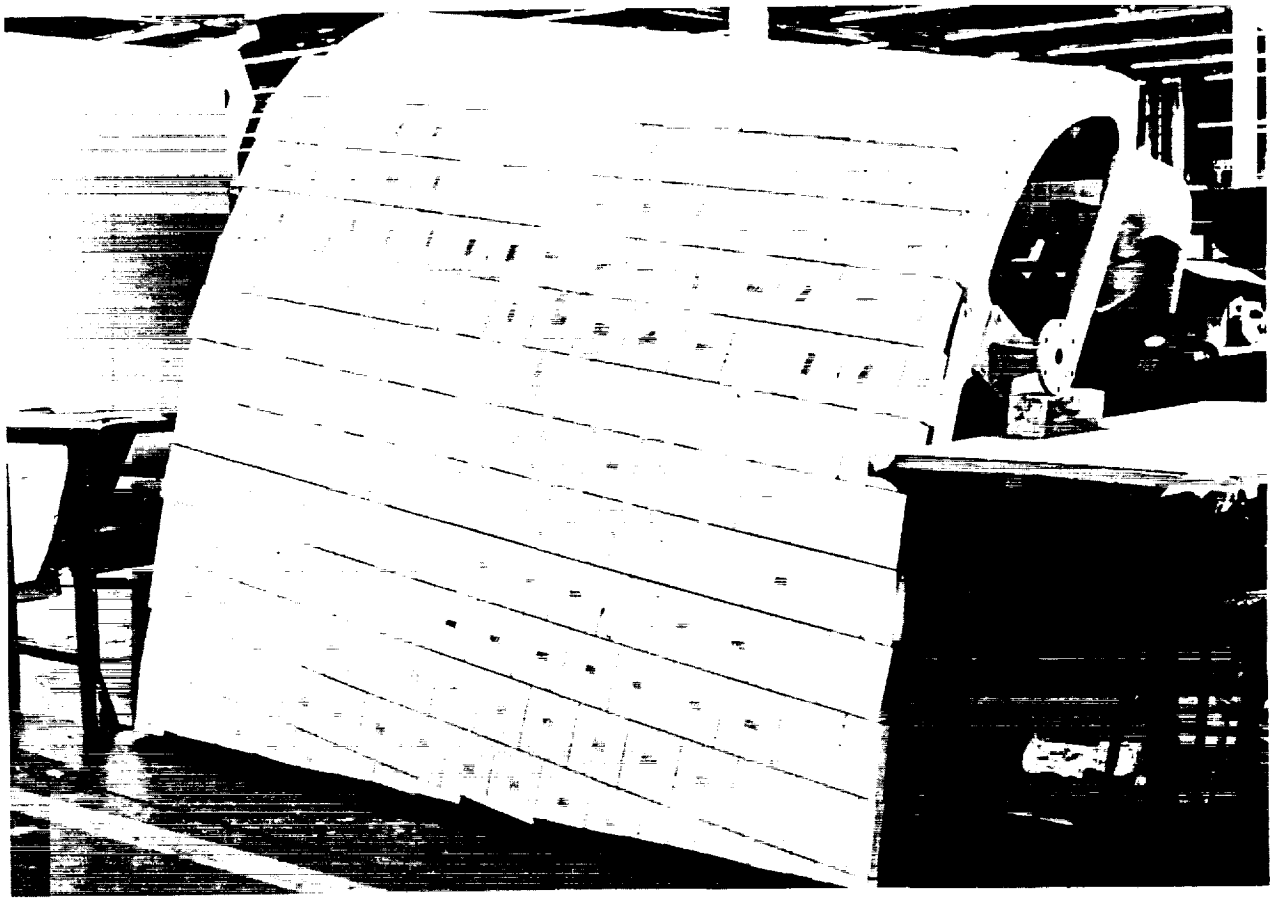

FIGURE 60 SMALL RADIUS TEST FIXTURE DURING TILE BONDING

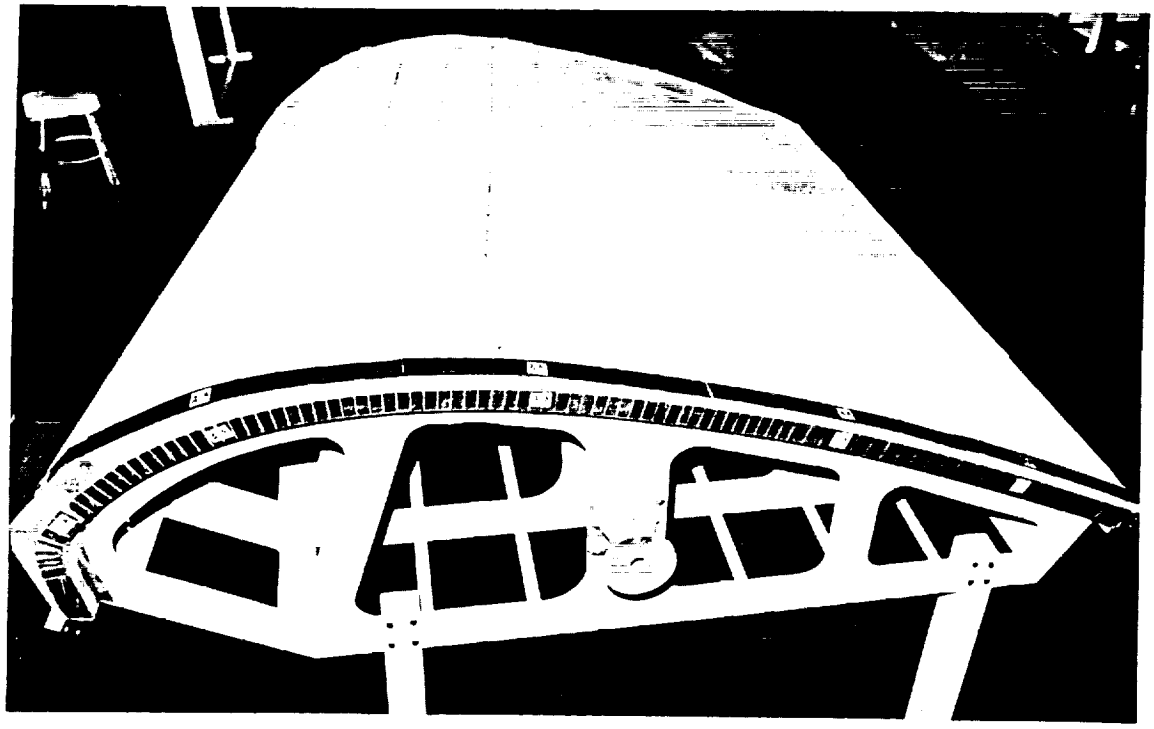

FIGURE 61 SMALL RADIUS ELECTRICAL TEST FIXTURE

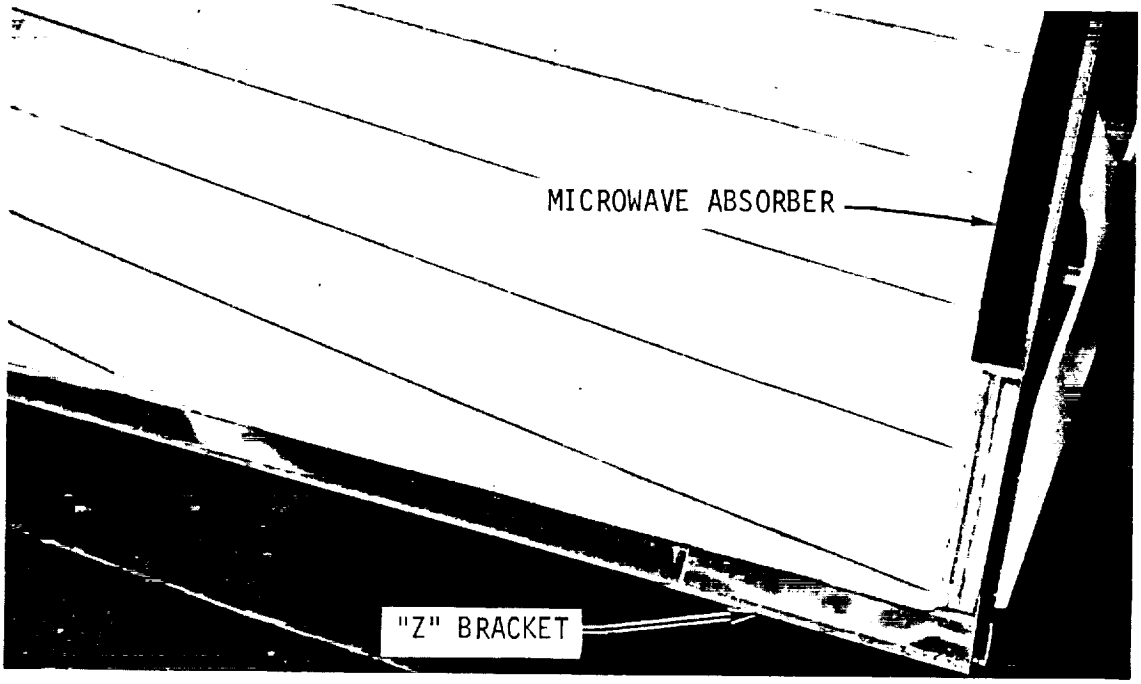

FIGURE 62 MICROWAVE ABSORBER ATTACHMENT CONFIGURATION

THIS PAGE INTENTIONALLY LEFT BLANK

REFERENCES

1. Gilreath, M. C. and Castellow, S. L., Jr.: High-Temperature Dielectric Properties and Candidate Space Shuttle Thermal-Protection-System and Antenna-Window Materials, NASA TN D-7523, June 1974

2. Stricklen, J. O.: "Shuttle TPS Dielectric Constant Tests," Rockwell International Memo No. 098-31-4057, 26 August 1974

3. Bailey, M. C. and Croswell, W. F.: "Pattern Measurements of Slot Radiators in Dielectric-Coated Metal Plates," IEEE Trans. Antennas and Propagation (Communications), Vol. AP-15, pp. 824-826, November 1967

THIS PAGE INTENTIONALLY LEFT BLANK

APPENDIX A

MATERIAL PROPERTIES

The material properties given below were used in the analyses performed in this program.

(1) REUSABLE SURFACE INSULATION (HRSI/LRSI)

	Thermal Conductivity (BTU/ft-hr-F)					
Temperature (°F)	P = 0.21 psf (P ∿ 0.076 torr)	P = 2.12 psf (P ∿ 0.76 torr)	P = 21.16 psf (P ∿ 7.6 torr)	P = 211.6 psf (P ∿ 76 torr)	P = 2116 psf (P ∿ 760 torr)	Specific Heat (BTU/lb-F)
-250.	0.0050	0.0075	0.0150	0.0216	0.0233	0.070
-150.	-	-	-	-	-	0.105
0.	0.0075	0.0100	0.0183	0.0250	0.0275	0.150
250.	0.0092	0.0125	0.0225	0.0316	0.0341	0.210
500.	0.0125	0.0167	0.0276	0.0400	0.0433	0.252
750.	0.0175	0.0216	0.0325	0.0492	0.0534	0.275
1000.	0.0233	0.0275	0.0392	0.0600	0.0658	0.288
1250.	0.0308	0.0350	0.0492	0.0725	0.0782	0.296
1500.	0.0416	0.0459	0.0617	0.0875	0.0942	0.300
1750.	0.0567	0.0610	0.0767	0.1060	0.1130	0.302
2000.	0.0734	0.0782	0.0942	0.1270	0.1360	0.303
2300.	0.0966	0.1020	0.1160	0.1550	0.1670	0.303

Density = 9.0 lb_m/ft^3

Emissivity = 0.8

Solar Absorptivity = $\begin{cases} 0.8 \text{ HRSI} \\ 0.32 \text{ LRSI} \end{cases}$

(2) STRAIN ISOLATOR PAD (SIP)

Temperature (°F)	Thermal Conductivity (BTU/ft-hr-F)				
	P = 0.21 psf (0.076 torr)	P = 2.12 psf (0.76 torr)	P = 21.16 psf (7.6 torr)	P = 211.6 psf (76 torr)	P = 2116 psf (760 torr)
-282	0.0050	0.0069	0.0090	0.0094	0.0094
-162	0.0050	0.0083	0.0130	0.0140	0.0140
92	0.0050	0.0120	0.0210	0.0230	0.0240
396	0.0090	0.0170	0.0300	0.0370	0.0380

Temperature (°F)	Specific Heat (BTU/lb_m-F)
-238	0.105
-148	0.124
-58	0.158
32	0.208
122	0.277
212	0.353
302	0.462
392	0.564

Density = 5.4 lb_m/ft^3

(3) INTERNAL INSULATION (TG-15000)

Temperature (°F)	Thermal Conductivity (BTU/ft-hr-F)				
	P = 0.0278 psf (P ∿ 0.01 torr)	P = 0.278 psf (P ∿ 0.1 torr)	P = 2.78 psf (P ∿ 1.0 torr)	P = 27.8 psf (P ∿ 10 torr)	P = 2116 psf (P ∿ 760 torr)
-300	0.0005	0.0006	0.0016	0.0035	0.0048
-200	0.0009	0.0012	0.0028	0.0061	0.0077
-100	0.0015	0.0018	0.0041	0.0088	0.0105
0	0.0021	0.0026	0.0056	0.0117	0.0138
100	0.0030	0.0038	0.0078	0.0150	0.0184
200	0.0042	0.0053	0.0107	0.0196	0.0245
300	0.0058	0.0078	0.0144	0.0250	0.0300
400	0.0078	0.0098	0.0182	0.0296	0.0354
500	0.0102	0.0127	0.0217	0.0342	0.0400
600	0.0127	0.0158	0.0259	0.0384	0.0450
700	0.0154	0.0192	0.0296	0.0421	0.0480

Density = 2.0 lb_m/ft^3
Specific Heat = 0.2 BTU/lb_m-°F
Emissivity = 0.2

(4) MISCELLANEOUS

Material	Density (lb_m/ft^3)	Specific Heat (BTU/lb_m-F)	Thermal Conductivity (BTU/ft-hr-F)	Emittance
RTV-560	88.0	0.35	0.18	
RTV-511	73.7	0.33	°F k 0 0.17 77 0.17 225 0.15 400 0.15	
Polyimide Fiberglass	112.4	0.40	0.184	
Eccosphere Insulation	5.7	0.19	0.058	
MLI	0.001	0.001	°F k -460 0.0006 -300 0.0012 -200 0.0028 -100 0.0068 0 0.016 100 0.026 200 0.040 300 0.060	0.2
2024-T8XX Al	178.	°F c_p -200 0.147 0 0.195 200 0.216 300 0.224 400 0.233 600 0.250	°F k -200 69.6 0 84.0 200 95.0 300 99.0 400 102.5 600 104.5	0.85
6061-T6 Al	169.3	Same as 2024-T8XX	96.8	0.8 0.9*

*Dust cover outside.

THIS PAGE INTENTIONALLY LEFT BLANK

APPENDIX B

ANTENNA THERMAL MODEL NODE LOCATIONS

1	Forward Radiating Element Insulation, Bottom
2	Forward Radiating Element Insulation, Bottom
3	Forward Radiating Element Ridge, Bottom
4	Forward Radiating Element Insulation, Bottom
5	Forward Radiating Element Ridge, Bottom
6	Forward Radiating Element Insulation, Bottom
7	Lateral Radiating Element Insulation, Bottom
8	Lateral Radiating Element Insulation, Bottom
9	Lateral Radiating Element Ridge, Bottom
10	Lateral Radiating Element Insulation, Bottom
11	Lateral Radiating Element Ridge, Bottom
12	Lateral Radiating Element Insulation, Bottom
13	Center Radiating Element Insulation, Bottom
14	Center Radiating Element Ridge, Bottom
15	Center Radiating Element Insulation, Bottom
16	Center Radiating Element Insulation, Bottom
17	Forward Radiating Element Insulation, Center
18	Forward Radiating Element Insulation, Center
19	Forward Radiating Element Ridge, Center
20	Forward Radiating Element Insulation, Center
21	Forward Radiating Element Ridge, Center
22	Forward Radiating Element Insulation, Center
23	Lateral Radiating Element Insulation, Center
24	Lateral Radiating Element Insulation, Center
25	Lateral Radiating Element Ridge, Center
26	Lateral Radiating Element Insulation, Center
27	Lateral Radiating Element Ridge, Center
28	Lateral Radiating Element Insulation, Center
29	Center Radiating Element Insulation, Center
30	Center Radiating Element Ridge, Center
31	Center Radiating Element Insulation, Center
32	Center Radiating Element Insulation, Center
33	Forward Radiating Element Insulation, Top
34	Forward Radiating Element Insulation, Top
35	Forward Radiating Element Ridge, Top
36	Forward Radiating Element Insulation, Top
37	Forward Radiating Element Ridge, Top
38	Forward Radiating Element Insulation, Top
39	Lateral Radiating Element Insulation, Top
40	Lateral Radiating Element Insulation, Top
41	Lateral Radiating Element Ridge, Top
42	Lateral Radiating Element Insulation, Top
43	Lateral Radiating Element Ridge, Top
44	Lateral Radiating Element Insulation, Top
45	Center Radiating Element Insulation, Top
46	Center Radiating Element Ridge, Top

APPENDIX B

(Continued)

47	Center Radiating Element Insulation, Top
48	Center Radiating Element Insulation, Top
49, 50	Forward Radiating Element Canister, Bottom
51, 52	Lateral Radiating Element Canister, Bottom
53	Center Radiating Element Canister, Bottom
54, 55	Forward Radiating Element Canister Side, Bottom
56, 57	Lateral Radiating Element Canister Side, Bottom
58	Center Radiating Element Canister Side, Bottom
59, 60	Forward Radiating Element Canister Side, Center
61, 62	Lateral Radiating Element Canister Side, Center
63	Center Radiating Element Canister Side, Center
64, 65	Forward Radiating Element Canister Side, Top
66, 67	Lateral Radiating Element Canister Side, Top
68	Center Radiating Element Canister Side, Top
69	Polymide Antenna Cover
70-79	Antenna Mounting Plate
80-84	Dust Cover Support Plate
85-88	TPS Bondline Over Antenna
89-103	Radiosity, Radiating Element Canisters
104-112	Forward Radiating Element Hybrid
113, 114	Forward Radiating Element Canister Stud
115, 116	Forward Radiating Element Canister Legs
117-123	Lateral Radiating Element Hybrid
124, 125	Lateral Radiating Element Canister Stud
126, 127	Lateral Radiating Element Canister Legs
128-133	Center Radiating Element Hybrid
134	Center Radiating Element Canister Stud
135	Center Radiating Element Canister Leg
136-141	Dust Cover Sides
142-145	Dust Cover Flange
146-160	Aluminum Skin and Stringers
161-172	TPS Bondline Away From Antenna
173-182	Circuit Board, Outboard
183-190	Radiosity, Dust Cover Sides and Dust Cover Flange
191-198	Radiosity, Circuit Board, Top
199, 200	Circuit Board Sides
201-208	Radiosity, Antenna Mounting Plate
209-224	RSI Inboard, Layer 1
225-234	Circuit Board, Inboard
235	Dust Cover Top
236,237	Radiosity, Circuit Board Side
238	Radiosity, Dust Cover Top, Inside
239-248	Radiosity, Circuit Board, Inboard
249-264	RSI Layer 2
265-271	TG-15000
272-275	MLI
276	Cabin Wall

APPENDIX B

(Continued)

277-292	RSI Layer 3
293-308	RSI Layer 4
309-324	RSI Surface, Layer 5

1. Refer to figure 4 for component locations.
2. Refer to figures 5 thru 9 for node locations.

THIS PAGE INTENTIONALLY LEFT BLANK

APPENDIX C

SAMPLE COMPUTER PROGRAM OUTPUT

HEATRAN*S-BAND ANTENNA INSTALLATION, LOWER ANTENNA ENTRY **76/01/19.*12.02.21.* PAGE 4 CASE= ENTRY SEQ= 1

(221)	207.6867	207.5366	207.2721	207.2864	178.7702	178.7734	178.7821	178.8058	178.8542	178.7702	(230)
(231)	178.7734	178.7821	178.8059	178.8544	176.3362	176.3215	178.3216	177.5355	177.6583	177.6595	(240)
(241)	177.6176	177.6652	177.6783	177.6583	177.6595	177.6176	177.6652	177.6783	242.1349	242.1486	(250)
(251)	246.7154	243.0026	242.8178	242.7628	246.5712	242.8866	242.9071	242.8027	242.5561	242.5283	(260)
(261)	247.8221	242.7105	242.5271	242.5466	162.9601	157.1170	151.1258	145.0403	138.9236	132.8457	(270)
(271)	126.8900	126.0008	125.1181	124.2316	123.3415	92.0000	346.7251	346.7380	349.9944	347.3183	(280)
(281)	347.2166	347.1789	349.8885	347.2401	347.2399	347.1705	347.0094	346.9863	347.1766	347.1032	(290)
(291)	346.9851	346.9994	670.5837	670.5923	672.3676	670.9045	670.8523	670.8327	672.3080	670.8623	(300)
(301)	670.8580	670.8210	670.7364	670.7224	670.8234	670.7842	670.7217	670.7294	1586.5509	1586.5510	(310)
(311)	1586.5622	1586.5529	1586.5526	1586.5525	1586.5618	1586.5527	1586.5526	1586.5524	1586.5519	1586.5518	(320)
(321)	1586.5524	1586.5522	1586.5518	1586.5518	(324)						

TIME = 500.0000 DEGREE FAHRENHEIT K2 = 29

(1)	179.0278	179.0277	179.0590	179.0344	179.0556	179.0243	179.0283	179.0249	179.0562	179.0350	(10)
(11)	179.0596	179.0282	179.0562	179.0893	179.0562	179.0553	179.0556	179.0340	179.0845	179.0415	(20)
(21)	179.0779	179.0274	179.0559	179.0278	179.0783	179.0417	179.0845	179.0340	179.0556	179.1075	(30)
(31)	179.0556	179.0786	179.1039	179.0911	179.1471	179.0896	179.1376	179.0810	179.1042	179.0815	(40)
(41)	179.1381	179.0899	179.1471	179.0912	179.1046	179.1612	179.1046	179.1200	179.0432	179.0428	(50)
(51)	179.0434	179.0436	179.0799	179.0663	179.0615	179.0621	179.0674	179.0937	179.0792	179.0724	(60)
(61)	179.0729	179.0789	179.1030	179.1108	179.0962	179.0970	179.1110	179.1282	179.2934	179.1335	(70)
(71)	179.0495	179.0898	179.1152	179.1284	179.1319	179.0471	179.0897	179.1149	179.1284	179.1418	(80)
(81)	179.1433	179.5035	179.5025	179.5100	188.8455	188.8103	188.8108	188.7434	178.7575	178.6022	(90)
(91)	178.6021	178.7576	178.7657	178.7642	178.6744	178.6744	178.7642	178.7655	178.7928	178.7626	(100)
(101)	178.7632	178.7928	178.7952	179.0426	179.0421	179.0428	179.0409	179.0401	179.0405	179.0397	(110)
(111)	179.0385	179.0387	179.0409	179.0401	179.0645	179.0599	179.0434	179.0428	179.0411	179.0410	(120)
(121)	179.0411	179.0393	179.0395	179.0408	179.0412	179.0605	179.0649	179.0798	179.0794	179.0781	(130)
(131)	179.0781	179.0769	179.0771	179.0782	179.0924	176.9523	176.9509	177.6135	177.6107	178.6453	(140)
(141)	178.6392	178.6524	178.6463	178.6323	178.8385	179.5204	179.5972	180.2520	180.2804	179.5805	(150)
(151)	179.6357	180.1101	180.0688	180.1061	179.9470	179.5127	179.5030	180.3211	180.0836	179.5046	(160)
(161)	188.5399	189.5926	190.7268	189.4602	188.8196	188.8387	190.5926	189.2795	189.3611	189.2113	(170)
(171)	189.4658	189.2652	179.0768	179.0538	179.0392	179.0380	178.8990	179.0772	179.0591	179.0395	(180)
(181)	179.0390	178.8992	177.7543	178.4690	178.7018	178.7479	177.7541	178.4687	178.7012	178.7488	(190)
(191)	178.7956	178.7467	178.6813	178.5735	178.7966	178.7468	179.6814	178.5735	178.8980	178.8982	(200)
(201)	178.8060	178.7710	178.7429	178.7518	178.8060	178.7710	178.7432	178.7525	217.6769	217.7029	(210)
(211)	221.7192	218.6507	218.2566	218.2241	221.5734	218.5044	218.5626	218.4330	218.1280	218.0987	(220)
(221)	218.5334	218.3325	218.0980	218.0960	178.7880	178.7922	178.8035	178.8345	178.8974	178.7880	(230)
(231)	178.7922	178.8036	178.8346	178.8977	176.1404	178.3410	178.3409	177.4570	177.5895	177.5908	(240)
(241)	177.5457	177.5977	177.6130	177.5895	177.5908	177.5457	177.5977	177.6130	282.2956	282.3133	(250)
(251)	286.3869	283.1152	282.9007	282.8570	286.2524	283.0029	283.0243	282.9239	282.6900	282.6619	(260)
(261)	282.9572	282.6476	282.6607	282.6746	162.2234	156.8145	151.3056	145.7348	140.1452	134.5838	(270)
(271)	129.0999	128.1693	127.2347	126.2960	125.3531	92.0000	458.2396	458.2531	461.1944	458.7922	(280)
(281)	458.6316	458.6496	461.0971	458.7188	458.7198	458.6546	458.5049	458.4828	458.6647	458.5952	(290)
(291)	458.4817	458.4939	860.4592	860.4678	862.1264	860.7642	860.7095	860.6920	862.0795	860.7241	(300)
(301)	860.7203	860.6850	860.6048	860.5913	860.6883	860.6508	860.5907	860.5977	1580.9456	1580.9457	(310)
(311)	1580.9627	1580.9487	1580.9481	1580.9480	1580.9621	1580.9483	1580.9483	1580.9479	1580.9471	1580.9469	(320)
(321)	1580.9479	1580.9476	1580.9469	1580.9470	(324)						

TIME = 600.0000 DEGREE FAHRENHEIT K2 = 33

(1)	179.1682	179.1660	179.2246	179.1804	179.2227	179.1637	179.1689	179.1644	179.2235	179.1811	(10)
(11)	179.2252	179.1667	179.2020	179.2635	179.2020	179.2003	179.2170	179.1736	179.2672	179.1915	(20)
(21)	179.2637	179.1589	179.2172	179.1695	179.2644	179.1916	179.2668	179.1733	179.1991	179.2948	(30)
(31)	179.1991	179.2410	179.2955	179.2671	179.3724	179.2744	179.3690	179.2605	179.2958	179.2612	(40)
(41)	179.3687	179.2748	179.3723	179.2672	179.2822	179.3885	179.2922	179.3096	179.1986	179.1982	(50)
(51)	179.1990	179.1992	179.2479	179.2375	179.2349	179.2356	179.2387	179.2715	179.2600	179.2565	(60)
(61)	179.2572	179.2590	179.2881	179.3177	179.3113	179.3125	179.3177	179.3369	179.6079	179.4249	(70)
(71)	179.3048	179.3213	179.3302	179.3393	179.4223	179.3007	179.3195	179.3299	179.3393	179.4380	(80)
(81)	179.4405	180.0262	180.0242	180.0359	193.2833	193.2246	193.2255	193.0830	178.9248	178.7593	(90)

ORIGINAL PAGE IS
OF POOR QUALITY

THIS PAGE INTENTIONALLY LEFT BLANK